5-2013

Mechanisms Underlying the Heterogeneous Sensitivities of Cancer Cells to Proteasome Inhibitors

Matthew C. White

MECHANISMS UNDERLYING THE HETEROGENEOUS SENSITIVITIES OF CANCER CELLS TO PROTEASOME INHIBITORS

by

Matthew Cooper White, B.S.

Approved:

_____

David J. McConkey, Ph.D.

Chair, Supervisory Committee

_____

Kevin A. Morano, Ph.D.

_____

Mary Ann Smith, Ph.D.

_____

Varsha Gandhi, Ph.D.

_____

Joya Chandra, Ph.D.

Approved:

_____

Dean, The University of Texas

Graduate School of Biomedical Sciences at Houston

MECHANISMS UNDERLYING THE HETEROGENEOUS SENSITIVITIES OF CANCER CELLS TO PROTEASOME INHIBITORS

A

DISSERTATION

Presented to the Faculty of
The University of Texas Health Science Center at Houston and
The University of Texas M.D. Anderson Cancer Center
Graduate School of Biomedical Sciences

in Partial Fulfillment
of the Requirements
for the Degree of

DOCTOR of PHILOSOPHY

by

Matthew Cooper White, B.S.
Houston, Texas
May, 2013

DEDICATION

To my beautiful wife, who has supported me over the course of this educational journey. Thank you for your patience, understanding, friendship, and love – I cannot say enough about who you are as a person. To my sweet daughters, Hadleigh and Lainey, your current and future presence has brought me great joy and motivated me to complete this work. To my father and brother, who instilled in me the hunger for knowledge and desire for higher education, and to my mother, whose encouragement over the years has been unwavering. Thank you for instilling in me my Christian faith, which now guides my life. I love you all – this work is dedicated to you.

ACKNOWLEDGEMENTS

There are many people who have helped me reach the completion of this work. First, I would like to thank my advisor Dr. David McConkey for training me in his laboratory. I truly appreciate all that you have invested in me throughout my doctoral research. Thank you for modeling scientific integrity, scholarship, and creativity, and for demonstrating a tireless work ethic while balancing family life with young children. You have been a great mentor.

I would also like to thank other faculty members who have impacted my graduate education. Dr. Kevin Morano, thank you for critical conversations, invitations to conferences, and overall advice – it was a conversation with you and your doodle on a piece of paper following candidacy that was the lightbulb moment of graduate school for me. Dr. Mary Ann Smith, thank you for teaching the best courses that I took while in GSBS, and for exposing me to toxicology and taking me under your wing at the SOT meetings, where I ultimately found my job. Dr. Varsha Gandhi, thank you for organizing an exceptional graduate program that has contributed greatly to my scientific development. Dr. Joya Chandra, thank you for serving on all my committees and for your input and suggestions. Thank you to all the other faculty members who have served on my committees or accepted me for research tuturials in their labs: Dr. Craig Logsdon, Dr. Peng Huang, Dr. Mike Van Dyke, and Dr. Xifeng Wu.

Thank you to all my fellow students and lab mates, past and present, for sharing in the joy of successful experiments and the misery of failed ones (which is often). Thank you also for all of the technical and scientific advice over the years – I owe a large portion of my training to my interactions with you all.

Thank you to the core facilities of the Smith Research building – Donna for help with immunohistochemistry and immunofluorescence, and to Dr. Robert Langley for help with microscopy. Thank you to Drs. Sol Bobst and Ben Thomas for serving as a valuable career mentors.

Lastly, I would like to thank all of my family and friends. Thank you Brittany and Hadleigh for enduring my work schedule over these last few months. Mom and Dad, thank you for all of your support, and Jeff, thank you for setting the bar high. To all of my extended family and my wife's family, thank you for all of your love and support over these last few years. BC, as the only one of my closest friends who understands what the Ph.D. process is like, thanks for always lending an ear and being someone with which to share frustrations and triumphs. To all of our friends at Memorial Baptist, thank you for being such an encouragement to our family during these years – you all have been a blessing.

MECHANISMS UNDERLYING THE HETEROGENEOUS SENSITIVITIES OF CANCER CELLS TO PROTEASOME INHIBITORS

Publication No.:_____

Matthew C. White, BS

Supervisory Professor: David J. McConkey, Ph.D.

The mechanisms underlying cellular response to proteasome inhibitors have not been clearly elucidated in solid tumor models. Evidence suggests that the ability of a cell to manage the amount of proteotoxic stress following proteasome inhibition dictates survival. In this study using the FDA-approved proteasome inhibitor bortezomib (Velcade®) in solid tumor cells, we demonstrated that perhaps the most critical response to proteasome inhibition is repression of global protein synthesis by phosphorylation of the eukaryotic initiation factor 2-α subunit (eIF2α). In a panel of 10 distinct human pancreatic cancer cells, we showed marked heterogeneity in the ability of cancer cells to induce eIF2α phosphorylation upon stress (eIF2α-P); lack of inducible eIF2α-P led to excessive accumulation of aggregated proteins, reactive oxygen species, and ultimately cell death. In addition, we examined complementary cytoprotective mechanisms involving the activation of the heat shock response (HSR), and found that induction of heat shock protein 70 kDa (Hsp72) protected against proteasome inhibitor-induced cell death in human bladder cancer cells. Finally, investigation of a novel histone deacetylase 6 (HDAC6)-selective inhibitor suggested that the cytoprotective role of the cytoplasmic histone deacetylase 6 (HDAC6) in response to proteasome inhibition may have been previously overestimated.

TABLE OF CONTENTS

LIST OF FIGURES

CHAPTER 1

CHAPTER 2 (No figures)

CHAPTER 3

CHAPTER 4

CHAPTER 5

CHAPTER 6

CHAPTER 7 (No figures)

LIST OF TABLES

CHAPTER 4

CHAPTER 5

Chapter 1. INTRODUCTION

1. Introduction

1.1 Chronic stress of cancer cells

At the most fundamental level, a cancer cell can be understood as aberrant. This deviation from normalcy does not come without consequences for the cancer cell; those qualities that support hallmarks of the malignant state such as heightened proliferative capacity also place an extraordinary burden on the cell's stress response systems (Figure 1.1), thus creating a window through which further disruption of intracellular homeostasis can preferentially kill some cancer cells over normal cells. This "chronic stress" condition was recently outlined by Luo, et. al.(1), describing the non-oncogene addiction of many cancers. Stress-response mechanisms, normally serving to help protect cells from insults, are pirated by cancer cells to support their malignant phenotype. For instance, HSF1, the master regulator of the heat shock response (HSR), which responds to proteotoxic stress in particular, has been shown to be required for both genetically and chemically induced tumorigenesis in murine models (2, 3). Likewise, upregulation of Nrf2, master regulator of the oxidative-stress response, by expression of oncogenes such as K-Ras, B-Raf, and Myc was found to play a crucial role in mitigating oncogene-induced oxidative stress and also promoted tumorigenesis (4). Further evidence suggests that Ras-driven cancers may also require high levels of a catabolic process known as autophagy to prevent metabolic stress and maintain energy for continued growth (5). In addition, the prevalence of aneuploidy, or abnormal chromosome number, in solid tumors is thought to be responsible for creating an elevated level of proteotoxic stress (6).

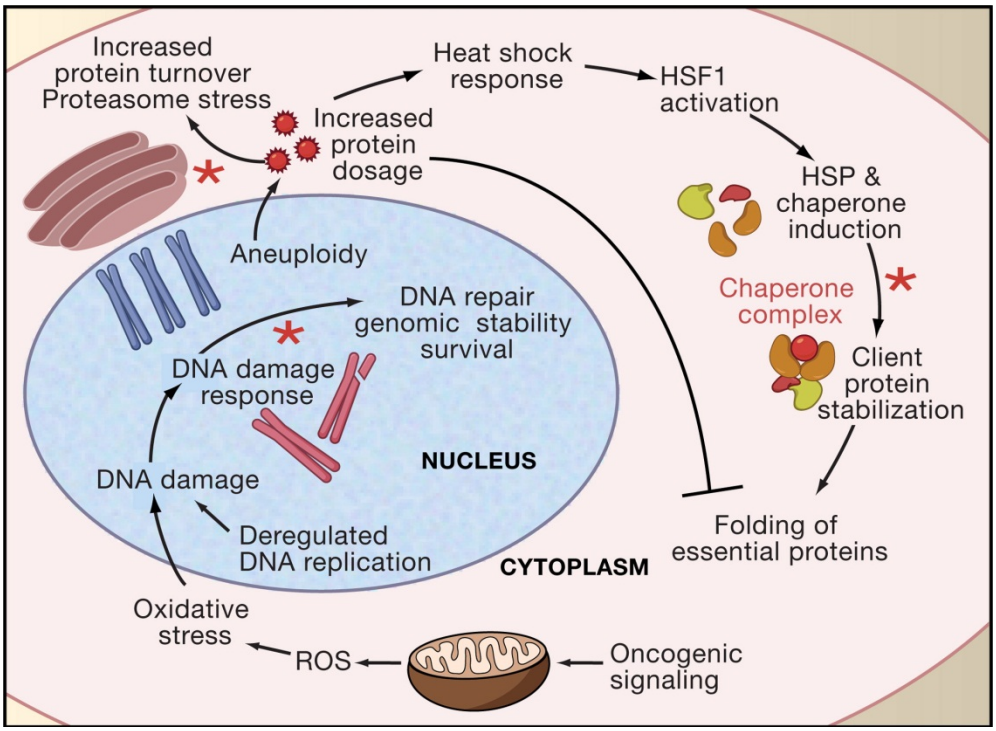

Figure 1.1.Intracellular stresses associated with the malignant phenotype and non-oncogene addiction. Because of the multitude of genetic changes associated with cancer, cancer cells often display heightened dependency on stress response pathways, such as those activated by oxidative stress, DNA damage, and heat shock/proteotoxic stress.

*Reprinted from *Cell*, 130(6), Solimini, NL, Luo, J, Elledge, SJ, Non-oncogene addiction and the stress phenotype of cancer cells, 986-988, Copyright (2007), with permission from Elsevier. Reference # (3).

1.2 Protein quality control and degradation in mammalian cells

Proteins are the primary functional components of a cell, responsible for everything from movement and cell division, to transcription, translation, and DNA repair. In *E. coli*, it has been estimated that intracellular protein concentrations can exceed 300 mg/ml (7), creating an extremely crowded working environment that is likely exacerbated in more complex mammalian cells. Thus, sophisticated quality control mechanisms to ensure proper protein folding and function have evolved, as well as efficient degradation systems to rid the nucleus and cytosol from expired and misfolded proteins. These pathways are increasingly being considered as novel drug targets in cancer as well as other protein folding diseases such as Alzheimer's, Parkinson's, and cystic fibrosis. Here I will discuss the primary protein quality control/folding network, and then discuss the two major degradation pathways for proteins that cannot be rescued.

1.2.1 The chaperone network

Newly synthesized polypeptides interact immediately with molecular chaperones, termed "heat shock proteins (Hsps)" for their discovery as part of a heat-induced stress response (8). Multiple families of heat shock proteins exist within mammalian cells, including the HSPA (Hsp70), HSPC (Hsp90), HSPH (Hsp110), DNAJ (Hsp40), and HSPB (small Hsp) families. Of these, the Hsp90 and Hsp70 families possess distinct functions and represent the major players in the chaperone network. Hsp90 family members primarily function to interact with folded substrates and ensure proper maturation, functionality, and interactions with other proteins. Hsp90 client proteins number in the hundreds, and include numerous oncoproteins such as AKT, HIF1α, MMP2, telomerase, and tyrosine kinases, providing the rationale for development of Hsp90 inhibitors in cancer (9). Conversely,

Hsp70 family members interact with nascent polypeptides immediately as they are being translated to ensure proper folding (10). This folding occurs through an ADP/ATP exchange cycle, and is facilitated by co-chaperones (Hsp40, HOP) and nucleotide exchange factors (Bag1, Hsp110). Hsp70 family chaperones represent some of the most highly conserved proteins in evolution, and are close homologs of the bacterial DnaK chaperone (11). In addition to the involvement of both the constitutively expressed Hsc70 and the inducible Hsp72 chaperones in the protein folding process, they are essential for preventing aggregation and determining the cellular fates of misfolded proteins. The chaperone complex senses misfolding by recognizing exposed hydrophobic residues, and then recruits specific ubiquitin ligases such as CHIP to promote the attachment of ubiquitin to lysine residues on the substrate (12), marking the substrate for degradation by mechanisms discussed in further detail below.

1.2.2 The ubiquitin-proteasome system

The primary protein degradation system in eukaryotic cells consists of the ubiquitin proteasome system (UPS) (Figure 1.2). In this elegant system, a small 7.6-kDa protein known as ubiquitin “marks” proteins for degradation (a process henceforth referred to as ubiquitylation). Ubiquitylation involves a series of enzymatic steps that first begins with ATP-dependent activation, or “charging” of the carboxy-terminus of the ubiquitin molecule by E1 ubiquitin-activating enzymes. The activated ubiquitin is then transferred to an E2 ubiquitin-conjugating enzyme via a thiolester linkage. Finally, the E2 enzyme interacts with an E3 ubiquitin-ligase enzyme that is bound to the substrate, and E3 catalyzes the transfer of the ubiquitin molecule from the E2 to the substrate (in some cases, ubiquitin can also be transferred to the E3 first and then subsequently the substrate). This cycle repeats itself

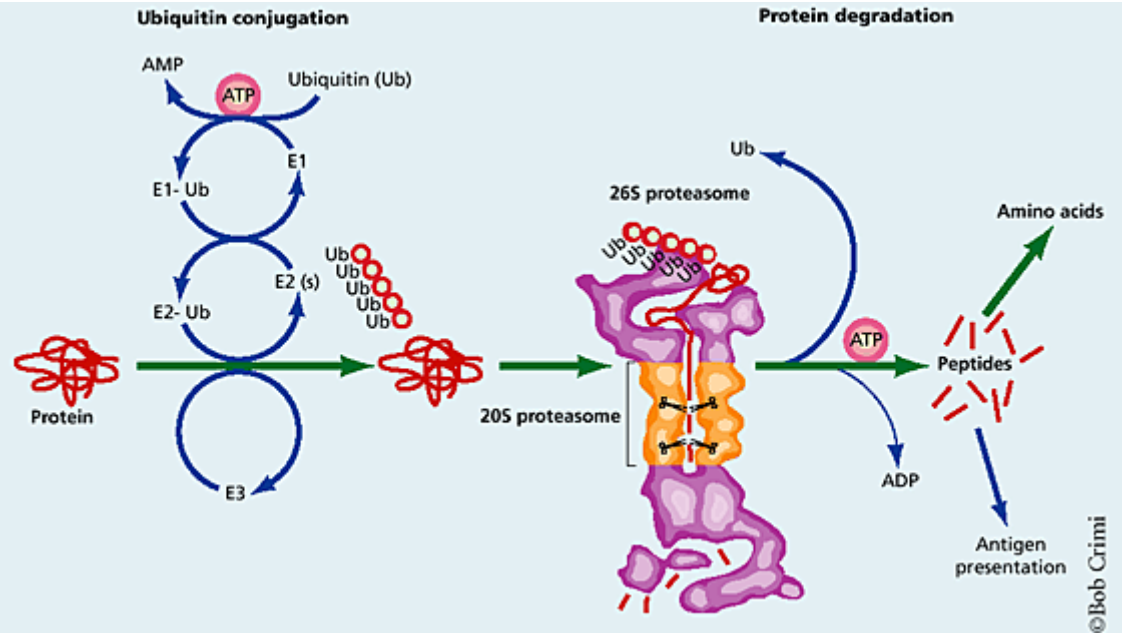

Figure 1.2 The ubiquitin-proteasome pathway. Misfolded proteins are tagged with ubiquitin in an ATP-dependent fashion by a series of enzymatic steps, which then marks the substrate for degradation and recycling to peptide fragments by the 26S proteasome.

multiple times to form a lysine-linked polyubiquitin chain. Several different lysine residues can be used for this linkage, with important functional consequences. Lys48-linked ubiquitin polymers most commonly signal proteasomal degradation, whereas Lys63-linked polymers have been implicated as signals for the aggresome pathway and autophagy (14). Additional ubiquitin polymers have also recently been discovered as markers for proteasomal degradation, such as Lys11. Once a Lys48 or Lys11 polyubiquitin chain has been attached to a substrate, it is recognized and degraded by the proteasome. The proteasome is a barrel-shaped protease that serves as the primary protein degradation machine in eukaryotic cells. Abundant in both the cytosol and nucleus, it consists of a cylindrical 20S core structure interacting with two 19S regulatory "cap" subunits at both ends. Collectively, this structure is referred to as the 26S proteasome. The 19S regulatory subunit is responsible for recognizing polyubiquitinated substrates and facilitates the unwinding and feeding of the substrate into the proteolytic 20S core in an ATP-dependent fashion (15). The proteolytic 20S core contains three different catalytic activities, the chymotryptic, the tryptic, and the caspase-like, which together mediate the cleavage of peptide bonds between any two amino acids.

1.2.3 The autophagy-lysosome system

Whereas the UPS serves as the primary degradation system for individual proteins, there also exists an alternative degradation system for bulk substrates such as organelles or large protein aggregates. These larger structures are degraded via a process known as autophagy, which terminates with the deposit of substrates into acidic, protease filled organelles known as lysosomes. Three distinct forms of autophagy exist: macroautophagy, microautophagy, and chaperone-mediated autophagy (CMA) (16). Macroautophagy

involves the sequestration and degradation of bulk substrates, including organelles and/or protein aggregates, and is often activated in response to starvation as a way to recycle macromolecules for energy (17). Conversely, microautophagy refers to the direct engulfment of the cytosol by invagination of the lysosomal membrane, whereas CMA refers to the transport of individual proteins to lysosomes by molecular chaperones that recognize specific KFERQ-like sequences in substrates (18). Importantly, proteasome inhibitors have been shown to be potent activators of macroautophagy (hereafter referred to as autophagy), and thus this will be the focus of the discussion here (19).

Autophagy begins with the formation of double-membraned vesicles termed autophagosomes, preceded by the recruitment of essential autophagy-related proteins (ATGs) to the phagophore-assembly site (PAS). The autophagosome then engulfs the substrate via a process facilitated by interactions between a core autophagosomal membrane protein, Atg8/LC3, and the autophagy cargo adaptor proteins p62/SQSTM1 and NBR1, which interact directly with ubiquitylated aggregates and present them to the autophagic membranes (20-22). Autophagosomes are then transported along the microtubule network, potentially through interactions with histone deacetylase 6 (HDAC6), to lysosomes for degradation of their contents. Once within the acidic environment of the lysosome, substrates are catabolized and translocated back out into the cytosol by lysosomal membrane permeases (23).

1.3 Proteasome inhibitors

Proteasome inhibitors were initially introduced as useful tools for biologists studying translation and degradation of particular proteins of interest, akin to other cell biology tools such as cycloheximide (a translation inhibitor) and actinomycin D (a transcription inhibitor).

These early inhibitors included peptide aldehydes (MG-132) and vinyl sulfones, as well as natural products such as β-lactones (lactacystin) and epoxyketones (epoxomicin). These inhibitors function in a similar fashion, forming covalent bonds with the catalytic threonine residue in the β5 chymotryptic-like site of the proteasome. These covalent interactions prevent nucleophilic attack on peptide bonds by the catalytic threonine residue, and block substrate cleavage. However, many of these compounds (with the exception of epoxyketones) produce undesirable off-target inhibition of other proteases such as cathepsins and calpains. In the late 1990's, the peptide aldehydes were modified by Julian Adams and colleagues to contain a boronate group, resulting in a novel class of potent, selective, and reversible inhibitors of the proteasome (24). The lead compound identified from these studies, PS-341, later became the first FDA- approved proteasome inhibitor for cancer therapy (specifically in multiple myeloma and mantle cell lymphoma), and is currently referred to as bortezomib, or Velcade® (25). Other PIs have since been developed, including marizomib, also known as salinosporamide A or NPI-0052 (Nereus Pharmaceuticals, Inc.) (26, 27) and carfilzomib or PR-171 (Proteolix, Inc.) (28). These new PIs offer irreversible inhibition of the proteasome and potentially higher systemic levels of sustained proteasome inhibition in patients. Clinical trials across several tumor sites are now ongoing using next generation PIs. In the following text, key cellular responses to proteasome inhibition will be discussed, as well as potential mechanisms mediating their toxicity in cancer cells, with a particular emphasis on bortezomib.

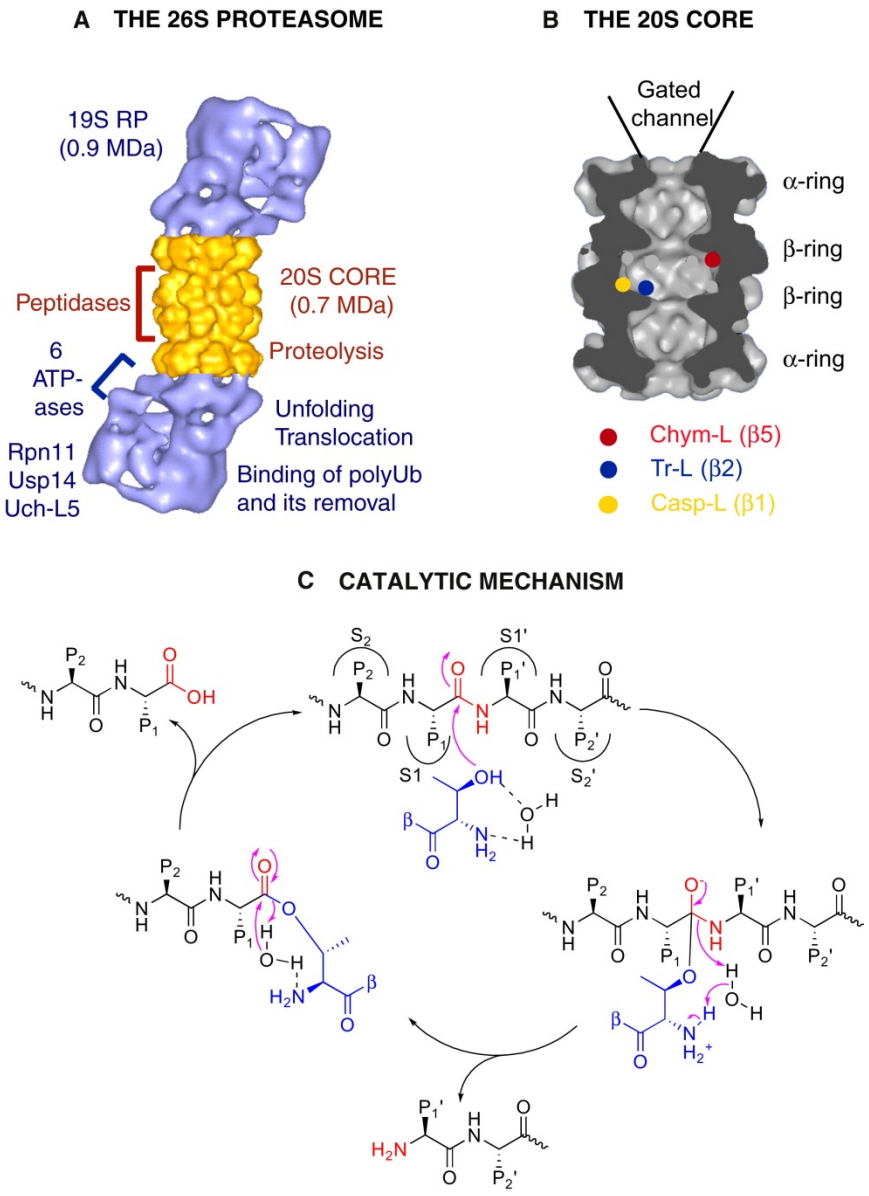

Figure 1.3 The proteasome: structure and mechanism. A) The complete 26S proteasome, B) The 20S core subunit, C) The catalytic mechanism of proteasome-mediated peptide cleavage.

*Reprinted from *Chemistry & Biology*, 19(1), Kisselev, AF, van der Lindin, WA, Overkleeft, HS, Proteasome inhibitors: An expanding army attacking a unique target. Copyright (2012), with permission from Elsevier. Reference #(29)

1.3.1 Cellular responses to proteasome inhibitors

1.3.1a The heat shock response

The heat shock response (HSR) is a highly conserved cytoprotective pathway involving the upregulation of molecular chaperones that is activated by proteotoxic stress in the cytosol. This can be caused by numerous stressors, including heat, heavy metals, arsenicals, viral and bacterial infections, and reactive oxygen species (30, 31). Importantly, numerous studies have demonstrated that proteasome inhibitors are potent inducers of the HSR (32-34). The HSR is regulated in eukaryotes by a family of transcription factors known as heat shock factors (HSFs). In mammalian cells, there exist three different isoforms (HSF1, 2, 4), with HSF1 being the dominant regulator of the stress-induced HSR (35). Under resting conditions, HSF1 exists as an inactive monomer bound by Hsp90 and/or Hsc70 and histone deacetylase 6 (HDAC6), a ubiquitin-binding protein deacetylase, in a repressive complex. Upon proteotoxic stress, misfolded proteins compete away the chaperones and HDAC6, leaving HSF1 free to trimerize and attain transcriptional activity. Activation of HSF1 also involves extensive post-translational modifications, including phosphorylation at multiple serine residues (36), with more recent evidence pointing to roles for acetylation (37) and sumoylation (38) in regulating HSF1 trans-activity. Activated HSF1 binds to specific sequences known as heat shock elements (HSE) in the promoters of target genes and drives transcription, often with the help of co-regulators (39). The target genes of HSF1 include the inducible chaperones of the Hsp70 (HSPA1A/HSPA1B), Hsp40 (DNAJB1), and small Hsp families (Hsp27/HSPB1), which serve to immediately cope with misfolded protein stress. Importantly, inducible Hsp70 and Hsp40 provide a negative feedback loop for “turning off” HSF1; once a sufficient amount of these chaperones are

present to restore proteostasis, they bind directly to HSF1's transactivation domain to attenuate the HSR (35). Although HSF1 is best known for its role in upregulating molecular chaperones, evidence suggests myriad other transcriptional targets (up to 3% of the genome in yeast) (40) and genome-wide acetylation (41), pointing to HSF1 as an extensive remodeler of the genomic landscape during proteotoxic stress.

1.3.1b eIF2α phosphorylation and the integrated stress response (ISR)

Mammalian cells retain tight control of protein synthesis during stress. Biologically, it makes sense to decrease the volume of new proteins being synthesized when facing a stress that is causing a buildup of misfolded proteins, such as proteasome inhibition. The primary mechanism used to control translation rates involves inhibitory phosphorylation of the eIF2 translation initiation factor at the Ser51 residue of its α subunit (42). In its active, unphosphorylated form, eIF2 bound with GTP and the Met-tRNA$_i$ assembles with eIF1, eIF1A, eIF3, eIF4F, and eIF5 to form the 43S pre-initiation complex. The complex scans the 5' cap of the mRNA being translated, and once the start codon is recognized, the eIF2-bound GTP is hydrolyzed to GDP and the initiator Met-tRNA binds to the 40S ribosome to provide the initial amino acid for the polypeptide (42). Inactivated eIF2-GDP is recycled back to its active GTP-bound form by eIF2B, a guanine nucleotide exchange factor (GEF). Upon proteotoxic stress, the α subunit of eIF2 is phosphorylated and directly binds to and inhibits the nucleotide exchange capacity eIF2B, thus dramatically decreasing eIF2-GTP levels and reducing translation rates.

Phosphorylation of eIF2α is mediated by four known stress-activated kinases in mammalian cells: HRI (EIF2AK1), PKR (EIF2AK2), PERK (EIF2AK3), and GCN2 (EIF2AK4). HRI (heme-regulated inhibitor) is best known for regulating protein synthesis in

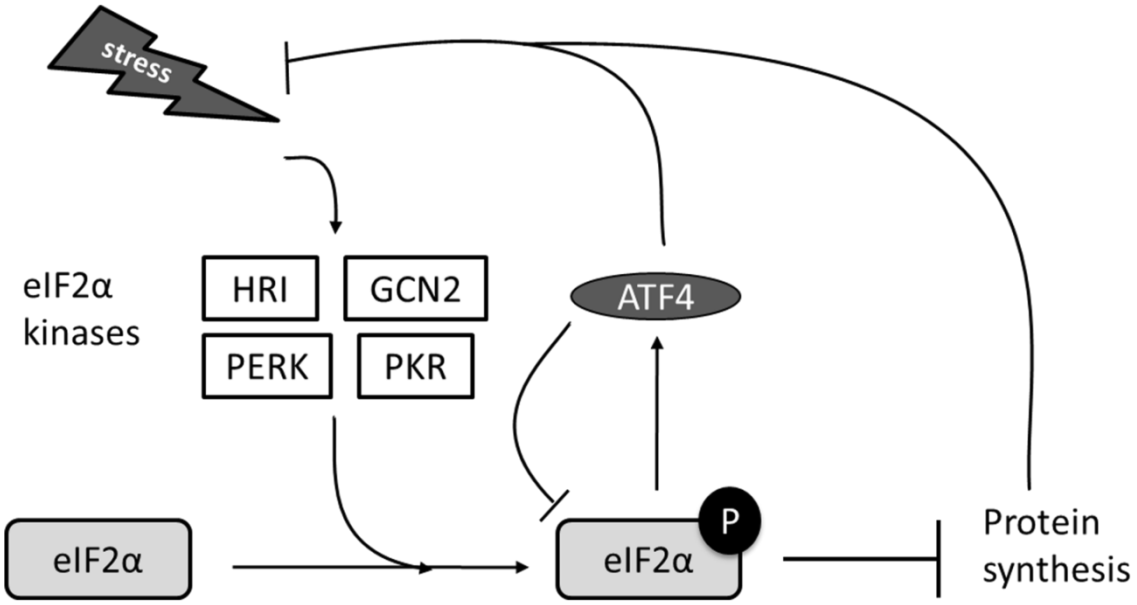

Figure 1.4. Schematic of stress-mediated translational repression by eIF2α phosphorylation. Stress (proteotoxic, viral, nutrient, hypoxic, hypoglycemic) serve to directly activate at least one of four known kinases (HRI, GCN2, PERK, or PKR), which then phosphorylate eIf2α at the Ser51 residue, effectively shutting off cap-dependent translation (protein synthesis). This allows for selective translational upregulation of the ATF4 transcription factor, which coordinates an integrated stress response (ISR) to alleviate stress. Phospho- eIf2α levels are reduced upon alleviation of stress by GADD34, a phosphatase upregulated by ATF4.

*Reprinted from *Advances in Cancer Research*, 116, David J. McConkey, Matthew C. White, Wudan Yan,, Chapter 4 – HDAC inhibitor modulation of proteotoxicity as a therapeutic approach in cancer, 131-163, Copyright (2012), with permission from Elsevier. Reference # (43).

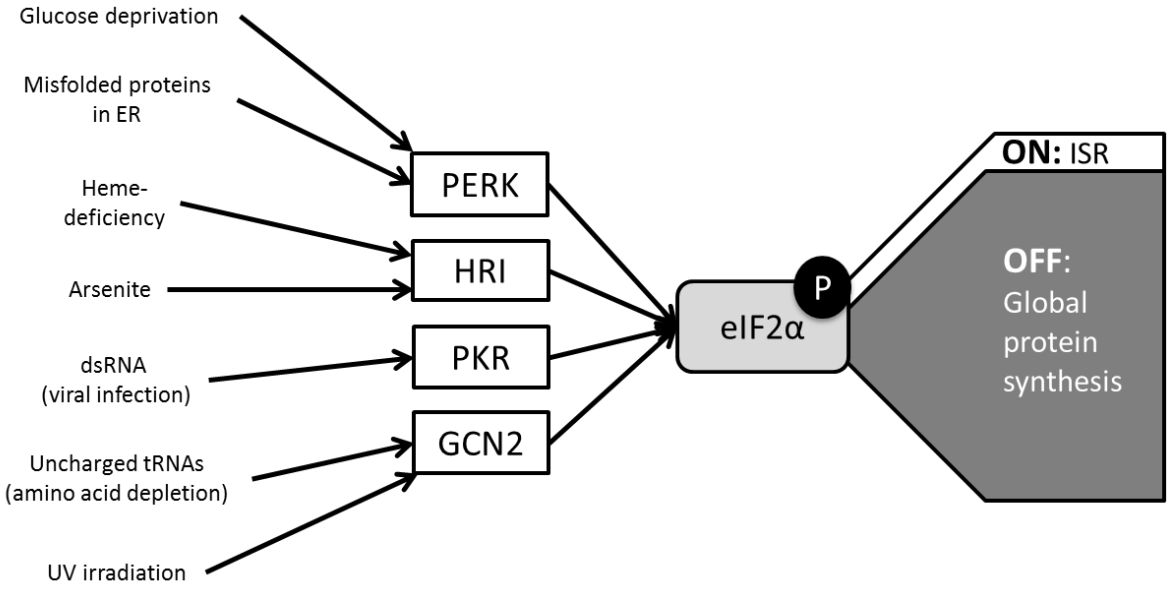

Figure 1.5. Phospho-eIF2α as a key signaling node for sensing multiple different stressors. The eIF2α kinases (HRI, GCN2, PKR, PERK) are evolutionarily optimized to sense a variety of unique upstream stress signals, but each serve to propagate the same downstream signaling event (eIF2α phosphorylation). Conceptually, this points to phospho-eIF2α as a "node" that controls protein synthesis and the integrated stress response (ISR) in response to multiple stressors.

*Reprinted from *Advances in Cancer Research*, 116, David J. McConkey, Matthew C. White, Wudan Yan, Chapter 4 – HDAC inhibitor modulation of proteotoxicity as a therapeutic approach in cancer, 131-163, Copyright (2012), with permission from Elsevier. Reference # (43).

erythroid cells in response to iron deficiencies (44); however, it also has been reported to be activated by a variety of cytosolic stresses, such as arsenic, heat shock, osmotic stress, and importantly, proteasome inhibition (45, 46). Interestingly, HRI appears to exist in a repressive complex with cytosolic chaperones (Hsp70), and can be activated when these chaperones dissociate to bind accumulating misfolded proteins in the cytosol (47, 48). PKR (protein kinase R) contains double-stranded RNA binding motifs, and is directly activated by viral infections as well as interferons (49, 50). PERK (PKR-like endoplasmic reticulum kinase), as its name suggests, functions exclusively in the ER, existing in a repressive complex with the ER chaperone Grp78/BiP until misfolded proteins compete away Grp78 from PERK, leading to PERK autophosphorylation, dimerization, and activation (51). In addition to activation by ER stress, PERK is also activated by glucose deficiency (52). Finally, GCN2 (general control nonderepressible 2) is the most highly conserved of these kinases (from yeast to mammals), and serves as a sensor of nutrient deprivation. GCN2 is activated by amino acid starvation conditions via direct binding of uncharged tRNAs to a histidyl-tRNA synthetase-related sequence (HisRS) near its carboxy terminus.

While the major function of eIF2α phosphorylation is to shut off global protein synthesis, it also works to activate the integrated stress response (ISR) via selective translational upregulation of certain mRNAs, such as activating transcription factor 4 (ATF4). This is accomplished through an elegant mechanism in which reduced amounts of active eIF2-GTP allow the scanning ribosome to bypass an inhibitory upstream open reading frame (uORF2) in the ATF4 mRNA, and resume translation at the ATF4 protein-encoding ORF. This regulatory mechanism resembles that of the yeast GCN4 mRNA and its corresponding protein Gcn4p, which serves to upregulate genes involved in amino acid

biosynthesis. ATF4 plays a similar but much broader role in mammalian cells by regulating expression of numerous stress-response genes involved in amino acid metabolism, protein folding, oxidative stress responses, autophagy, and cell death (53, 54). Once the cellular stress is resolved, ATF4 also serves to upregulate part of a negative feedback loop involving GADD34, a protein phosphatase that dephosphorylates eIF2α and attenuates the ISR, Evidence also suggests that under certain conditions, eIF2α phosphorylation can propagate cell death through a terminal unfolded protein response (55, 56). A well-known target of the ATF4 transcription factor that is translationally upregulated by eIF2α phosphorylation is the CHOP/DDIT3/GADD153 transcription factor (hereafter referred to as CHOP). Induction of CHOP gene expression is thought to promote apoptosis; studies suggest that this may occur through transcriptional binding and upregulation of BIM protein promoter regions (57), or through inhibition of Bcl-2 expression. CHOP expression is tightly linked to eIF2α phosphorylation, as mutant MEFs expressing a knock-in serine to alanine mutation in eIF2α that prevents phosphorylation fail to induce CHOP expression following ER stress (58). However, despite the absence of CHOP expression, these mutant cells display heightened sensitivity to ER stress, suggesting that CHOP is not required for stress-induced apoptosis, and that it may have other important functions that have not been revealed (59).

1.3.1c Endoplasmic Reticulum (ER) Stress and Unfolded Protein Response (UPR)

The endoplasmic reticulum (ER) is responsible for folding of secretory and membrane proteins. The ER lumen is uniquely tuned for high-capacity protein folding as an oxidative environment, also containing high levels of calcium (Ca^{2+}) and molecular chaperones. ER-specific homologs of cytosolic Hsp70 and Hsp90 proteins, Grp78/BiP and Grp94, interact with substrates in the lumen to promote proper folding. A multitude of other

ER-specific chaperones and folding cofactors are also present: Erdj1-5 (Hsp40 homologs) stimulate Grp78 ATP:ADP exchange, calnexin and calreticulin function as lectin chaperones for glycans, and protein disulfide isomoerases (PDIs) promote disulfide bond formation. In addition to folding, proteins undergo extensive post-translational modifications in the ER, such as N-linked glycosylation, carboxylation and hydroxylation of amino acids, and attachment of glycosylphosphatidylinositol. Proteins that are unsuccessfully folded are transported out of the ER for degradation by the proteasome through the Sec61 pore complex via a process called ER-associated degradation (ERAD). Perturbations in the folding milieu of the ER lumen are specifically referred to as ER stress and can arise from many different cellular insults, such as oxidative stress, low glucose, depletion of luminal Ca^{2+} stores, and inhibition of the 26S proteasome. Several compounds are known inducers of ER stress: thapsigargin (TG) blocks the sarcoplasmic reticulum Ca^{2+} ATPase and results in release of ER calcium stores (60), tunicamycin (TM) prevents the first step of protein glycosylation within the ER (61), and dithiothreitol (DTT) reduces disulfide bonds within the oxidative ER lumen. ER stress is directly sensed by ER chaperones, primarily Grp78, as the concentration of misfolded proteins rises. The exposed hydrophobic residues of the misfolded substrates competitively inhibit Grp78 binding of three ER transmembrane signaling proteins. Once released from Grp78, these proteins become activated via autophosphorylation and propagate an elaborate downstream stress response known collectively as the unfolded protein response, or UPR. The three arms of the UPR signaling apparatus are IRE1, ATF6, and PERK. IRE1 is a transmembrane kinase that is also an endonuclease. Upon dimerization and autophosphorylation, IRE1 directly splices the mRNA

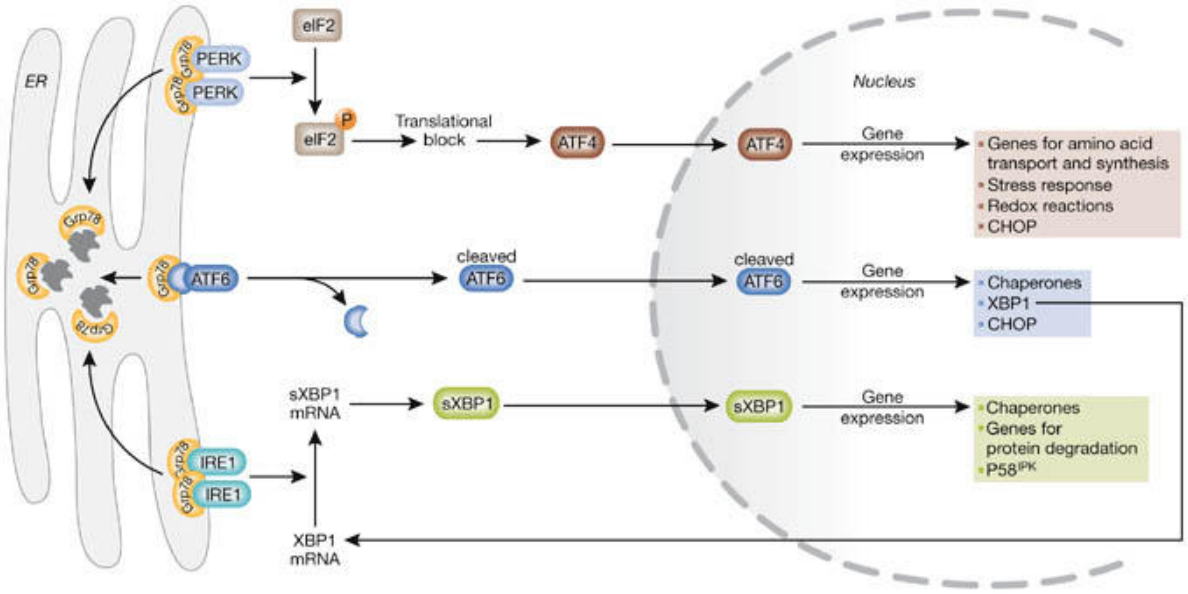

Figure 1.6 The unfolded protein response (UPR). The accumulation of unfolded proteins in the ER activates a three-armed signaling cascade, orchestrated by ATF6, PERK, and IRE1, that seeks to restore ER homeostasis.

*Reprinted by permission from Macmillan Publishers Ltd: [EMBO reports], (62), copyright (2006).

of a key UPR-specific transcription factor known as XBP1, thereby activating XBP1 and promoting upregulation of multiple ERAD and ER chaperone genes (Figure 1.3). ATF6 is a transcription factor that upon release from Grp78, gets processed into its active form in the Golgi apparatus, then translocates to the nucleus where it also upregulates ER chaperones as well as the transcription factor CHOP, which may promote apoptosis if the stress is unresolved. PERK is a transmembrane kinase that upon Grp78 release forms homodimers and undergoes autophosphorylation and activation. Activated PERK phosphorylates the cytosolic eukaryotic initiation factor 2 on its α-subunit (eIF2α), which serves to halt global protein synthesis and translationally upregulate the ATF4 transcription factor. ATF4 serves as a master regulator of the integrated stress response (ISR) (53) by inducing expression of genes involved in promoting ER homeostasis, ERAD, and amino acid and antioxidant stress responses. ATF4 also upregulates CHOP, which, in addition to its known pro-apoptotic functions, also induces expression of the GADD34 phosphatase cofactor that recruits the PP1 phosphatase complex to eIF2α to attenuate phosphorylation and restore protein synthesis (63).

1.3.1d Aggresomes and Autophagy

Under conditions of extreme proteotoxic stress, such as proteasome inhibition where the cell's primary protein degradation system is compromised, or accumulation/ overexpression of mutant aggregate-prone proteins (e.g. CFTR, mutant Huntington), additional degradation routes must be exploited. Thus, the autophagy-lysosomal system (ALS) is activated in as an alternative mechanism (see Section 1.2.3c). Because the ALS functionally differs from the ubiquitin-proteasome system (UPS) in that it targets larger bulk substrates as opposed to specific individual proteins, accumulating misfolded proteins

coalesce to the microtubule-organizing center (MTOC) to form large aggregates termed "aggresomes" that are thought to be novel substrates for autophagy (64). Aggresome formation is not random, but rather is an active, multi-stepped process that represents an important part of the cytoprotective response to PIs. In the early stages of the aggresome pathway, misfolded ubiquitin-tagged proteins that cannot be degraded by the proteasome begin to form small aggregates or aggresomal particles through interactions with exposed hydrophobic residues. These smaller aggregates are bound by a unique protein deacetylase known as HDAC6 (histone deacetylase 6 – see Chp. 5) capable of binding both ubiquitin and dynein motors (65). Evidence suggests that the type of polyubiquitin chain, either Lys^{48} or Lys^{63} –linked (K48 and K63, respectively), may be important for HDAC6 recognition and recruitment to aggresomes. K48-linked chains are traditionally associated with proteasomal degradation because they are more efficiently degraded by proteasomes (66), whereas K63-linked chains appear to be preferentially recognized by HDAC6 and p62/SQSTM1(p62) and facilitate degradation by the aggresome-autophagy pathway (67, 68). These minus-end-directed dynein motors transport HDAC6 and its bound ubiquitylated substrates along the microtubule network from multiple cytosolic locations to a centralized perinuclear region near the MTOC (64). It is hypothesized that aggresomes form around the MTOC because the peri-centriolar region is enriched in 20S proteasomes, proteasomal activators, and molecular chaperones (69, 70). However, clearance of aggresomes formed without the use of PIs is only partially inhibited upon the addition of PIs, suggesting that the major route of aggresomal clearance is proteasome-independent, regardless of how the aggresome was formed. Accordingly, we found that in some solid tumor cells, aggresomes were only seen upon dual inhibition of both autophagy and the proteasome (71). In addition, p62/SQSTM1,

a ubiquitin-binding cargo-adaptor protein that interacts directly with Atg8/LC3 on autophagosome membranes and facilitates autophagic degradation of aggregates, co-localizes to aggresomes (72, 73). Overall, the data suggest that aggresomes are a unique bulk substrate for the ALS.

1.3.2 Mechanisms of anti-tumor activity

Because of the myriad intracellular consequences of proteasome inhibition, it has been difficult to conclusively determine how PIs kill cancer cells. Here, we discuss several of the most promising hypotheses. In a broad sense, much of the original rationale for investigating proteasome inhibitors as anti-cancer agents stemmed from knowledge of the proteasome's central role coordinating the cell cycle and mitosis through degradation of cell cycle regulators (24). In addition to cell cycle regulation, the proteasome was also found to control the activity of NFκB, a pro-survival transcription factor associated with inflammatory stimuli and thought to promote the viability of cancer cells (74). The proteasome controls NFκB activity through degradation of an endogenous inhibitor of NFκB known as IκBα, which when bound to NFκB, prevents translocation into the nucleus and blocks transcriptional activity (75). However, upon phosphorylation by IKK, IκBα is ubiquitylated and degraded by the proteasome, thus activating NFκB. NFκB is activated at high levels in MM and pancreatic cancer, and is known to prevent apoptosis (76, 77). This provided enthusiasm and rationale for the use of PIs as NFκB inhibitors in cancer; however, later studies using selective inhibitors of the IKK kinase (PS-1145) proved that direct inhibition of NFκB was much less cytotoxic than bortezomib (76, 78), suggesting that PI-induced cell-killing was not driven by NFκB inhibition.

The proteasome is also essential for controlling levels of proteins associated with apoptosis, another potential explanation for the anti-tumor effects of PIs. For example, bortezomib stabilizes the pro-apoptotic BH3-only protein Bim, and this was found to be required for reversal of paclitaxel resistance by bortezomib (79). In colon, lung, and ovarian carcinomas, bortezomib was found to promote accumulation of another BH3-only protein Bik, but not other members of the BCL-2 family (Bak, Bax, Bcl-XL, Bcl-2), and increased levels of Bik correlated with sensitivity to bortezomib (80). Perhaps the most consistent effect of PIs on pro-apoptotic BH3-only proteins is the induction of Noxa expression both at the mRNA and protein levels. High-doses of PS-341 (now bortezomib) were shown to cause Noxa-dependent cell death in squamous cell carcinoma. In this study, the authors also found that Noxa upregulation appeared to be dependent on eIF2α phosphorylation and the UPR (81). Similar results were also found in melanoma and myeloma cells, where the PIs MG-132, lactacystin, and bortezomib all increased Noxa transcript and protein levels, and siRNA-mediated knockdown of Noxa significantly reduced cell death in response to all three agents (82).

As previously discussed, the proteasome is the backbone of intracellular protein degradation. More compelling, perhaps, than the stabilization/accumulation of individual proteins are the effects of PIs on proteins *en masse*. In broad terms, inhibition of the proteasome immediately blocks the route of choice for misfolded and expired proteins, for which removal is a significant task for the cell (new synthesis alone is estimated to be ~30% defective) (83, 84). Thus, perhaps the strongest hypothesis for PI-induced toxicity suggests that the buildup of misfolded and aggregating proteins is the toxic event that kill cells. Evidence from MM supports this concept of PI-induced proteotoxicity. Obeng, et. al.

demonstrated that PIs caused a “terminal” UPR in MM cells that seemed to correlate with high amounts of immunoglobulin (IgG) retention (55). Furthermore, Meister, et. al. used an elegant model system in which subclones of MM cells were manipulated to either express low or high levels of IgG, and found that increased IgG production sensitized the subclones to bortezomib (85). Indeed, the physiologic role of normal plasma cells (antibody production) requires an extensive ER-Golgi network, and MM cells usually retain this “hard-wiring” for protein production and secretion. Overall, the robust clinical activity of bortezomib (clinically Velcade®) in MM supports the idea that proteotoxic stress dictates the anti-tumor activity of PIs. Our data discussed in Chapter 3 with respect to eIF2α-P and protein aggregation also provide strong evidence in support of this mechanism of action for PIs.

Recently, another intriguing explanation for PI-induced cell death was outlined (86). Here, Suraweera, et al. proposed that PIs severely deplete amino acid pools, which elicits a GCN2- eIF2α-P- mediated stress response culminating in CHOP production and ultimately cell death. By supplementing cells with cysteine and/or asparagine/aspartate, they were able to rescue cells from bortezomib-induced death. However, cysteine is a known anti-oxidant, which could be an alternative explanation for its protective capabilities (see Chapter 3 for data/discussion on the role of ROS production in PI-induced cell death). Because the proteasome generates a significant amount of free amino acids through the recycling of peptides (15), this is an attractive hypothesis that bears further exploration. Indeed, the proteasomal generation of amino acids was found to be required for protein synthesis under conditions of nutrient restriction in HeLa cells (87). It is therefore conceivable that blocking the proteasome perturbs the free amino acid pool to an extent that activates GCN2,

especially in cancer cells which often have higher rates of protein synthesis than normal cells (88).

1.4 Summary and scope of dissertation

In this dissertation, I seek to better understand how molecular heterogeneity among cancer cells influences response to the proteasome inhibitor bortezomib. Here, I present three separate but related research projects evaluating different components of the PI-induced stress response and determining each of their respective contributions to cancer cell survival. First, in Chapter 3, I highlight the central role of HRI activation and eIF2α-P in protecting pancreatic cancer cells from BZ-induced cell death. This represents the first such study evaluating heterogeneous eIF2α-P in solid tumor cells, and the first to suggest that this correlates with BZ sensitivity. In Chapter 4, I demonstrate that Hsp72 induction protects bladder cancer cells from BZ, and for the first time outline that heterogeneity exists among bladder cancer cells in both basal and inducible Hsp72 expression that is associated with Hsp72 (HSPA1A) promoter methylation. Finally, in Chapter 5, I evaluated a novel HDAC6-selective inhibitor in pancreatic and bladder cancer cells through a series of *in vitro* tests, demonstrating inhibitor specificity at low micro-molar doses as well as investigating its potential for combination therapy with BZ.

In multiple myeloma, where PIs are frontline therapy, response rates to Velcade® are only ~35-40% (89), meaning that roughly 60% of patients do not respond. Lymphomas (mantle cell lymphomas, indolent non-Hodgkin's, refractory B-cell non-Hodgkin's) typically show response rates up to 45-60% (90, 91). In solid tumors, less impressive response rates have been seen thus far (92), with non-small cell lung cancer (NSCLC) responding at around 8% (93), with minimal responses in melanoma (94), recurrent glioma

(95), and metastatic breast cancer (96). As such, there is much need for a better understanding of how molecular heterogeneity among tumor cells can influence response to PIs, and this dissertation seeks to make a valuable contribution towards this aim.

Chapter 2. MATERIALS AND METHODS

2.1 Materials and Methods for Chapter 3

2.1.1 Cell lines and culture - HPDE immortalized pancreatic ductal epithelial cells were a gift from Dr. Craig Logsdon (Department of Cancer Biology, U.T. M.D. Anderson Cancer Center). BxPC3, Panc1, HS766t, MiaPaCA-2, and CF-Pac1 pancreatic cancer cells were obtained from ATCC (American Type Culture Collection, Manassas, VA). Suit2, SU86.86, and T3M4 pancreatic cancer cells were obtained from Eric Collisson (UCSF). mPanc96 pancreatic cancer cells are a genetically identical but phenotypically distinct variant of AsPC1 cells. The identities of all of the human cell lines were validated by DNA fingerprinting, performed in the MD Anderson Characterized Cancer Cell Line Core. All pancreatic cancer cells (except for BxPC3) were maintained in DMEM supplemented with 10% fetal bovine serum (HyClone/Thermo Scientific, Waltham, MA), MEM vitamins, sodium pyruvate (Mediatech/Corning Cellgro, Manassas, VA), L-glutamine, non-essential amino acids, Penicillin/Streptomycin (Lonza, Switzerland), and HEPES. BxPC3 cells were cultured in RPMI-1640 supplemented with 10% fetal bovine serum (HyClone/ Thermo Scientific), MEM vitamins, L-glutamine, sodium pyruvate, non-essential amino acids, Penicillin/Streptomycin, and HEPES. HPDE cells were maintained in serum-free keratinocyte media supplemented with EGF and BPE (Gibco/Life Technologies, Grand Island, NY). Wild-type eIF2α^{51SS} and eIF2α^{51AA} knock-in mutant MEFs were obtained from Dr. David Ron (NYU/ University of Cambridge) and grown as described previously (71). All cells were grown in a humidified incubator at 37° C under an atmosphere of 5% CO_2 in air.

2.1.2 Chemicals and antibodies - Bortezomib was purchased from ChemieTek (Indianapolis, IN). Thapsigargin, cycloheximide, and propidium iodide (PI) and *N*-acetyl-L-cysteine (NAC) were purchased from Sigma-Aldrich (St. Louis, MO). Antibodies were purchased from the following sources: phospho-eIF2α, GCN2, PERK and lamin A/C (Cell Signaling Technology, Beverly, MA), eIF2α, (Invitrogen/Life Technologies, Grand Island, NY), HRI and ubiquitin (Santa Cruz Biotechnology, Santa Cruz, CA), phospho-GCN2 (Abcam, Cambridge, MA), LC3 (MBL International, Woburn, MA), β-actin (Sigma-Aldrich), and anti-mouse/ anti-rabbit HRP-labeled secondary antibodies (Promega, Madison, WI).

2.1.3 Immunoblotting – Cells (~70% confluency) were collected via scraping on ice, and lysed by vigorous vortexing using a 1% NP-40 buffer containing 50mM Tris-HCl (pH 7.4), 150mM NaCl, 5mM EDTA, 0.1% Triton X-100, 25mM NaF, 100mM Na_3OV_4, 10mM glycerophosphate, 10mM PMSF, and complete protease inhibitors. Lysates were clarified by centrifugation and then protein concentrations were quantified using a commercial Bradford assay (Bio-Rad, Hercules, CA). Equal amounts of protein (15-20μg) were separated by 6-10% SDS-PAGE and transferred to nitrocellulose membranes. Membranes were blocked with either 5% bovine serum albumin (BSA) or 5% nonfat dried milk dissolved in TBS-T, then probed overnight in the same solutions with primary antibodies. Membranes were then washed and incubated with species-specific horseradish peroxidase-labeled secondary antibodies. Immunoblots were developed by chemiluminescence (GE Healthcare Life Sciences, Piscataway, NJ), and densitometry was performed using ImageJ.

2.1.4 Measurement of cell viability - Cells were plated in 6-well plates and allowed to attach overnight. Cells (~40-60% confluency) were then exposed to drugs for 48 hours and collected by trypsinization. Cell pellets were washed once in PBS and then resuspended in

0.5mL of fresh PBS. Propidium-iodide (PI) solution (100μg/mL) was added in a 1:10 dilution immediately prior to analyzing the samples. PI–positive (non-viable) cells were measured by FACS (fluorescence activated cell sorting) analysis on the FL3 channel of a Beckman Coulter FC500 flow cytometer.

2.1.5 ^{3}H-leucine incorporation assays – Equal numbers of cells were plated in 6-well plates (~2-3 x 10^5 cells/well) and allowed to attach overnight. Cells were exposed to bortezomib (30nM) or cycloheximide (20μM) as indicated. Following incubation, drugs were removed and cells were pulsed for 1-2 hours with 1 μCi/mL L-[4,5- ^{3}H(N)] leucine (Perkin-Elmer, Waltham, MA) in leucine-free media (MP Biomedicals, Solon, OH) supplemented with 10% dialyzed FBS, vitamins, L-glutamine, antibiotics, and HEPES. Cells were trypsinized and pellets lysed in a 1% Triton X-100 buffer containing 25mM Tris-HCl, 300mM NaCl, and 10mM PMSF plus complete protease inhibitors by rotation for 20-30 minutes at 4˚ C. Lysates were clarified via centrifugation and proteins were precipitated overnight at 4˚ C in 5% trichloroacetic acid (TCA). The resulting precipitates were collected via centrifugation and dissolved in 0.1% KOH. Samples were aliquoted in triplicate and combined with scintillation fluid (ThermoFisher Scientific, Waltham, MA). CPMs were measured by a Beckman Coulter LS6500 scintillation counter.

2.1.6 Leucine deprivation – Following overnight attachment, complete DMEM was removed from cells and cells were washed 1x in PBS. Leucine-free media (see above) was added for 2 hours prior to harvesting.

2.1.7 Quantitative real-time PCR – Cells were harvested at ~70% confluency and total RNA was isolated using the *mir*VANA miRNA isolation kit (Ambion/ Life Technologies, Grand

Island, NY). Final RNA isolates were checked for quality and concentration using a NanoDrop ND-1000 spectrophotometer (NanoDrop/ThermoFisher Scientific). Specific primers for GRP78, CHOP, and HSPA1A (Applied Biosystems/Life Technologies) were amplified by Taqman-based one-step real-time PCR (Ambion/Life Technologies; ABI 7900HT Fast Real-Time PCR System).

2.1.8 Immunofluorescence - Cells were plated on either 4-well (50,000 cells/well) or 8-well (20,000 cells/well) chamber slides and allowed to attach overnight. Following drug exposure, cells were fixed and permeabilized with either acetone or 4% paraformaldehyde and 100μg/mL digitonin. Slides were blocked in 5% horse serum and 1% goat serum and then the primary antibody was added overnight. Fluorescent secondary antibodies, Cy3 or DyLight 549 anti-mouse (Jackson Immunoresearch Labs, West Grove, PA) were added for 1 hour at room temperature. Nuclei were counterstained with a 1:10,000 dilution of Sytox Green and coverslips mounted using propyl gallate. Cells were imaged using a Zeiss Axioplan 2 fluorescent microscope mounted with a Hamamatsu ORCA-ER camera.

2.1.9 Detergent-insoluble protein aggregates assay - Cells (50-70% confluency) were exposed to bortezomib for 24 hours and collected via scraping on ice. Cells were lysed by gentle rotation for 15 minutes at 4°C in the 1% Triton X-100 buffer described previously. Detergent-soluble and -insoluble fractions were isolated by centrifugation at maximum speed (16,000x *g*) for 15 minutes. The resulting supernatants were saved as the detergent-soluble fraction, while the resulting pellets were resuspended in a 6M urea-containing sample buffer by sonication for 15 seconds and saved as the detergent-insoluble fractions. Proteins were resolved by 10% SDS-PAGE and membranes probed with an anti-ubiquitin antibody. Densitometry was performed using ImageJ.

2.1.10 Measurement of reactive oxygen species (ROS) – Cells (50-70% confluency) were plated in 6-well plates and allowed to attach overnight. Where indicated, 10 mM NAC was added 1 hour prior to bortezomib exposure. Cells were then exposed to bortezomib for 18 hours. One hour prior to harvesting, 1μM of the redox-sensitive dye 2',7'-dichlorodihydro-fluorescein diacetate (H_2DCFDA) (Invitrogen/Life Technologies, Grand Island, NY) was added to each well. Cells were then collected by trypsinization and washed 1x in cold PBS. H_2DCFDA fluorescence was measured on the FL1 channel of a Beckman Coulter FC500 cytometer. Histograms overlays were generated using FlowJo software (Tree Star, Inc., Ashland, OR).

2.1.11 siRNA-mediated gene silencing assays - Cells were transfected with ON-TARGETplus SMARTpool siRNAs specific for GCN2, HRI, PERK, or PKR, or a non-targeting control (Dharmacon RNAi Technologies/Thermo Scientific). All targets were silenced via the reverse-transfection protocol included with the RNAiMAX transfection reagent (Invitrogen/ Life Technologies) for 72 hours before exposing cells to drug. Target-specific knockdown was verified by quantitative RT-PCR.

2.1.12 Statistics – Statistical analyses were performed using Student's *t* test functions from GraphPad Prism 5 software and Microsoft Excel. P-values of < 0.05 were considered statistically significant.

2.2 Materials and Methods for Chapter 4

2.2.1 Cell lines and reagents: Bladder cancer cell lines were obtained from the MD Anderson Bladder Cancer SPORE Cell Line Repository and maintained in MEM

supplemented with 10% fetal bovine serum (FBS) (Omega Scientific, Tarzana, CA). The authenticity of all of the cell lines was confirmed at deposit by DNA fingerprinting, and their identities were routinely confirmed during experimentation in the MD Anderson Characterized Cell Line Core (97). Bortezomib was purchased from ChemieTek (IN, USA). For *in vitro* experiments, bortezomib was dissolved in DMSO at a stock concentration of 10 mM, sterilized by filtration through a 0.22 µm syringe filter, with aliquots stored at -20°C until use. Prior to use, the stock was diluted in medium to the desired concentrations. For injection of mice, bortezomib was dissolved in saline containing 10 mg/mL mannitol just before treatment.

2.2.2 Cell viability assays: Cells were exposed to bortezomib, collected at the indicated time points by trypsinization, and resuspended in 500 µl PBS. Fifty µl PBS, pH 7.4, containing 100 µg/ml propidium iodide (PI) was added to the resuspended cells, and PI uptake (indicative of cell death) was analyzed immediately by flow cytometry (FACS) on a Cytomics FC 500 with CXP Software (Beckman Coulter, Inc., Fullerton, CA. For trypan blue exclusion, cells were collected by trypsinization, stained with 0.4% trypan blue (Invitrogen), and cells were counted using a hemocytometer. The experiment was conducted in triplicate.

2.2.3 Microarray analyses: Microarray experiments were performed as described previously (98) with minor modifications. RNA was isolated from cells using the TRIzol Reagent (Invitrogen), followed by cleanup with RNeasy Mini kits (Qiagen). RNA was used for the synthesis of biotin-labeled cRNA, which was prepared using the Illumina RNA amplification kit (Ambion, Inc.), and then hybridized to Illumina Human-HT12 (Illumina, Inc.) chips. Washed chips were scanned with BeadStation 500x (Illumina) and the signal

intensities quantified with BeadStudio (Illumina). The heatmap was made using Cluster 3.0 and Java Treeview from Eisen lab (http://www.eisenlab.org/eisen/).

2.2.4 mRNA extraction, reverse transcription and quantitative real-time PCR: mRNA extraction and reverse transcription were performed as described previously (99). RNA was isolated from cells using the TRIzol Reagent (Invitrogen), and cDNA synthesis was performed using SuperScript III First-Strand Synthesis System for RT–PCR (Invitrogen). Real-time PCR for HSPA1A, HSPA8, HSPB1, DNAJB1, and glyceraldehyde-3-phosphate dehydrogenase (GAPDH) was performed using a StepOne real-time PCR system (Applied Biosystems). The TaqMan primer sets for HSPA1A (Hs00359163_s1), HSPA1B (Hs00271244_s1), pan-HSPA1A & HSPA1B (Hs00271229_s1)HSPA8 (Hs03045200_g1), HSPB1 (Hs03044127_g1), DNAJB1 (Hs00428680_m1), and for GAPDH (4333764F) were purchased from Applied Biosystems. The amplification protocol consisted of one cycle at 50°C for 2 min, one cycle at 95°C for 10 min, followed by 40 cycles at 95°C for 15 s and 60°C for 60 s, and transcript levels were quantified using the comparative C_T method. The resulting data were analyzed with StepOne software and expressed as the mean of ratios (relative expression to control) ± SE, and GAPDH served as the internal loading control.

2.2.5 Treatment of cells with 5-aza-2'-deoxycytidine (5-AzdC): Cells were plated at low density (~$5x10^4$ cells/well) in 6-well plates and allowed to attach overnight. Cells were then exposed to 5μM 5-AzdC dissolved in 50% acetic acid for 5 days. Bortezomib (30nM) was then added to appropriate wells 6 hours prior to harvesting on day 5, and then cells were collected for RNA isolation.

2.2.6 DNA Methylation Analysis: Genomic DNA was isolated using a genomic DNA isolation kit (Qiagen). DNA (1 μg) was converted with sodium bisulfite using the EpiTect Bisulfite Kit (Qiagen) according to the manufacturer's instructions. The bisulfite-modified DNA was then subjected to methylation-specific PCR (MSP). The primers used for MSP were designed using Methprimer. The primer set for converted methylated DNA was 5'-TGTTTTTTTTATTCGGATTAGTTAAC-3' (forward) and 5'-CCACCTACTCGCTAAAACTACGTA-3' (reverse); The primer set for converted unmethylated DNA was 5'- TTTTTTTTATTTGGATTAGTTAATGT -3' (forward) and 5'-CCCACCTACTCACTAAAACTACATA -3' (reverse). The PCR protocol included an initial incubation at 95 °C for 10 min, followed by 35 cycles of 95 °C for 30 s, 49 °C for 30 s and 72 °C for 40 s, followed by one cycle of 72 °C for 10 min. MSP PCR products were separated on 2% agarose gels and visualized by ethidium bromide staining. Fully methylated control DNA and unmethylated control DNA were used as controls.

2.2.7 Immunoblotting: Cells were harvested by trypsinization and lysed in buffer containing 20 mM Tris-HCl (pH 7.5),150 mM NaCl,1 mM Na_2EDTA,1 mM EGTA, 1% Triton, 2.5 mM sodium pyrophosphate, 1 mM beta-glycerophosphate, 1 mM Na_3VO4, 1 μg/ml leupeptin and 1mM PMSF. Whole-cell extracts (20 μg total protein) were subjected to sodium dodecyl sulfate-10% polyacrylamide gel electrophoresis (SDS-PAGE) and transferred to nitrocellulose membranes (Bio-Rad, Hercules, CA). Membranes were probed first with either a monoclonal antibody specific for the Hsp72 (SPA-810, Stressgen) or human beta-actin (Sigma, St. Louis, Mo.), and then with appropriate horseradish peroxidase-

conjugated second antibodies (Santa Cruz). Immunodetection was performed using ECL (Amersham, Piscataway, N.J.) according to manufacturer's instructions.

2.2.8 Chromatin Immunoprecipitation: Chromatin Immunoprecipitation (ChIP) was performed with the ChIP-IT™ Express Enzymatic kit, and ChIP-IT™ Control Kit (Active Motif) according to the manufacturer's protocol. Control and bortezomib-treated 253JB-V and UM-UC13 cells (1.5×10^7 each) were fixed for 8 minutes at room temperature and sheared by enzymatic digestion for 10 minutes. The sheared chromatin yielded bands between 200-1500 bp as visualized by agarose gel electrophoresis. DNA bound to HSF1 was precipitated with an anti-HSF1 antibody (Stressgen, SPA901). To amplify the HSF1-bound HSPA1A promoter, the precipitated DNA was subjected to real-time PCR using the TaqMan® Gene Expression Master Mix with Custom TaqMan® Gene Expression Assay primers (ABI) corresponding to the HSF-1-binding region of the HSPA1A promoter (-10 to -180) (100, 101). Real-time PCR was performed using ABI StepOne with following conditions: 5 minutes at 50°C; 10 minutes at 95°C; then 40 cycles of 95°C for 15 seconds, 60°C for 60 seconds. The data presented represent results from three separate ChIP experiments and were normalized to reactions performed with 1% of input. End-point PCR reactions were also performed as described previously (37) to confirm the real-time PCR results. Normal IgG antibody was used as a control.

2.2.9 Molecular modulation of HSPA1A gene expression: The lentiviral pLKO.1-based constructs TRCN0000008762 and TRCN0000008757 specifically targeting the Hsp72 gene were purchased from Open Biosystems, Inc. The empty pLKO.1 vector was used as a

control. Recombinant viruses were produced by calcium phosphate transfection of HEK293T cells using standard protocols. At day 2–3 post-culture, 253J BV cells were incubated with shRNAs and polybrene (6 µg/ml) for 16~24 hours, and the transduced cells were selected in 1 µg/ml puromycin. For overexpression of HSP72, the Precision LentiORF RFP control (OHS5832) and Precision LentiORF individual clone for HSPA1A (OHS5897-100998480) were purchased from Open Biosystems, Inc. Transduced cells were selected in 5 µg/ml blasticidin and FACS sorting of GFP positive cells.

2.2.10 Lysosomal integrity assays: Cells (~1-2x10^5) were plated in 6-well plates and allowed to attach overnight. Cells were then exposed to bortezomib for 24 h. Following drug treatments, 100nM LysoTracker Red DND-99 (Molecular Probes/ Life Technologies, Grand Island, NY) was added to cells for 30 minutes prior to harvest. Cells were trypsinized, washed once with PBS, and resuspended in fresh PBS, and fluorescence was measured using a Beckman Coulter FC500 flow cytometer.

2.2.11 Xenograft studies: Nude mice (NIH, 6 weeks of age) were inoculated subcutaneously (s.c.) with 2X10^6 253J B-V cells transduced with the HSPA1A shRNA construct (253JB-V.KDHsp72) or a non-targeting control construct (253JB-V.NT) (10 mice/group). When tumors became palpable (5~7 days), the mice were randomly assigned to control or treatment groups. The mice were treated i.v. (via the tail vein) biweekly with 1 mg/kg bortezomib formulated in saline containing 10 mg/mL mannitol in a volume of 100 µl or with 100 µl saline containing 10 mg/mL mannitol as a vehicle control. Caliper measurements of the longest perpendicular tumor diameters were performed twice a week after the start of treatment, and the volumes of tumors were calculated using the formula: W*W*L/2 (where W and L represented transverse diameter, and longest longitudinal). For

H&E analysis, tumors were collected from mice 24 hours after the second drug treatment and then fixed in OCT and 10% formalin.

2.2.12 UCSC Genome Browser: The UCSC Genome Browser (102) was used to identify the presence of a CpG island surrounding the HSPA1A promoter region, Within the Genome Browser, the encyclopedia of DNA elements consortium (ENCODE) database (103) was used to identify the presence of methylation in other cell types. The UCSC Genome Browser is publically available at the following site: http://genome.ucsc.edu/

2.2.13 Statistics: Statistics were performed as described previously in 2.1.12

2.3 Materials and Methods for Chapter 5

2.3.1 Cell lines, culture, and chemicals – Human pancreatic cancer cells and bladder cancer cells were obtained and grown as described above (Chps. 3 and 4 Materials and Methods, respectively). Cell line identities were confirmed using DNA fingerprinting analysis in the MD Anderson Characterized Cell Line Core. Multiple myeloma cells MM1, U266, RPMI-8226, and OPM-2 cells were obtained from Robert Orlowski at MD Anderson and grown in suspension in RPMI media supplemented with L-glutamine. Bortezomib and propidium iodide were obtained as described in Chp. 2.1.

2.3.2 Antibodies and immunoblotting –Antibodies were purchased from the following sources: HDAC6 (Santa Cruz Biotechnology, Santa Cruz, CA), HDAC1, total α-tubulin, acetylated α-tubulin, histone H3, and acetylated histone H3 (Cell Signaling Technology, Beverly, MA). Anti-mouse and anti-rabbit HRP-conjugated secondary antibodies were obtained from Promega, Madison, WI. Immunoblotting was done as described in Chp. 2.1.

2.3.3 Measurement of cell viability – Propidium iodide-uptake assays (measuring outer membrane integrity and total cell death) were performed as described in Chp 2.1. DNA fragmentation was analyzed on the same samples; following collection and measurement of membrane integrity, cells were washed and resuspended in 500µL DNA fragmentation buffer (50µg/mL propidium iodide in PBS + sodium citrate). Cells were incubated in the dark at 4˚C for at least 1 hour prior to FACS analysis on the FL3 channel of a Beckman Coulter FC500 cytometer. Sub G_0-G_1 cells were gated and quantified as the percentage of cells with fragmented DNA (subdiploid).

2.3.4 MTT assays –L3.6pl pancreatic cancer cells (5×10^3) were plated in 96-well plates and allowed to attach overnight before exposing them to the indicated concentrations of bortezomib, Compound A, SNDX-275, or SAHA inhibitors for 48 hours. Conversion of MTT (3-(4,5-dimethylthiazol-2-yl)-2,5-diphenyltetrazolium bromide) to formazan salt was used to measure relative numbers of viable cells in each well. Following drug exposure, 50 µL of MTT solution (50µg/ml in PBS) was added to each well and cells were incubated for 2 more hours. Next, medium was aspirated and replaced with DMSO (100 µL). A colorimetric assay using a standard micro-plate reader was used to determine the amount of MTT in each well via absorbance at 600 nm.

2.3.5 siRNA-mediated transient silencing assays – HDAC1, 2, 3, and 6 siRNAs ONTARGETplus SMARTpool siRNAs as well as a non-targeting control siRNA were purchased from Dharmacon/Thermo Scientific. Genes were silenced for 48-72 hours as described in Chp. 2.1 prior to drug exposure. Knockdown efficiencies were verified by qRT-PCR with primers specific for each target (Applied Biosystems/ Life Technologies).

2.3.6 shRNA-mediated stable gene knockdown assays – Cells were plated at ~30-40% confluency and allowed to attach overnight. pGIPZ plasmids containing hairpin sequences directed against HDAC6 or HDAC1 and a puromycin resistance gene(Open Biosystems) were packaged in lentiviral vectors and delivered to cells with polybrene in antibiotic-free medium (5µg/mL). After a 24h incubation with lentivirus, medium was replaced and cells grew to confluency. After several days, cells were selected and maintained with puromycin (5-10µg/mL) and knockdown levels were confirmed at the RNA and protein level.

Chapter 3. LACK OF INDUCIBLE eIF2A PHOSPHORYLATION IS ASSOCIATED WITH SENSITIVITY TO BORTEZOMIB IN PANCREATIC CANCER CELLS

3.1 Introduction

As detailed in Chapter 1 (Section 1.3.2b), eIF2α phosphorylation effectively shuts off global protein synthesis in response to stress, and also selectively upregulates the ATF4-mediated ISR. This phosphorylation is thought to be controlled by one of the four known stress-activated kinases, HRI, GCN2, PKR, and PERK, each activated by distinct stresses (see Fig. 1.5). Our group became interested in eIF2α through our work on the mechanisms underlying the cytotoxicity of proteasome inhibitors (PIs) in solid tumor models (71, 88, 104, 105). This work led to discovery of heterogeneity in PI-induced cytotoxicity among panels of cell lines both within and across tissue types. In addition, we noticed that only certain subsets of cancer cells appeared to phosphorylate eIF2α upon stress, and only certain subsets of our cancer cell lines formed large centralized aggregates known as aggresomes following PI exposure, indicating differences in protein aggregation levels (104). Perhaps the most convincing hypothesis for PI-induced cell death revolves around a proteotoxicity-based mechanism of action (see Section 1.3.3b); specifically, our view was that accumulation of aggregated proteins following proteasome inhibition precipitated cell death. The results of our work and others' led to the hypothesis that perhaps eIF2α phosphorylation is the central mechanism controlling proteostasis upon proteasome inhibition, and that cells that failed to phosphorylate eIF2α and shut off protein synthesis would be susceptible to enhanced protein misfolding/aggregation and thus be more sensitive to PIs.

Pancreatic cancer is an attractive disease site to study proteotoxic stress for several reasons. The pancreas is a secretory organ, containing small populations of islet (isle of Langerhaan's) cells responsible for secreting insulin and glucagon, while the majority of the organ is composed of acinar cells that secrete digestive enzymes into the intestine. PERK, as

previously described, is the only known ER-membrane resident eIF2α kinase known, and phosphorylates eIF2α in response to misfolded proteins and ER stress (106). Studies from P*ERK* $^{-/-}$ mice (52) provided strong evidence that PERK-eIF2α signaling is particularly important to the pancreas. Zhang, et al. showed that, contrary to most other tissues, the wild-type pancreas has high levels of phosphorylated-eIF2α. This phosphorylation was shown to be controlled by glucose availability: when the mice were injected with glucose after fasting, phosphorylation levels dropped fivefold, while serum insulin levels rose dramatically. Correspondingly, expression of PERK was also high in the wild-type pancreas. Expectedly, *Perk*$^{-/-}$ mice showed a loss of islet cells leading to decreased insulin and diabetes early in the postnatal growth period, and also showed a decrease in secretion of digestive enzymes, leading to digestive problems. It is unclear as to which of the three pancreatic cell types, ductal, acinar, or islet, is the cell of origin for pancreatic cancer (107, 108). In culture, our pancreatic cancer cell models do not retain the secretory protein expression profile seen in acinar cells, possibly because they originated from non-secretory pancreatic ductal cells, or perhaps because of changes as a result of malignant transformation or even the cell culture process (109). Importantly, when compared with their malignant counterparts, normal pancreatic cells possess lower overall translation rates and a better ability to attenuate translation in response to stress (88), (Jennifer Choe, unpublished results).

Therefore, we sought to understand the relationship between eIF2α phosphorylation and BZ sensitivity among a panel of 10 distinct pancreatic cancer cell lines derived from human tumors. Through the course of this study we also sought to characterize the nature of intracellular stress caused by proteasome inhibition. Our work and others' (88, 105, 110) has suggested that PI's induce significant ER stress; however, the cytosolic heat shock

response is also known to be strongly activated by PIs as well (32, 33). By examining the etiology of PI-induced stress, we hoped to gain a better understanding of the downstream stress response and identify new, rationale targets that may be inhibited to overcome BZ resistance. Activation of autophagy is also thought to be a significant compensatory response to PIs that lies downstream of the initial stress response (71). Another major goal of our study was to identify the specific eIF2α kinase (either HRI, GCN2, PKR, or PERK) that is activated by BZ. If eIF2α phosphorylation is indeed cytoprotective, it follows that blocking phosphorylation by targeting the BZ-activated eIF2α kinase would sensitize cells to BZ.

Here, we show that BZ sensitivity correlates with a lack of inducible eIF2α phosphorylation among a panel of human pancreatic cancer cell lines. The sensitive cells failed to sufficiently arrest translation, and this led to extensive protein aggregation that was associated with oxidative stress and ultimately, cell death. BZ appeared to more strongly induce expression of cytosolic stress response chaperones (Hsp72) than ER stress chaperones (Grp78/BiP) and transcription factors (CHOP/GADD153). Accordingly, we identify the cytosolic eIF2α kinase HRI as most strongly activated by BZ, and demonstrate that knockdown of HRI can reverse resistance to BZ. Overall, this work provides important clarification regarding how molecular heterogeneity of the eIF2α stress response pathway influences BZ-induced cytotoxicity in pancreatic cancer cells, and identifies new targets for therapy (HRI) within this pathway.

3.2 Results

3.2.1 *Heterogeneous effects of bortezomib on cell death and eIF2α phosphorylation in pancreatic cancer cells* - We previously observed significant heterogeneity among human pancreatic cancer cell lines in the levels of apoptosis induced by proteasome inhibitors (104). Here we examined a new panel of cells to determine their sensitivities to a clinically relevant concentration of bortezomib (BZ) using a plasma membrane integrity assay (PI-uptake) that measures cumulative cell death. Immortalized normal pancreatic ductal epithelium cells (HPDE) were used as a control and were relatively resistant to BZ, as was reported previously using DNA fragmentation assays (104). Among the cancer cells we observed a wide range of responses indicative of inter-tumoral heterogeneity in drug sensitivities (Fig. 3.1). We performed time course experiments to measure eIF2α phosphorylation in two drug-sensitive (CF-Pac1, T3M4) and two drug–resistant (mPanc96, Suit2) cell lines. Neither BZ nor the ER stress-inducing agent thapsigargin (TG) induced eIF2α phosphorylation in the sensitive cell lines, whereas both compounds promoted strong induction in the resistant lines (Fig. 3.2). We then compared the effects of BZ and TG on eIF2α phosphorylation in the rest of the cell lines in the panel. Overall, there was an excellent correlation between lack of eIF2α phosphorylation and BZ sensitivity (Fig. 3.2-3.3). Only two of the cell lines that exhibited intermediate drug sensitivities (L3.6pl and Panc1) did not conform to this pattern (Fig. 3.3).

3.2.2 *Effects of bortezomib on translation and protein aggregation* - We hypothesized that lack of inducible eIF2α phosphorylation might prevent efficient translational attenuation leading to toxic accumulation of misfolded protein aggregates. To test this hypothesis, we utilized a L-[4,5-^{3}H(N)] leucine incorporation assay to measure rates of protein synthesis in**A**

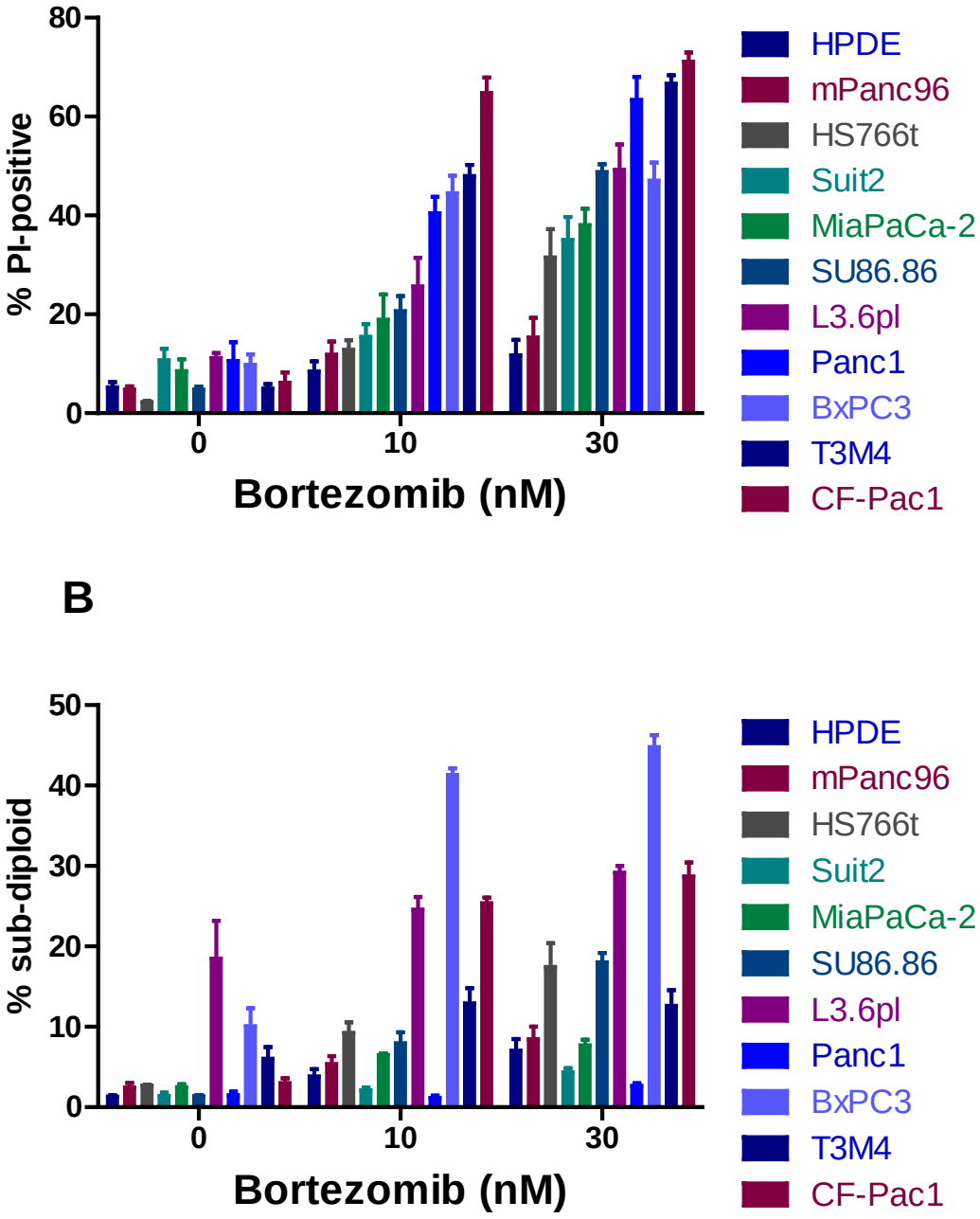

Figure 3.1. Heterogeneous sensitivities of pancreatic cancer cell lines to bortezomib. 10 distinct human pancreatic cancer cell lines and one normal immortalized pancreatic ductal epithelial cell line (HPDE) were exposed to 10 and 30 nM concentrations of bortezomib (BZ) for 48 hours. A) Viability was measured by outer membrane integrity using PI-uptake/FACS analysis (A). B) Apoptosis was determined by PI-based cell cycle analysis of sub G_0-G_1 cells. Columns represent mean $\pm$ SE (n=3).

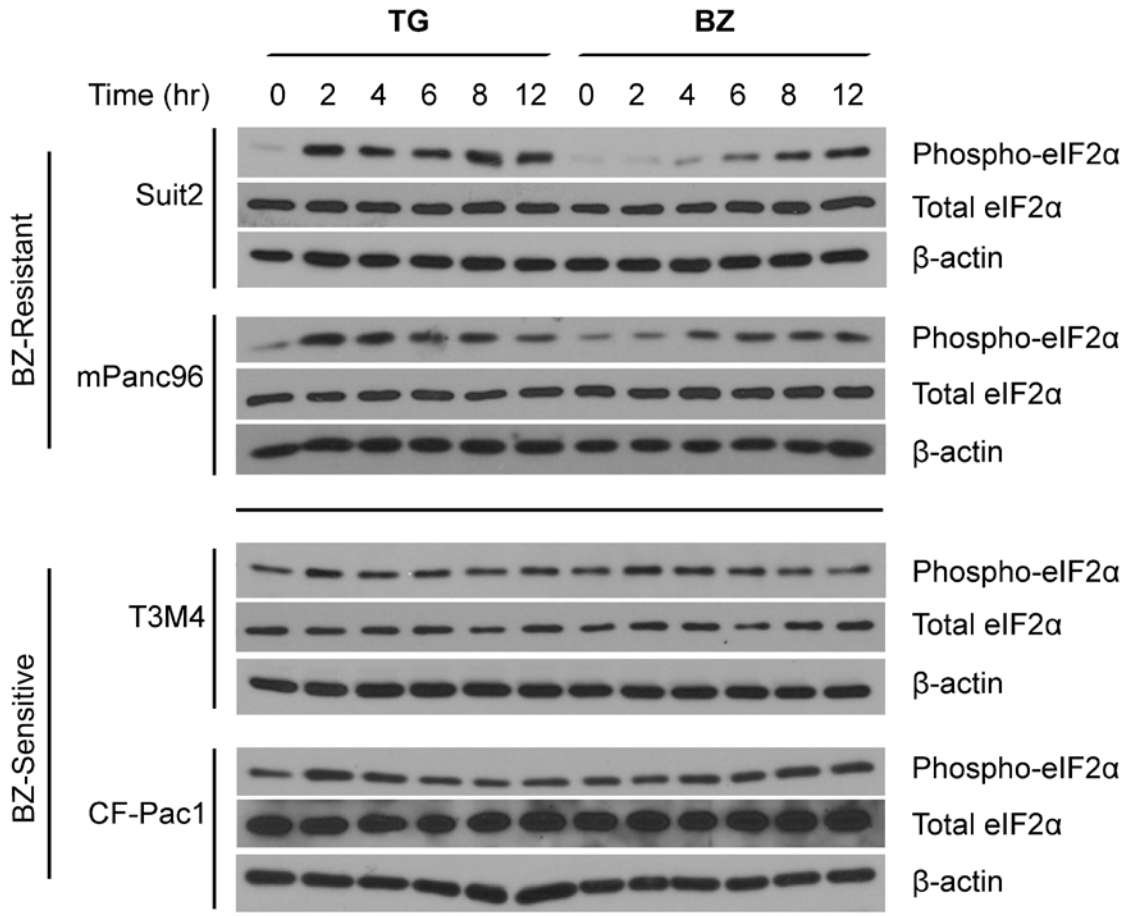

Figure 3.2. Bortezomib sensitivity correlates with lack of inducible eIF2α phosphorylation in human pancreatic cancer cells. Time-course of eIF2α phosphorylation. BZ-resistant (Suit2, mPanc96) and BZ-sensitive (T3M4, CF-Pac1) were exposed to 10μM thapsigargin (TG) or 10nM BZ (BZ) for the indicated times and the levels of phosphorylated and total eIF2α were measured by immunoblotting, with β-actin serving as a loading control. Data are representative of n=3.

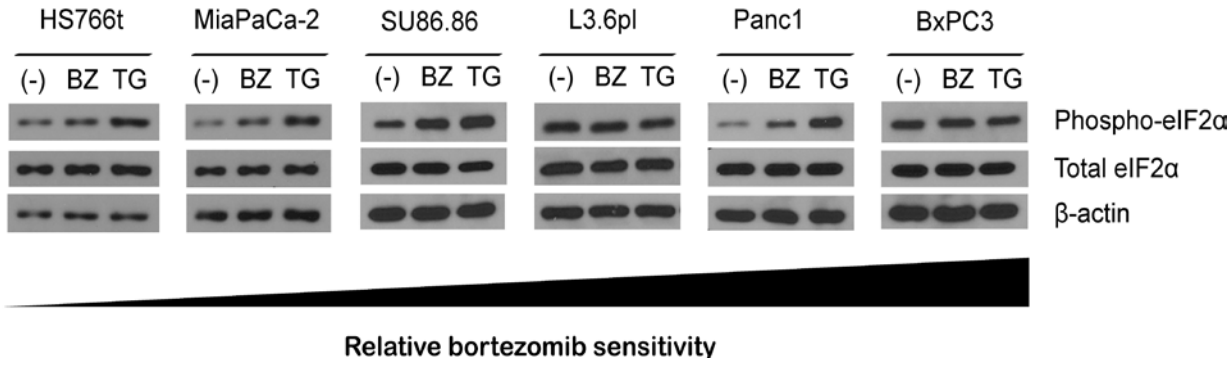

Figure 3.3. Characterization of eIF2α phosphorylation in additional cell lines. Cells were exposed to 10nM BZ for 6 hours (BZ) or 10μM thapsigargin for 2 hours (TG) and eIF2α phosphorylation was measured by immunoblotting. Data are representative of duplicate experiments.

cells exposed to BZ. The results (Fig. 3.4) confirmed that translation attenuation was delayed in the BZ-sensitive cell lines, which continued incorporating leucine into protein at $\geq$ 100% of control levels for up to 8 hours after BZ exposure, whereas the resistant cells down-regulated translation much earlier (2-4 hours). The results were not related to differences in the basal protein synthesis rates among sensitive and resistant cells (Fig. 3.5A). Sensitivity of the assay was also validated using the translation inhibitor cycloheximide (CHX), which caused similar levels of translational inhibition in all of the cell lines (Fig. 3.5B).

Based on the protein synthesis data, we suspected that the BZ-sensitive cell lines would accumulate protein aggregates more readily than the resistant cells. We examined the time-dependent effects of BZ on the accumulation of ubiquitin-positive aggregates in the sensitive CF-Pac1 and T3M4 cells using anti-ubiquitin immunofluorescence microscopy, and the results revealed that visible aggregates began to form at 12 hours (Fig. 3.6). We then used the same assay to measure protein aggregation in the resistant cells at this time point. Strikingly, immunofluorescence analyses revealed almost no ubiquitin-positive aggregates in either of the BZ-resistant cells (mPanc96 or Suit2) (Fig. 3.7). To confirm these results with a different method, we used a variation of a detergent-insoluble protein aggregation assay reported previously (111). Again, BZ induced higher levels of ubiquitin-positive aggregates in the insoluble fractions of CF-Pac1 and T3M4 than in mPanc96 or Suit2 cells (Fig. 3.8). To explore whether a causal link existed between protein aggregation and cell death, we pre-incubated BZ-sensitive cells with CHX prior to exposing them to BZ and examined the effects on BZ-induced protein aggregation and cell death (Fig. 3.9). Immunofluorescence confirmed that CHX prevented BZ-induced protein aggregation in CF-

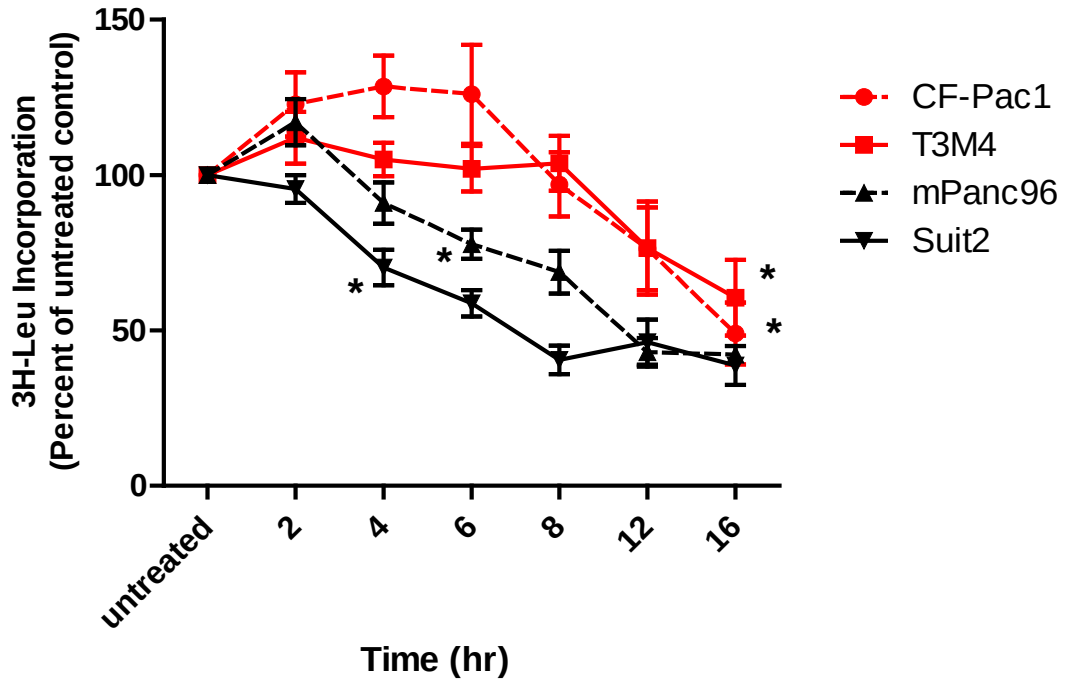

Figure 3.4. Bortezomib-sensitive cells display impaired translation attenuation. Measurement of bortezomib (BZ)-induced translational arrest. Left panel, BZ-resistant (Suit2, mPanc96) and BZ-sensitive (CF-Pac1, T3M4) cells were exposed to 30nM bortezomib for the indicated times, and protein synthesis was measured by L-[4,5- ^{3}H(N)] leucine incorporation. Points represent mean $\pm$ SE (n=4). *Represents time point at which values became significantly different from untreated controls ($P < 0.05$).

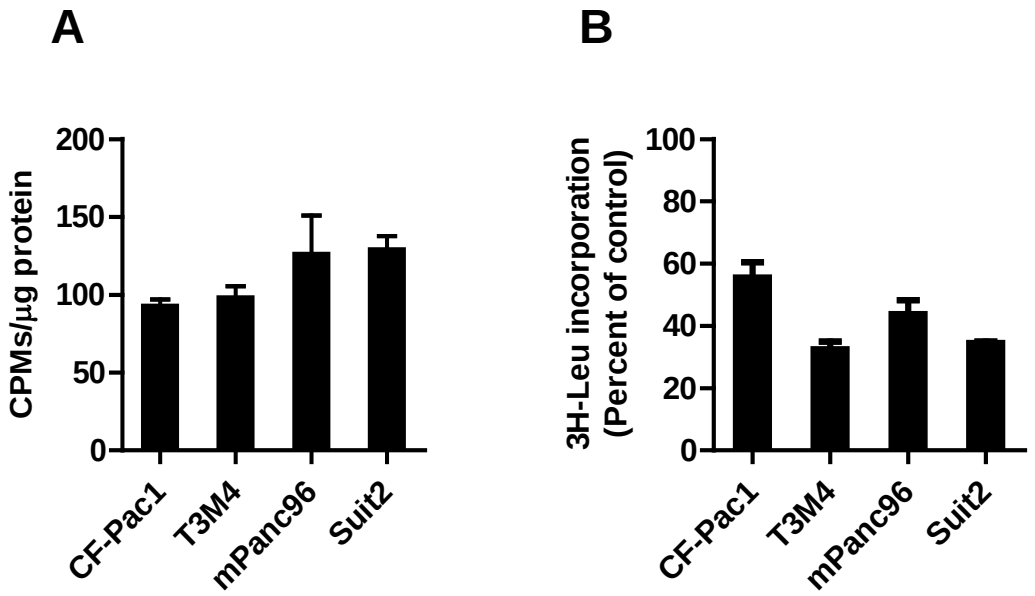

Figure 3.5. Differences in translation attenuation are not due to inherent differences in protein synthesis rates between cell lines or to L-[4,5- ^{3}H(N)] leucine incorporation assay sensitivity. A) Basal levels of protein synthesis among sensitive (CF-Pac1, T3M4) and resistant (mPanc96, Suit2) cells, normalized to CPMs per µg of protein loaded. B) Sensitivity of L-[4,5- ^{3}H(N)] leucine incorporation assay validated by cycloheximide, a positive control for inhibition of translation. Columns represent mean $\pm$ SE (n=3).

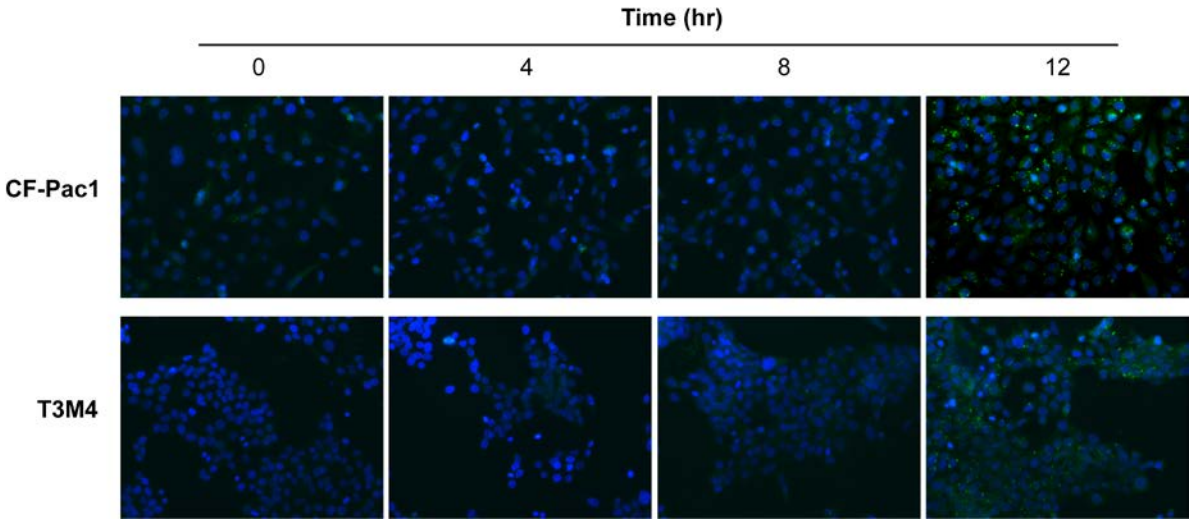

Figure 3.6. Bortezomib-sensitive cells form ubiquitin-positive protein aggregates following exposure to bortezomib. Measurement of ubiquitin-positive aggregates by immunofluorescent staining. CF-Pac1 and T3M4 were exposed to 10nM BZ for indicated times. Blue = nuclear stain; green = ubiquitin. Magnification = 20x. Images are representative of 2 independent experiments..

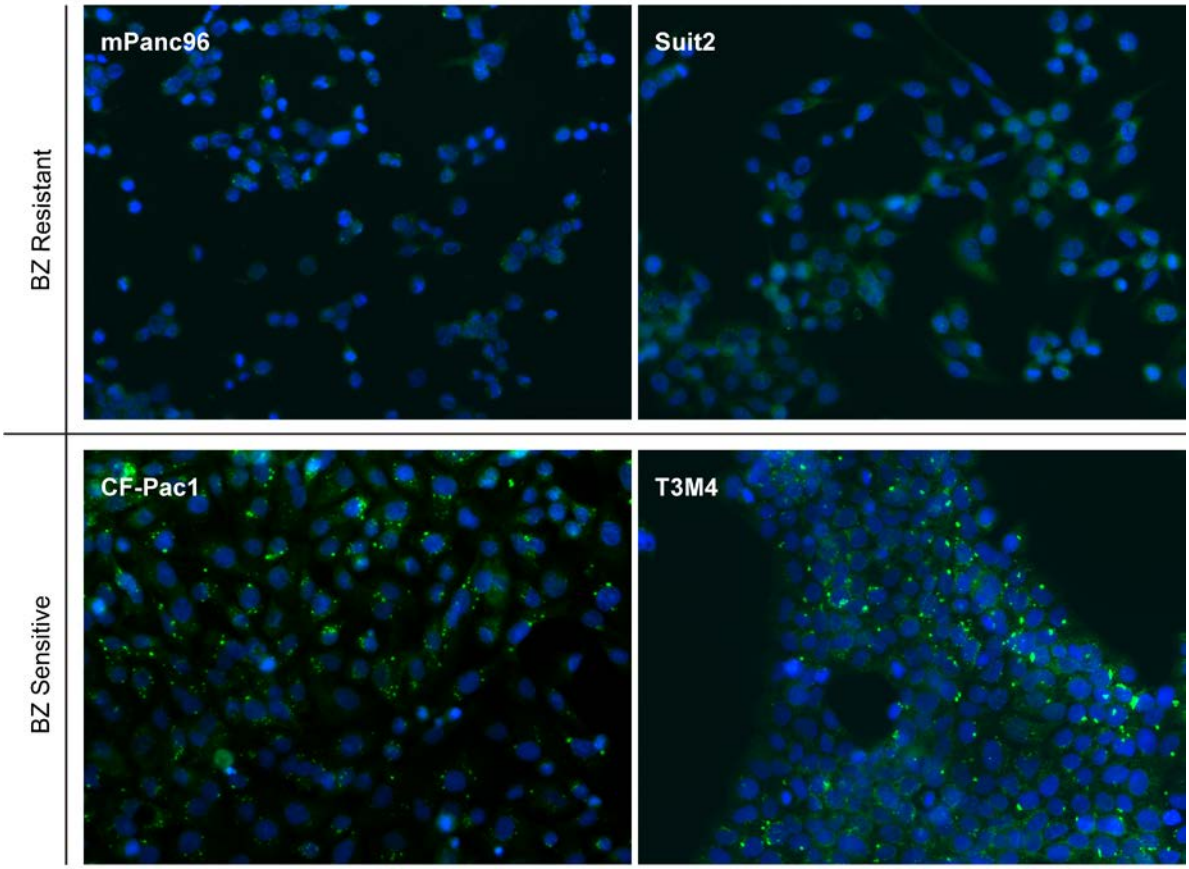

Figure 3.7. Bortezomib induces different levels of visible ubiquitin-positive aggregates in sensitive and resistant cells. *A*, ubiquitin immunofluorescent staining. mPanc96, Suit2, CF-Pac1, and T3M4 were plated in chamber slides and exposed to 10nM BZ for 12h. After fixation, cells were stained for ubiquitin (green) and nuclei (blue). Magnification = 20x. Images are representative of 2 independent experiments.

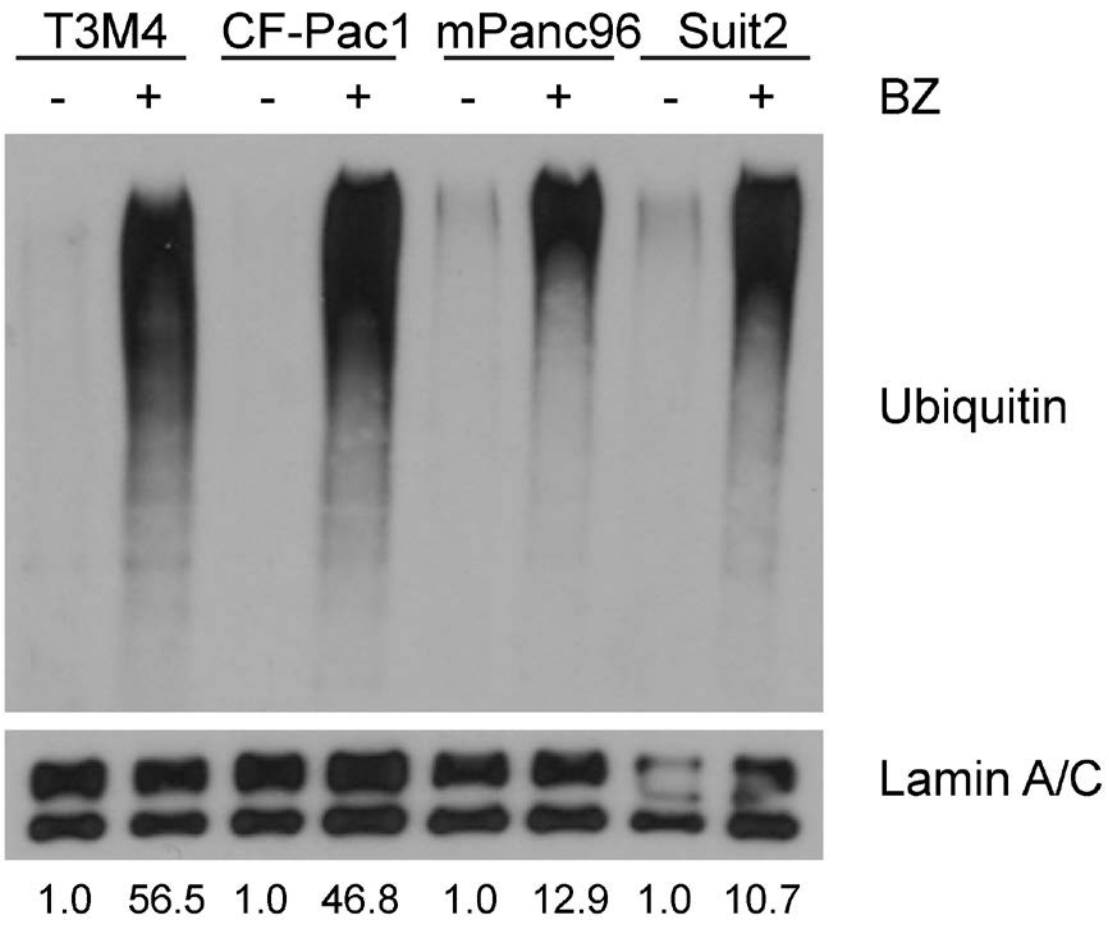

Figure 3.8. Bortezomib-sensitive cells have higher levels of ubiquitin in detergent-insoluble fraction after bortezomib exposure. T3M4, CF-Pac1, mPanc96, and Suit2 cells were exposed to 10nM bortezomib (BZ) for 24h, detergent insoluble fractions were isolated, and ubiquitin-positive aggregates were detected by immunoblotting. Lamin A/C served as a loading control. The numbers located below each lane correspond to levels of ubiquitin, as determined by densitometry and adjusted to lamin A/C levels. Results are representative of 3 independent experiments.

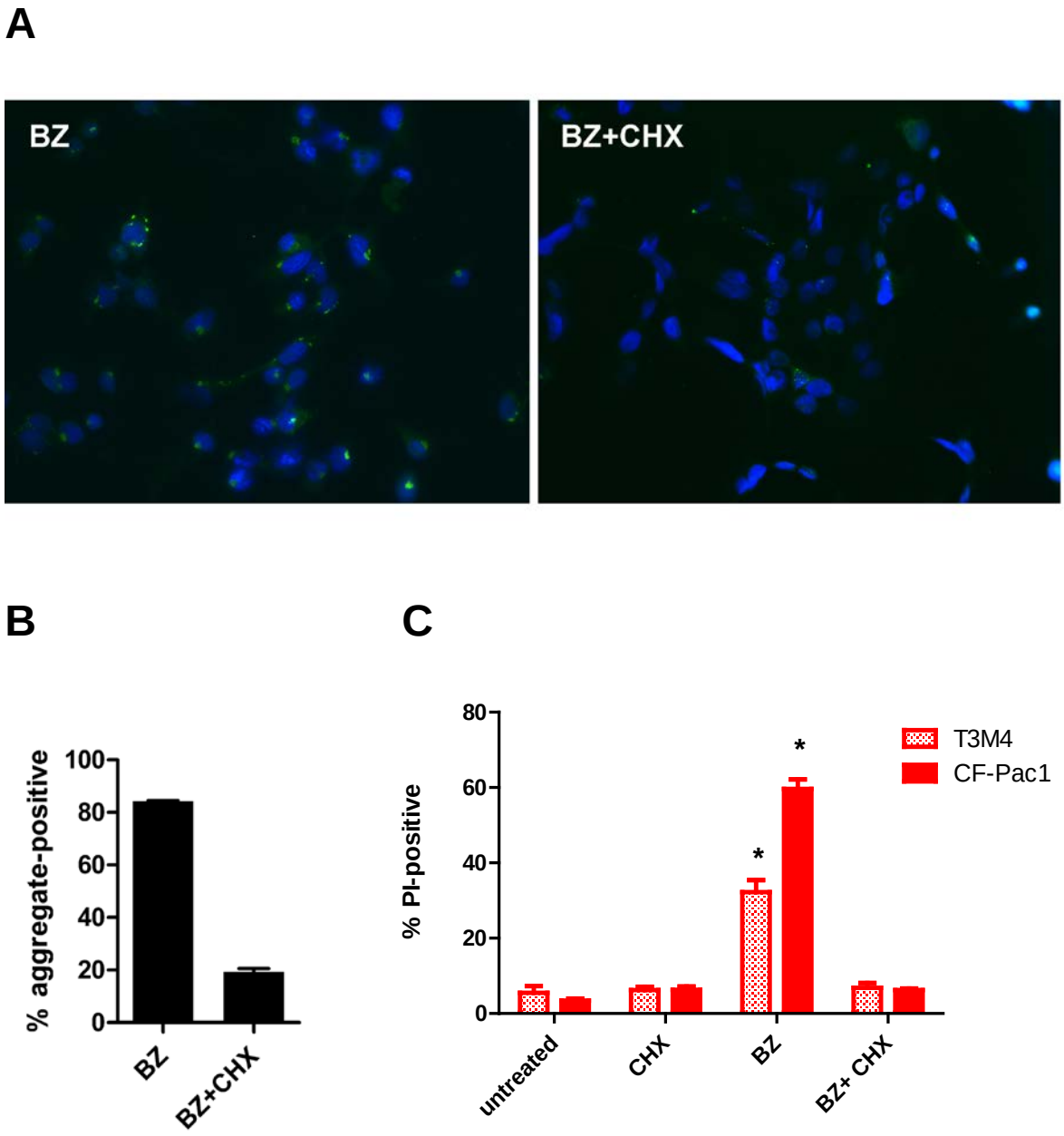

Figure 3.9. Chemical inhibition of translation prevents bortezomib-induced protein aggregation and cell death. *A,* ubiquitin immunofluorescence. CF-Pac1 cells with and without a 2 hour preincubation with 20μM cycloheximide (CHX) were exposed to 30nM bortezomib (BZ) for 24 hours, then fixed and stained. Green represents ubiquitin, blue represents the nuclear stain. Magnification = 20x. Right panel, >100 cells from at least 2 representative images from 2 independent experiments were scored for the presence/absence of at least one ubiquitin-positive aggregate. Columns represent mean ± SE. (n=2). *B,* effects of cycloheximide (CHX) on bortezomib-induced cell death. T3M4 and CF-Pac1 cells with and without a 2 hour preincubation with 20μM CHX were exposed for 48 hours to 30nM BZ as indicated. Cell viability was determined by PI-uptake/FACS analysis. Columns represent mean ± SE (n=3). *P <0.01 compared with BZ alone.

Pac1 cells (Fig. 3.9A,B). The inhibitor also prevented BZ-induced death in the CF-Pac1 and T3M4 cells (Fig. 3.9C).

3.2.3 *Bortezomib-induced oxidative stress mediates cell death* – Protein misfolding and aggregation have been implicated in the production of ROS (112-115). It therefore seemed possible that ROS production might underlie the protein aggregate-associated toxicity of BZ in pancreatic cancer cells. To test this, we measured intracellular BZ-induced peroxide production with 2',7'-dichlorodihydro-fluorescein diacetate (H_2DCFDA). Following exposure to BZ for 18h (a time point which follows initial aggregate formation but precedes cell death), the sensitive cell lines BxPC3, CF-Pac1, and T3M4 displayed significant rightward shifts in H_2DCFDA fluorescence, indicating increased production of ROS, whereas the resistant cell lines mPanc96, Suit2, and MiaPaCa-2 did not (Fig. 3.10). Furthermore, the thiol antioxidant *N*-acetyl-L-cysteine (NAC) prevented both BZ-induced ROS production and cell death (Figs. 3.11, 3.12).

3.2.4 *Bortezomib induces Hsp72 mRNA levels but not Grp78/BiP or CHOP/GADD153* – To better understand the BZ-induced stress response, we measured biomarkers associated with either cytosolic or ER stress responses. BZ induced similar levels of ER stress (as measured by Grp78/BiP levels) in both sensitive and resistant cell lines (Fig. 3.13A). In addition, levels of CHOP/GADD15, were also similar following BZ exposure (Fig. 3.13B). Strikingly, when compared with a classic ER stressor such as TG, BZ was a relatively weak inducer of both Grp78 and CHOP, but it was a much more potent inducer of the cytosolic and heat shock-inducible homolog of Grp78, Hsp72 (Fig. 3.13C). In addition, TG did not induce significant cytotoxicity in any of the cell lines (Fig. 3.14). Previous work implicated CHOP in proteasome inhibitor-induced cell death (5). We therefore also examined the

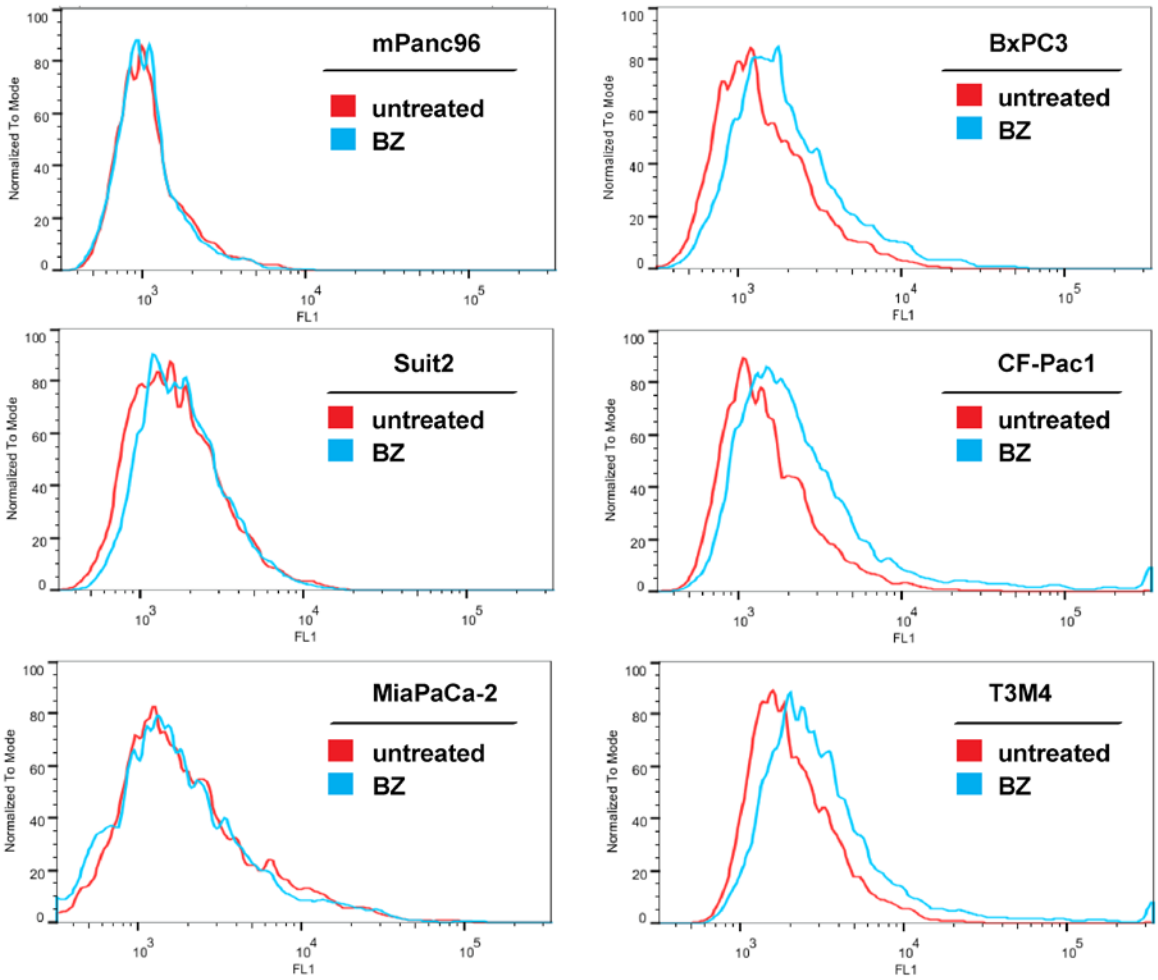

Figure 3.10. Bortezomib induces reactive oxygen species (ROS) in sensitive cells. ROS levels in resistant (mPanc96, Suit2, MiaPaCa-2) and sensitive (BxPC3, CF-Pac1, T3M4) cells measured by H_2DCFDA fluorescence (FL1 channel) after an 18 h exposure to 30nM BZ. Data are representative of three independent experiments.

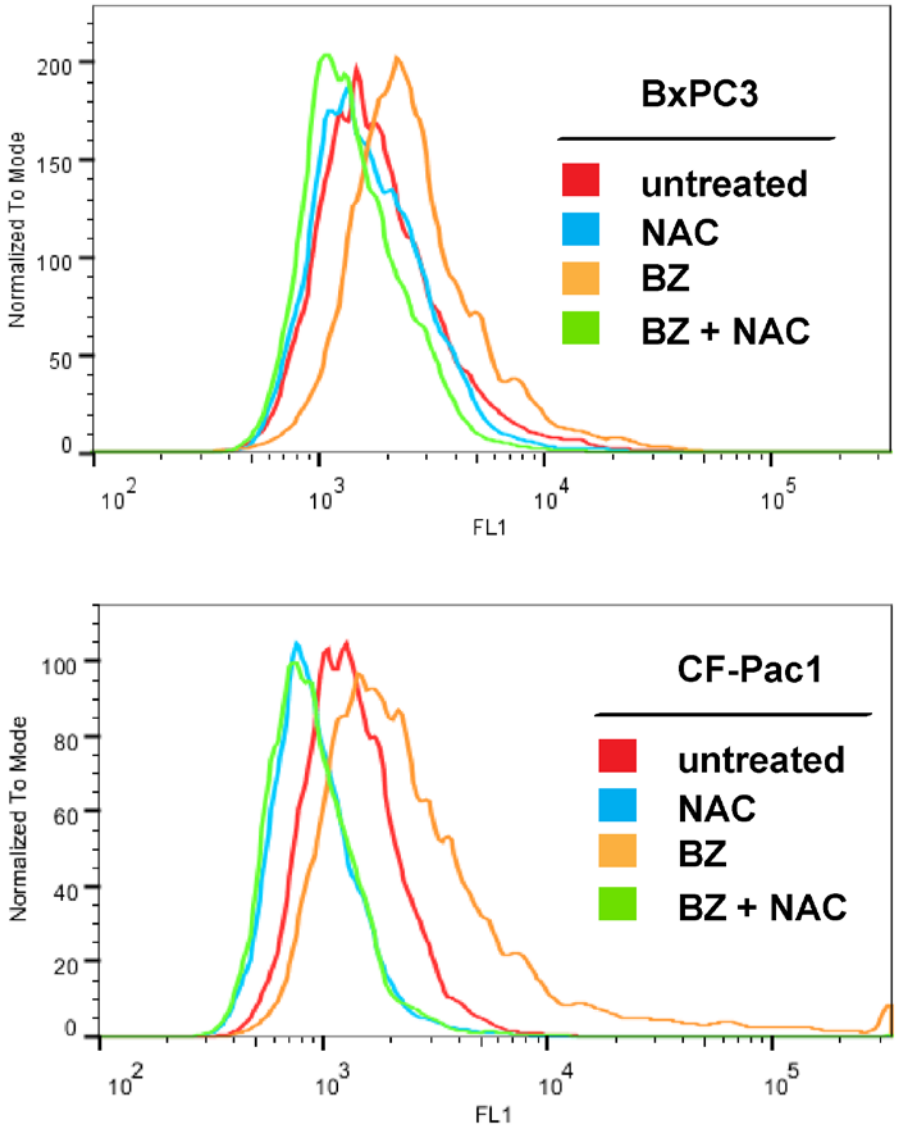

Figure 3.11. Antioxidants block bortezomib-induced ROS production. Pre-treatment with 10mM of the antioxidant *N*-acetyl-L-cysteine (NAC) blocks ROS production following an 18 hour exposure to 30nM BZ in two sensitive cell lines, BxPC3 and CF-Pac1. Data are representative of three independent experiments.

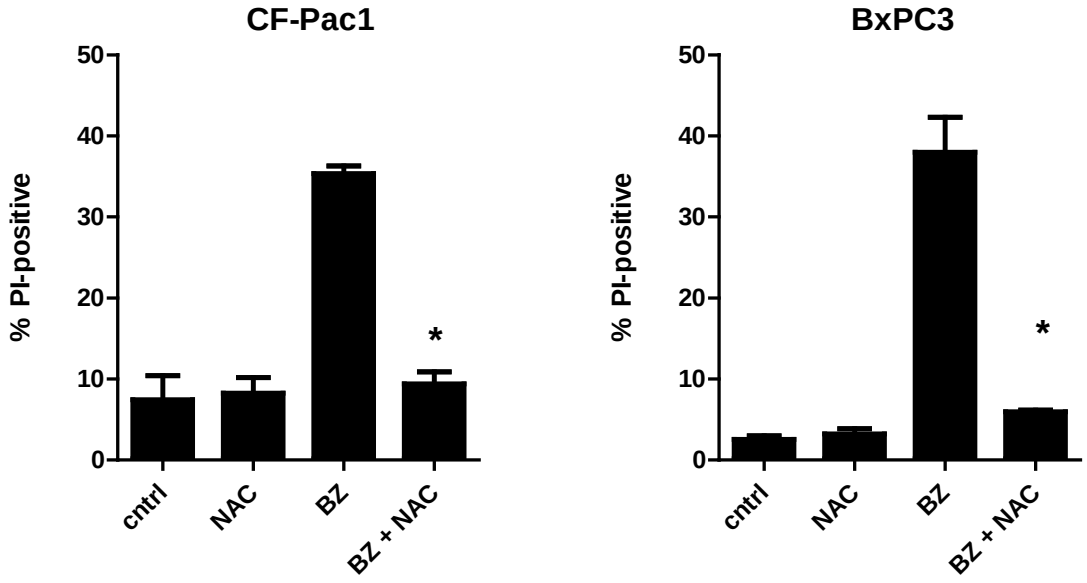

Figure 3.12. The antioxidant N-acetyl-L-cysteine (NAC) prevents bortezomib-induced cell death. CF-Pac1 and BxPC3 cells were pre-exposed to 10mM NAC for 1 hour prior to a 48 hour BZ exposure. Cell death was measured by PI-uptake/FACS analysis. Columns represent mean of dead cells $\pm$ SE. *P < 0.02 compared to BZ column.

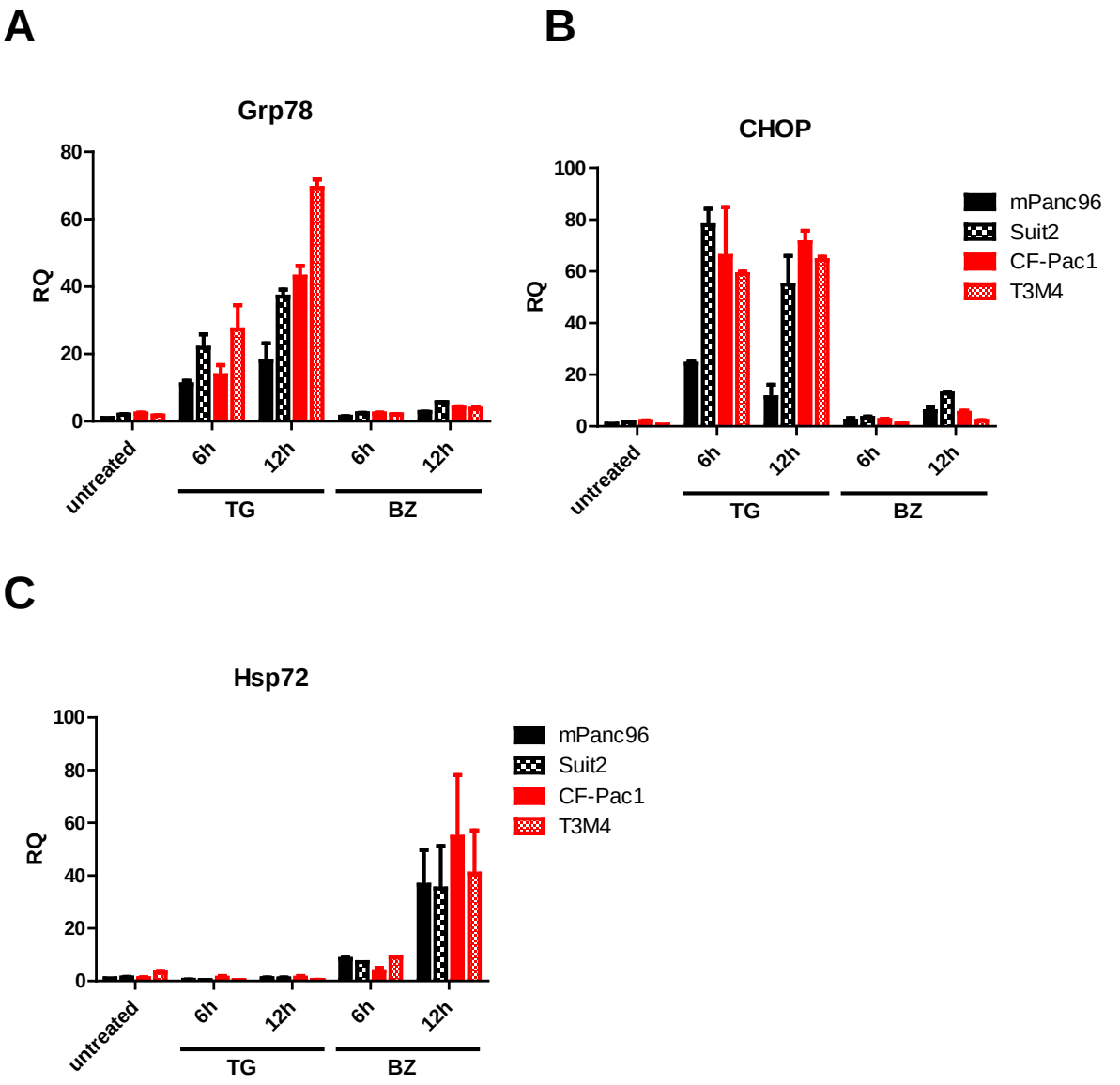

Figure 3.13. Effects of bortezomib on biomarkers of ER and cytosolic stress. *A,* effects on the ER stress marker Grp78/BiP; *B,* effects on the ER stress marker CHOP/GADD153; *C,* effects on the cytosolic stress marker Hsp72. mPanc96, Suit2, CF-Pac1, and T3M4 cells were exposed to 10μM thapsigargin (TG) or 10nM bortezomib (BZ) as indicated. Expression levels were determined by one-step quantitative RT-PCR. RQ, relative quantity as normalized to the internal control (cyclophilin A). Columns represent mean ± SE (n=3).

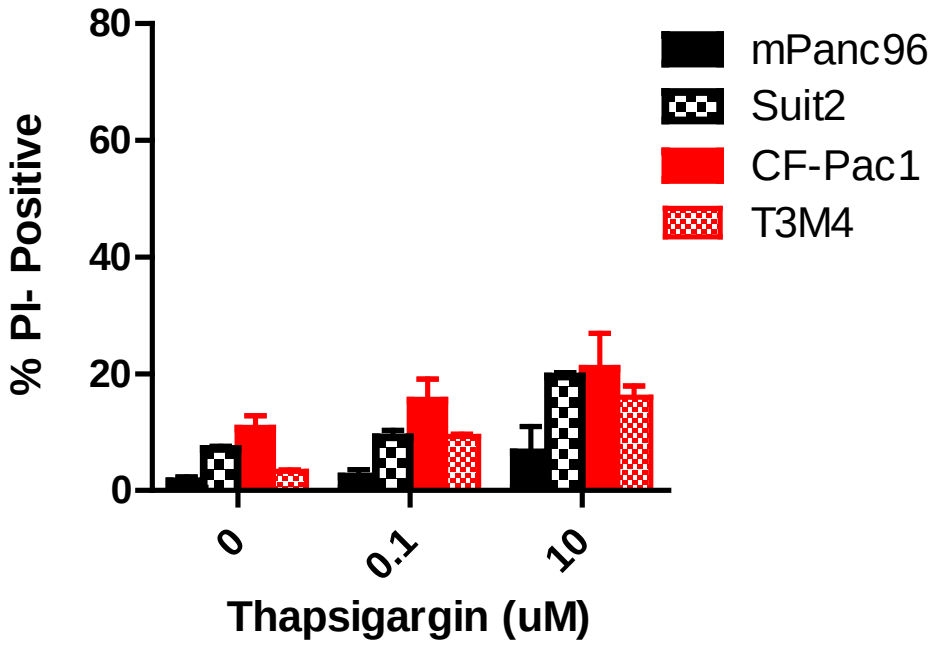

Figure 3.14. Dichotomy between bortezomib-sensitive and -resistant cells does not exist when exposed to the ER stress-inducing agent thapsigargin. Thapsigargin (TG)-induced ER stress does not induce significant cell death. mPanc96, Suit2, CF-Pac1, and T3M4 cells were exposed to TG for 48 hours at the concentrations indicated. Cell death was measured by PI-uptake/FACS analysis. Columns represent mean ± SE (n=3).

effects of CHOP knockdown on BZ-induced cell death in the Suit2 and CF-Pac1 cells. In contrast with the previous work, CHOP knockdown actually promoted cell death (Fig. 3.15). Therefore, the nature of the proteotoxic stress caused by BZ appears to be more similar to heat shock than to ER stress, and is primarily cytosolic in origin.

3.2.5 *Identification of BZ-activated eIF2α kinase(s)* – Given that BZ induced primarily cytosolic stress, it seemed likely that an eIF2α kinase other than PERK might be primarily responsible for the BZ-induced eIF2α phosphorylation observed in the resistant cells. We therefore examined the concentration-dependent effects of BZ on activation of the eIF2α kinases HRI, PERK, and GCN2 by immunoblotting. As positive controls we used amino acid starvation (leucine deprivation) and TG to induce activation of GCN2 and PERK, respectively. We monitored GCN2 activation using a phospho-specific antibody, and we measured HRI and PERK activation indirectly by monitoring the appearance of slower migrating species of the kinases by SDS-PAGE and immunoblotting because reliable commercial phospho-specific antibodies were not available. Bortezomib caused dramatic HRI mobility shifts in the Suit2 and CF-Pac1 cells, whereas its effects on PERK were much more modest, especially when compared to the effects of TG (Fig. 3.16). Neither BZ nor TG had any detectable effect on GCN2 phosphorylation (Fig. 3.16). Importantly, BZ induced similar effects on HRI and PERK in the drug-sensitive and –resistant cells, indicating that the lack of increased eIF2α phosphorylation in the sensitive cells was not caused by defective kinase activation. Basal levels of HRI and GCN2 were slightly higher in BZ-sensitive versus –resistant lines but none of the kinases were upregulated by BZ (Fig. 3.17).

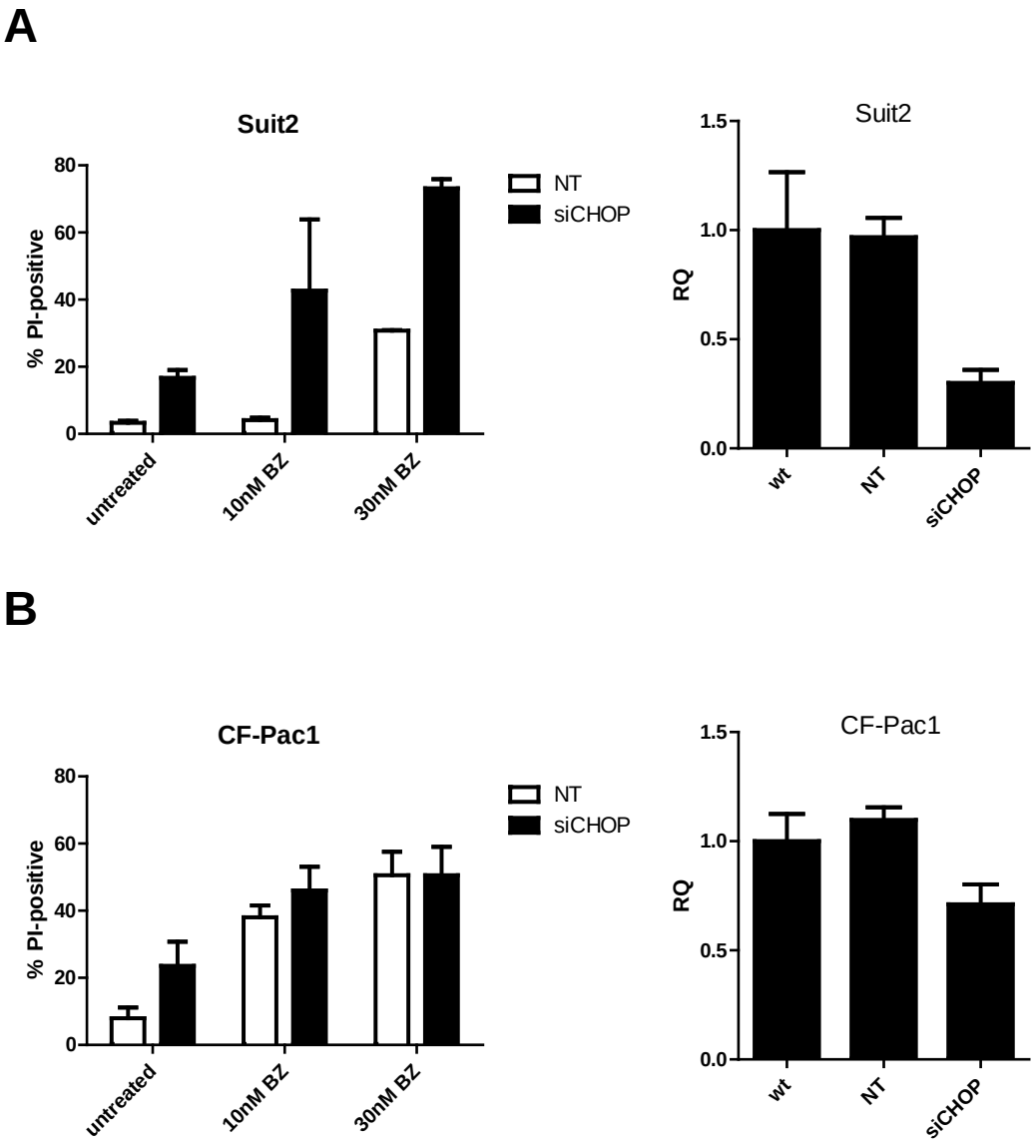

Figure 3.15. CHOP knockdown promotes cell death and sensitizes cells to bortezomib. (A) Suit2 and (B) CF-Pac1 cells were transfected with siRNA specific for CHOP (siCHOP) as well as a non-targeting control siRNA (NT). Cells were then exposed to indicated concentrations of BZ for 48h, and cumulative cell death measured by PI-uptake/FACS analysis. Left panels, columns represent mean cell death $\pm$ SE (n=2). Right panels, knockdown efficiencies for CHOP determined by one-step quantitative RT-PCR. RQ, relative quantity as normalized to the internal control (cyclophilin A). Columns represent mean $\pm$ SE (n=2).

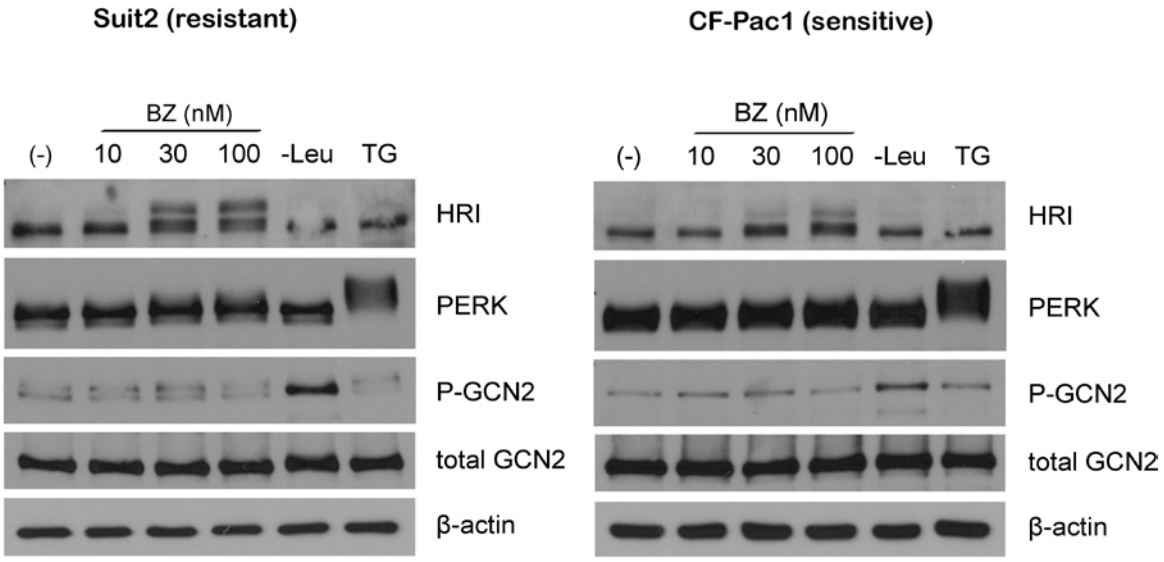

Figure 3.16. Identification of bortezomib-activated eIF2α kinase(s). Analysis of HRI, PERK, and GCN2 activation following bortezomib exposure. Suit2 and CF-Pac1 cells were either exposed to indicated concentrations of bortezomib (BZ) for 6 hours, leucine-starved for 2 hours, or exposed to 10 μM thapsigargin (TG) for 2 hours. Phosphorylated and total kinase levels were measured by immunoblotting. Data are representative of three independent experiments.

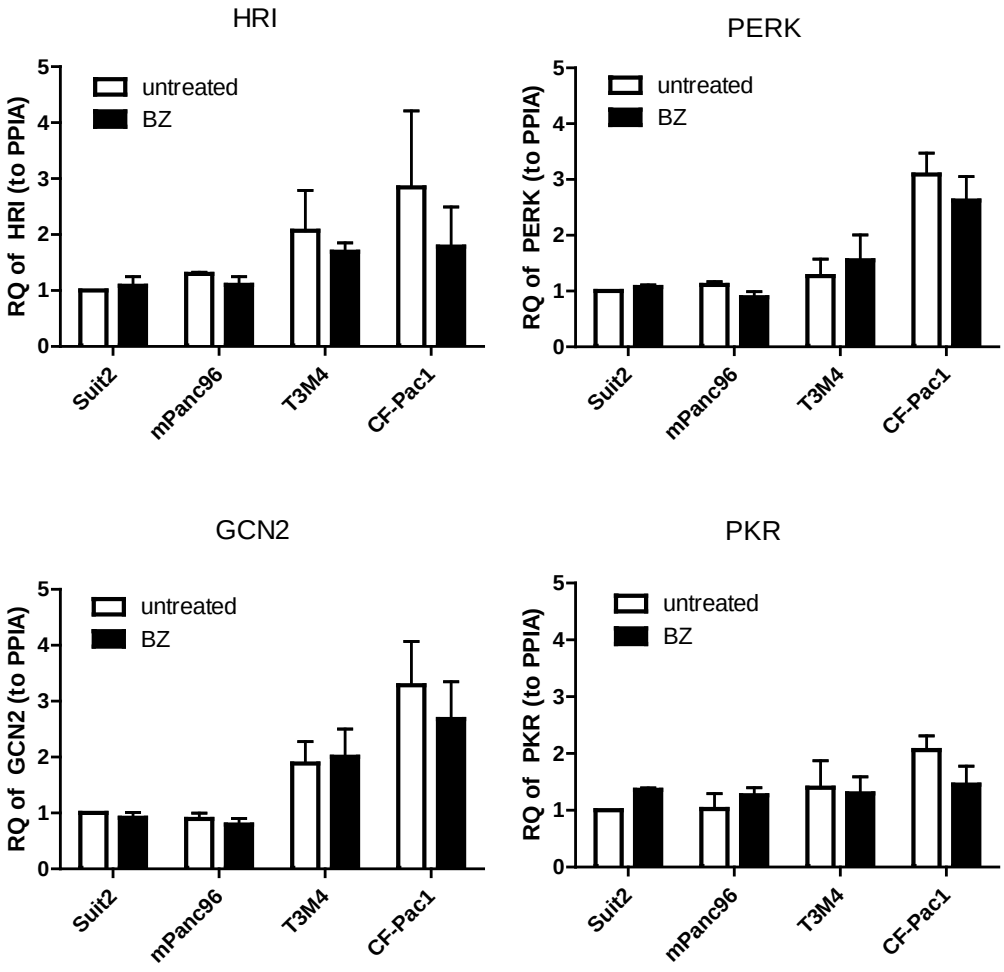

Figure 3.17. eIF2α kinase expression among bortezomib-sensitive and-resistant cells. Suit2, mPanc96, T3M4, and CF-Pac1 cells were left untreated or exposed to 10nM BZ for 6h (BZ), and HRI, GCN2, PKR, and PERK mRNA levels were measured by one-step quantitative RT-PCR. Columns represent mean ± SE (n=2).

3.2.6 *GCN2 controls constitutive phosphorylation of eIF2α*– We noticed that most of the BZ-sensitive cell lines had elevated levels of phospho-eIF2α at baseline (Fig. 3.2). We confirmed this by immunoblotting (Fig. 3.18A, left panel), and the differences between sensitive (CF-Pac1, T3M4) and resistant (mPanc96, Suit2) cells were significant (Fig. 3.18A, right panel). To identify the responsible kinase, we used RNAi to knock down expression of HRI, GCN2, and PERK in the CF-Pac1 cells and examined phospho- and total-eIF2α levels by immunoblotting (Fig. 3.18B, left panel) and confirmed knockdown efficiencies by RT-PCR (Fig. 3.19). The results revealed that GCN2 knockdown resulted in a significant reduction in basal phospho-eIF2α levels, whereas knockdown of the other kinases or transfection with a non-targeting control had no effect (Fig.3.18B, right panel).

3.2.7 *Inhibition of inducible eIF2α phosphorylation sensitizes cells to bortezomib* – To more directly determine the contribution of eIF2α phosphorylation to cell death, we compared the effects of BZ in MEFs expressing either wild-type (51SS) or knock-in mutant (51AA) forms of eIF2α. The mutant 51AA cells were significantly more sensitive to BZ than the wild-type 51SS cells (Fig. 3.20). We next tested whether knockdown of eIF2α kinases would sensitize cells to BZ (Fig. 3.21-22). Based on the kinase activation data (Fig. 3.16), we expected that knockdown of HRI, and to a lesser extent PERK, would promote cell death. Consistent with our expectations, HRI knockdown strongly promoted BZ-induced cell death in two resistant cell lines (Suit2, MiaPaCa-2). PERK knockdown produced some sensitization but less than HRI knockdown. GCN2 and PKR knockdown also modestly increased cell death over the non-targeting control, but the differences were not statistically significant (Fig. 3.21). Overall, the results demonstrate that HRI-mediated eIF2α phosphorylation antagonizes BZ-induced cell death.

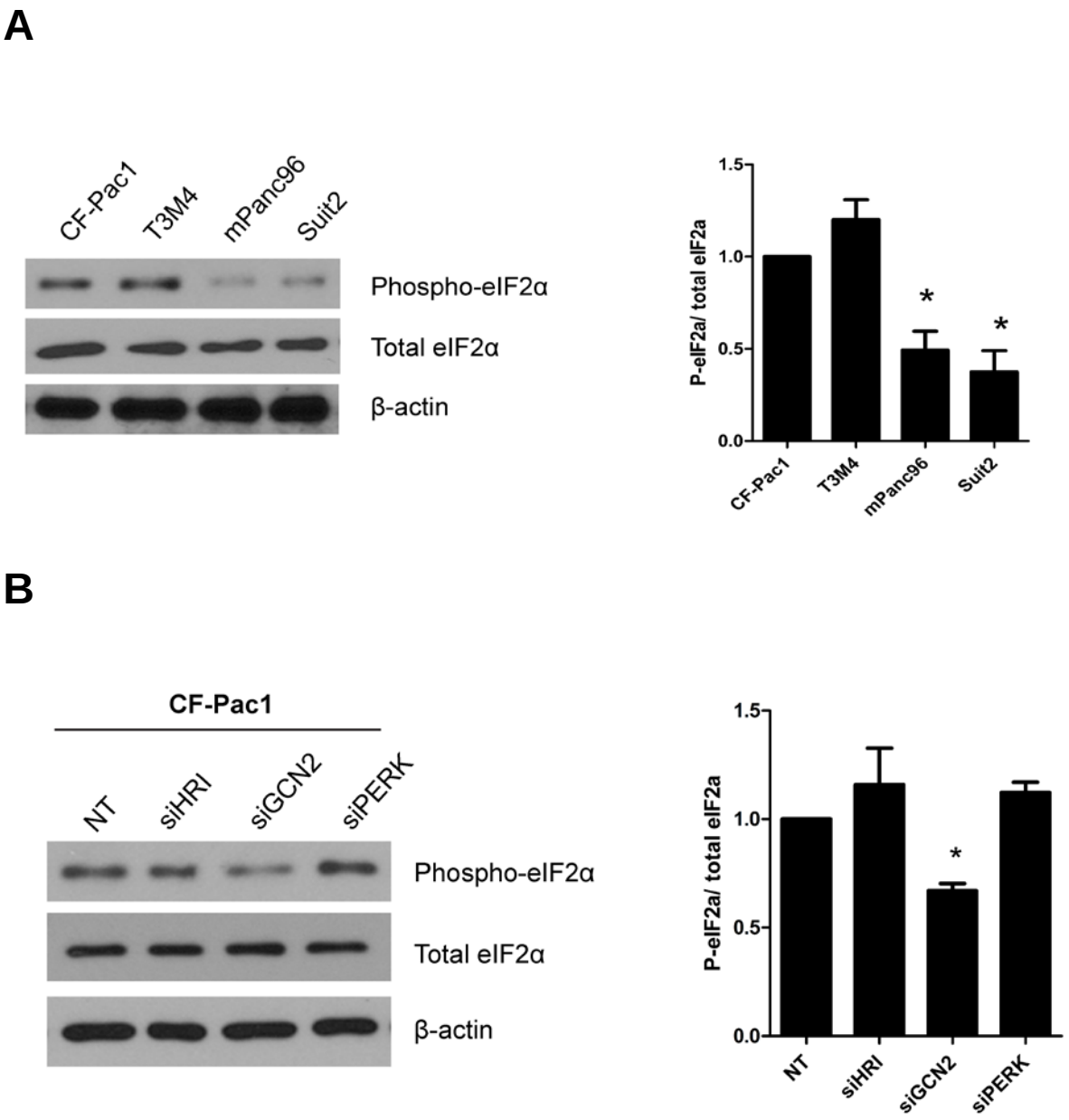

Figure 3.18. GCN2 controls constitutive eIF2α phosphorylation bortezomib-sensitive cells. A), Basal phospho-eIF2α levels in BZ-sensitive and BZ-resistant cells. Left panel, untreated lysates were analyzed for phospho- and total eIF2α levels by immunoblotting. Right panel, quantification of phospho- eIF2α levels by densitometry. Columns represent mean $\pm$ SE (n=6).*P < 0.001, compared with CF-Pac1 and T3M4. B) Effects of silencing eIF2α kinases on basal phospho- eIF2α levels. CF-Pac1 cells were transfected with siRNAs specific for HRI, GCN2, or PERK, or a non-targeting control siRNA (NT). Right panel, columns represent the mean $\pm$ SE (n=3). P < 0.05 compared to NT.

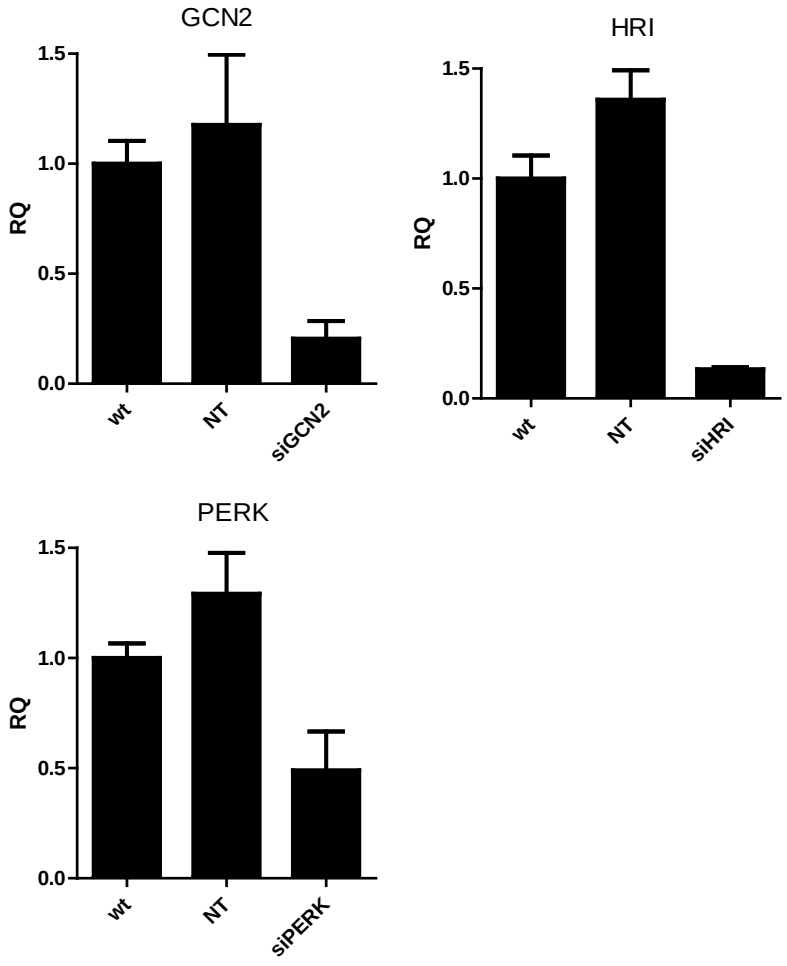

Figure 3.19. Knockdown efficiencies for eIF2α kinase siRNAs in CF-Pac1. *A,* CF-Pac1 cells were transfected with siRNA specific for HRI, GCN2, or PERK for 72h, and kinase expression levels were measured by one-step quantitive RT-PCR. Columns represent mean ± SE (n=3).

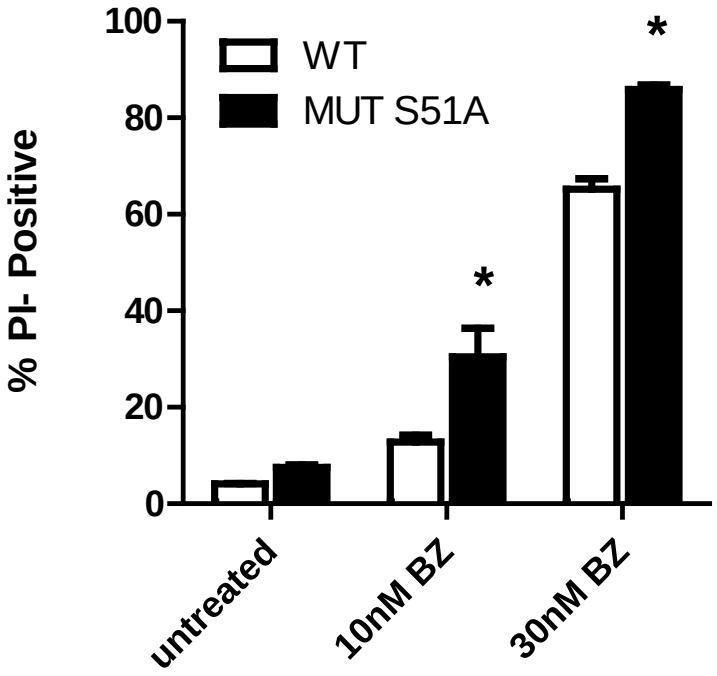

Figure 3.20. Genetic ablation of eIF2α phosphorylation sensitizes cells to bortezomib. Effects of BZ on cell death in wild-type (51SS) and phosphorylation-deficient mutant (51AA) MEFs. Cells were exposed to 10nM bortezomib (BZ) for 72 hours, and cell viability was measured by PI-uptake/FACS analysis. Columns represent mean $\pm$ SE (n=3).*P < 0.05 compared to wild-type 51SS BZ-treated values.

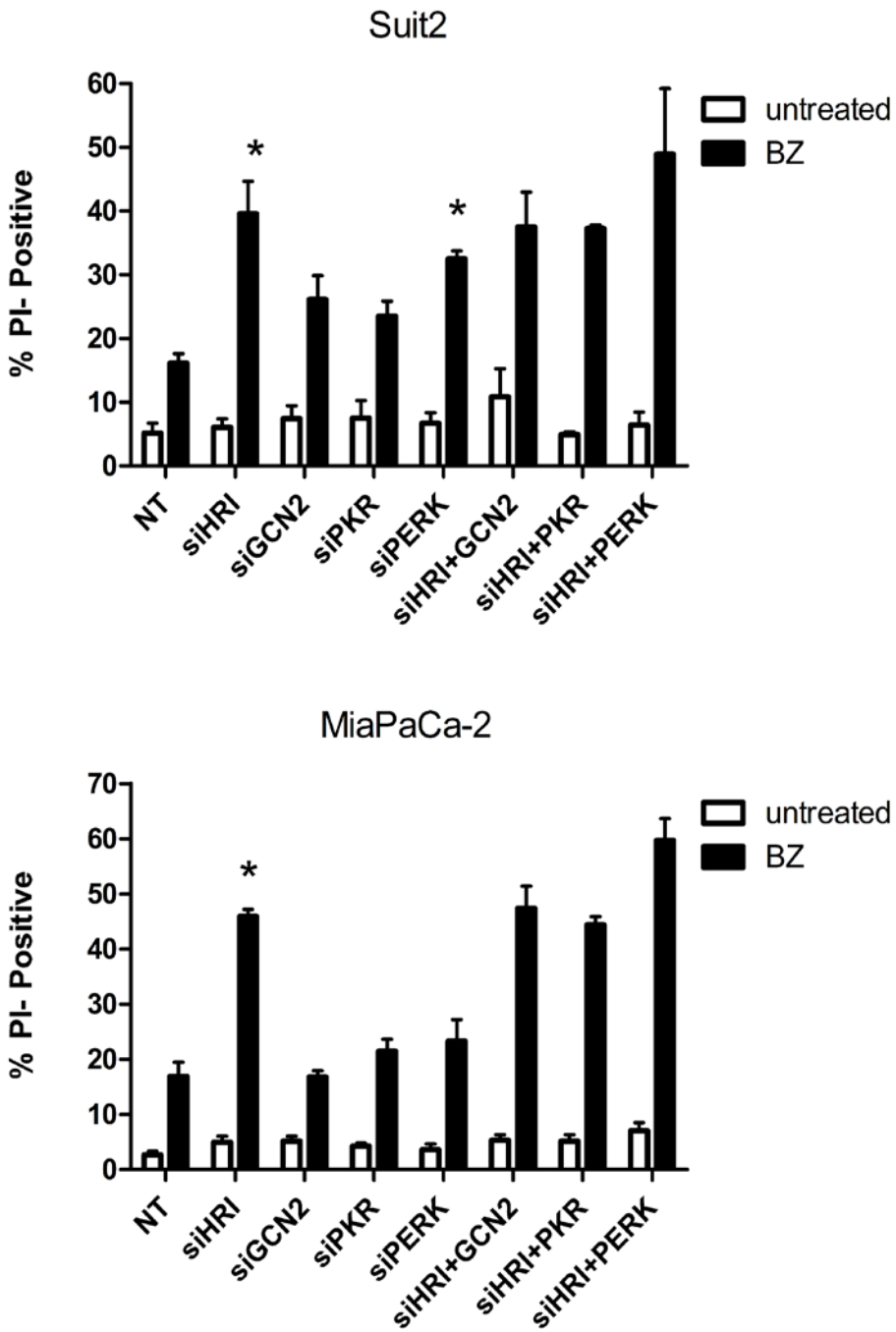

Figure 3.21. HRI knockdown sensitizes cells to bortezomib. siRNA screen examining the effects of eIF2α kinase knockdown on bortezomib sensitivity. Suit2 and MiaPaCa-2 cells were transfected with siRNAs specific for HRI, GCN2, PKR, or PERK, as well as a non-targeting (NT) control siRNA for 72 hours. The cells were then exposed to 30nM bortezomib (BZ) for 48 hours, and cell viability was measured by PI-uptake/FACS analysis. Columns represent mean $\pm$ SE (n=3).*$P < 0.05$ compared to NT BZ-treated values.

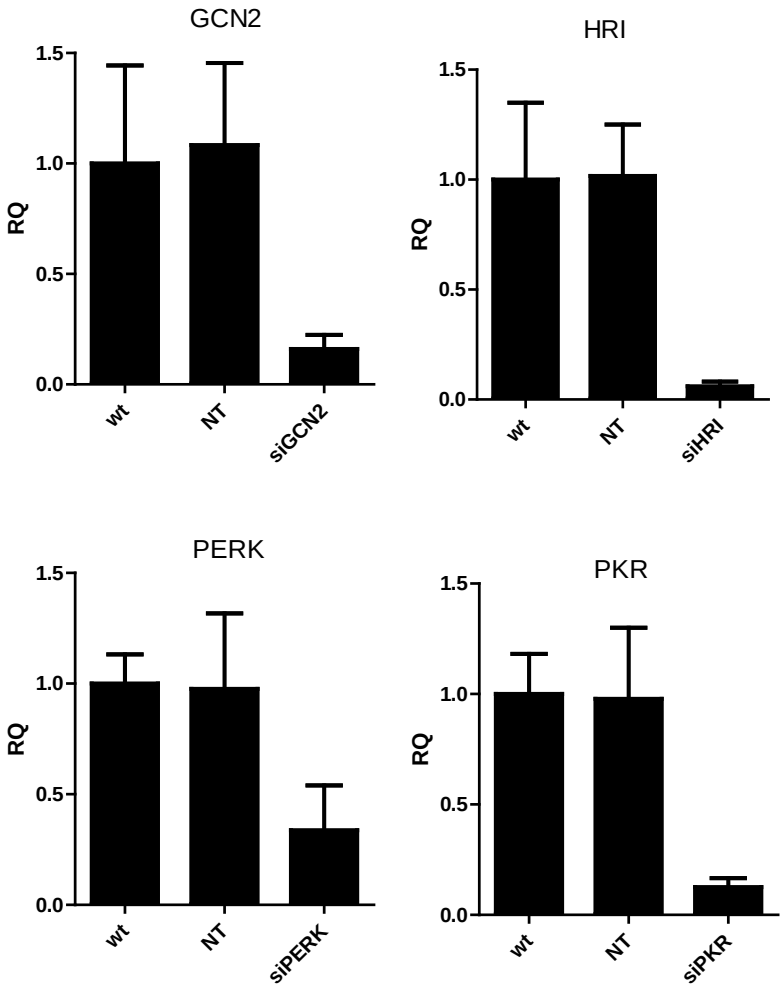

Figure 3.22. Knockdown efficiencies for eIF2α kinase siRNAs in Suit2. Suit2 cells were transfected with siRNA specific for HRI, GCN2, PKR, or PERK for 72h, and kinase expression levels were measured by one-step quantitive RT-PCR. Columns represent mean ± SE (n=3).

3.2.8 *LC3 punctae correlate with phospho-eIF2α levels* – Activation of autophagy has been shown to be a crucial compensatory mechanism in response to proteasome inhibition (116). We previously demonstrated a coupling between eIF2α phosphorylation and autophagy induction following exposure to proteasome inhibitors (71); this coupling has also been observed in cells exposed to other stress stimuli (117, 118). It therefore seemed likely to us that the heterogeneity in eIF2α phosphorylation among our cell lines might also contribute to heterogeneous levels of both basal and drug-induced autophagy. To test this, endogenous microtubule-associated protein light chain 3 (LC3) punctae were measured by immunofluorescence in representative bortezomib-sensitive and -resistant cells. LC3 is conjugated to phosphatidylethanolamine (PE) and incorporated into autophagosomal membranes upon autophagy induction, and visualization of LC3 punctae is a reliable method for measuring formation of autophagosomes and autophagy induction (119, 120). Our data revealed both higher levels of basal autophagy in bortezomib-sensitive T3M4 and CF-Pac1 cells (Fig. 3.23A), and also a less significant increase in bortezomib-induced LC3 punctae formation in these cells when compared with the bortezomib-resistant cell lines (Fig. 3.23B). This is consistent with the pattern of eIF2α phosphorylation seen in our cells, and suggests that inefficient induction of autophagy is another consequence of the impaired eIF2α response that contributes to bortezomib sensitivity in pancreatic cancer cells.

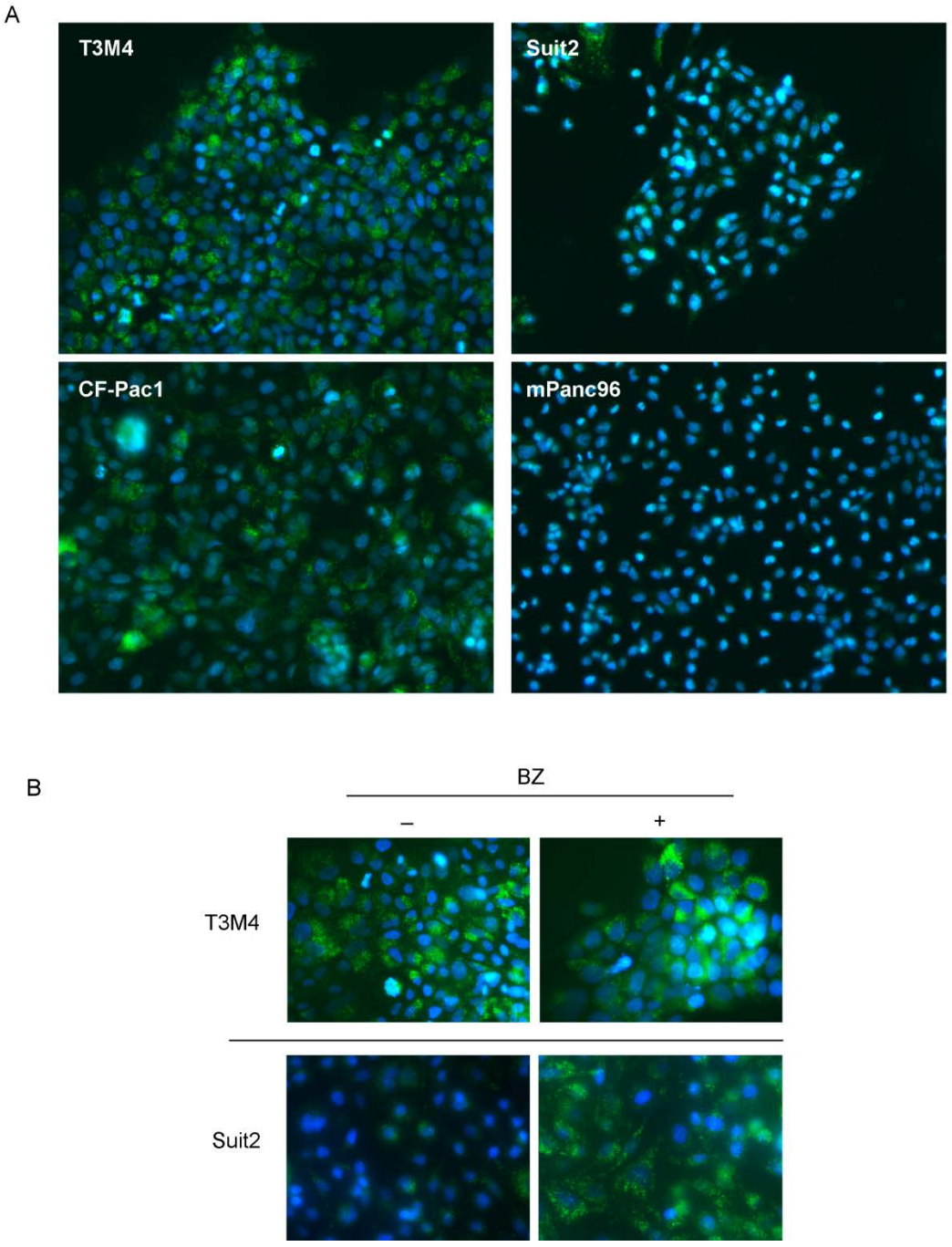

Figure 3.23. High basal eIF2α-P correlates with constitutively high levels of autophagy. A). Basal LC3 immunofluorescence. T3M4, CF-Pac1, Suit2, and mPanc96 cells plated on chamber slides and then probed for LC3 punctae formation. B) BZ-induced LC3 punctae formation. T3M4 and Suit2 cells were exposed to 10nM BZ for 18h prior to staining. Green represents LC3, blue represents nuclear stain. Images are representative of multiple images taken from at least 3 independent experiments.

3.3 Discussion

By attenuating translation and preventing the accumulation of misfolded and aggregated proteins, eIF2α phosphorylation serves to protect cells from proteotoxic stress. Our results show a clear relationship between lack of inducible eIF2α phosphorylation and BZ sensitivity. In highlighting the importance of translational control following proteasome inhibition, our data support the results of a recent study from Millenium Pharmaceuticals in which knockdown of other translation initiation factors (*EIF4E, EIF4G1*) prevented BZ-induced death (121). Similarly, high levels of protein synthesis are known to sensitize multiple myeloma cells to PI's (85). A critical role for eIF2α phosphorylation in resistance to PI's is also supported in MM, where resistant cells phosphorylate and then de-phosphorylate eIF2α in response to PI's, but inhibition of this de-phosphorylation was shown to be sufficient to reverse resistance (122). Others have suggested a pro-apoptotic role for eIF2α phosphorylation following proteasome inhibition (with MG-132) (58), which is contrary to our conclusions. Thus, although induced phosphorylation of eIF2α that remains at high levels and is not attenuated may lead to cell death, our model suggests that transient, inducible, phosphorylation protects cells (see Fig. 3.23), whereas constitutive, un-inducible phosphorylation sensitizes cells to PI's. We discovered that the GCN2 kinase controls this constitutive phosphorylation, but it is presently unclear as to why GCN2 would be activated at baseline in our BZ-sensitive cell lines. It is possible that this is an indication of an underlying metabolic stress resulting from a specific malignant phenotype. Interestingly, GCN2 mRNA expression was 2-3 fold higher in our BZ-sensitive cells (Fig. 3.16). It is unclear as to why the BZ-sensitive cells are unable to modulate levels of phospho- eIF2α in response to stress (both BZ and TG). This could simply be a result

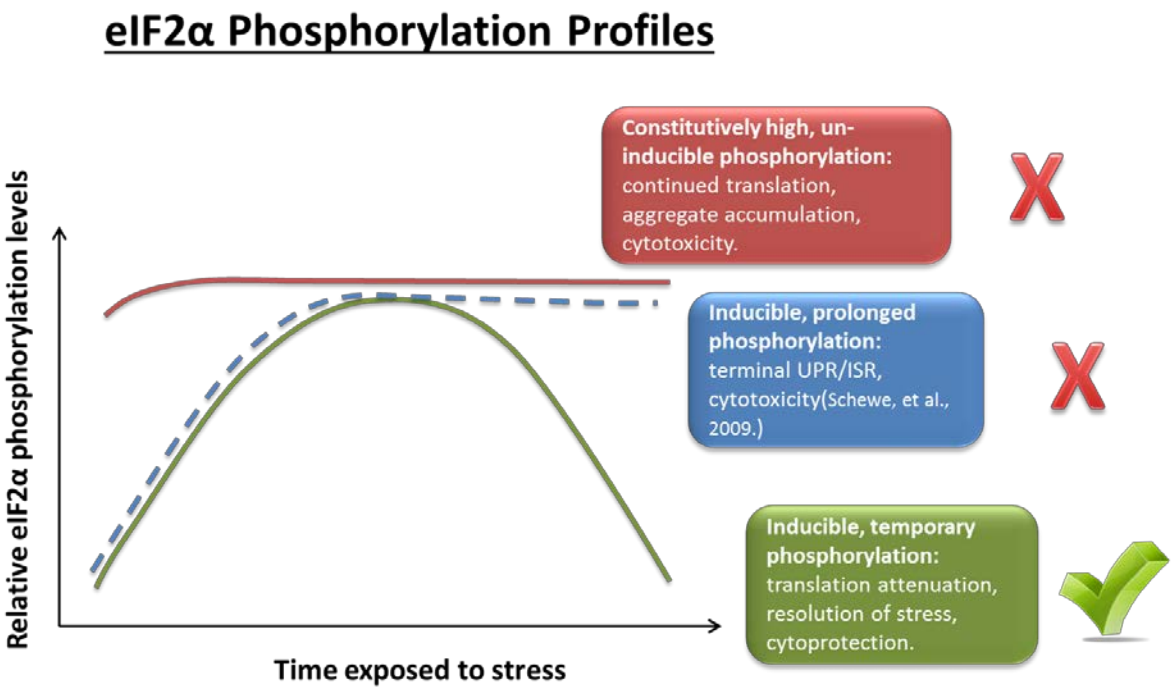

Figure 3.24. Proposed schematic of eIF2α phosphorylation profiles upon proteotoxic stress. Based on data from our study and others, we suggest 3 distinct forms of eIF2α phosphorylation with different downstream consequences: 1) Inducible, temporary phosphorylation = resolution of stress and cytoprotection; 2) Inducible, prolonged phosphorylation = terminal UPR and cytotoxicity (Schewe, et al. 2009); 3) Constitutive, un-inducible phosphorylation = continued protein synthesis and buildup of aggregates, cytotoxicity.

of these cells already having maximal (saturated) phosphorylation, or perhaps be related to a more complex mechanism involving differential regulation of a specific phosphatase (potentially GADD34). Data from lung cancer links high phospo- eIF2α levels to better overall survival (123), and our data suggest that the possibility of constitutive eIF2α phosphorylation as a biomarker for BZ sensitivity should be further explored. In addition, the observation that levels of autophagy vary among our cell lines is particularly relevant in light of a recent study implicating high levels of basal autophagy in pancreatic cancer cells as essential for tumor growth (124). Our study extends these observations by demonstrating that heterogeneity in autophagy levels exists among pancreatic cancer cells that is associated with basal eIF2α phosphorylation. Given that this basal phosphorylation is controlled by the amino acid- and nutrient-sensitive kinase GCN2, it seems likely that the high phospho-eIF2α levels are a symptom of some basal nutrient stress that is driving constitutive autophagy and potentially contributing to bortezomib sensitivity.

We propose that the mechanism behind the toxicity of the aggregates in the BZ-sensitive cell lines is ROS production. Oxidative stress is known to be associated with misfolded protein accumulation in both neurodegenerative (112, 113), as well as non-disease causing proteins (114). Proteasome inhibitors have also been shown to induce ROS (125-127), and recent clinical data in mantle cell lymphoma shows an association between higher ROS levels and improved outcomes following BZ treatment (128). The exact mechanism for how misfolded and aggregated proteins stimulate ROS production is presently unclear, although one possibility is through damaging interactions with cellular phospholipid membranes. Misfolding often exposes buried hydrophobic residues on the surface of proteins, resulting in either an amphipathic or net positive charge. Through electrostatic and

hydrophobic interactions, these toxic species can interact with and destabilize lipid membranes, potentially disrupting membrane receptors and ion pumps. Through this mechanism, ROS (superoxide) could leak through a destabilized outer mitochondrial membrane directly from the intermembrane space, or this could be stimulated by influx of Ca^{2+} ions (129). Increases in intracellular Ca^{2+} levels correlate with exposure to aggregate-prone proteins (130), and we have previously shown that increased Ca^{2+} levels are also associated with proteasome inhibition (88). Our present data strengthen the link between protein aggregation and ROS, and even though our data do not identify the exact mechanism(s) by which protein aggregates stimulate ROS production, oxidative stress is an attractive explanation for the toxicity of protein aggregates.

The nature of the initial and primary stress elicited by PI's is an important unanswered question. Roles for both a cytosolic, heat shock-like stress and ER stress are well documented (32, 33, 110). Through an unbiased, quantitative analysis of both cytosolic (Hsp72) and ER stress (Grp78, CHOP) biomarkers, our data argue that in pancreatic cancer cells, the cytosolic stress component is greater. Induction of Grp78 and CHOP expression by BZ was minimal when to compared to a classic ER stressor such as TG; conversely BZ was a strong inducer of Hsp72 expression whereas TG was not. This model of BZ-induced stress is supported by our kinase activation data, indicating that HRI is more strongly activated than PERK. The concept of BZ as a cytosolic stressor that primarily activates HRI is supported by work detailing similar activation of HRI in erythroid cells following exposure to other cytosolic stressors such as heat shock, arsenic, and osmotic stress (45). HRI has also been linked to BZ-induction of stress granule formation (131). The strong shifts seen in total HRI bands upon BZ exposure (Fig. 3.16) are consistent with activation of HRI by extensive

autophosphorylation (in particular Thr485) (132). The mechanism by which BZ activates HRI likely resembles activation of PERK during ER stress. HRI exists in inactive complexes with molecular chaperones (Hsc70/Hsp72, Hsp90). Upon sensing proteotoxic stress, the repressive chaperones leave HRI to bind misfolded proteins, leaving HRI to become activated. Overall, our model suggests that the shift towards misfolded protein accumulation is the initial stress elicited by BZ, and subsequently HRI is the primary kinase activated. This is contrary to a recent high-profile study arguing that amino acid depletion was the primary stress caused by PI's, and that this led to GCN2 activation and ultimately CHOP-dependent cell death (86). It is highly plausible that by blocking the proteasome, the pool of free amino acids would be perturbed; however, we found no GCN2 activation by BZ in our experiments (Fig. 3.16). In addition, we were unable to prevent BZ-induced cell death by CHOP knockdown, suggesting that CHOP acts differently in our cell lines (Fig. 3.15)

Taken together, our data suggest targeting HRI as a novel strategy to prevent cytoprotective eIF2α phosphorylation and overcome resistance to BZ. $HRI^{-/-}$ mice display normal, fertile phenotypes, with the only complications being minor hematologic defects (44). This points to HRI as potentially amenable to pharmacologic inhibition; presently no specific HRI inhibitors exist, and our study supports the development of such inhibitors for combination with PI's.

Chapter 4. INDUCTION OF HSP72 AS A CYTOPROTECTIVE RESPONSE TO BORTEZOMIB IN BLADDER CANCER CELLS

4.1 Introduction

The heat shock response (HSR) is strongly activated by proteasome inhibition. Many similarities exist between heat shock and proteasome inhibition: they both function primarily to increase the titer of misfolded proteins within the cytosol. The major chaperone induced by the HSR is an inducible isoform of the Hsp70 family; Hsp72, which functions to ensure proper protein folding and prevent aggregation. In addition, other cytoprotective functions have been attributed to Hsp72 such as lysosomal stabilization and inhibition of apoptosis (133-135). The centrality of Hsp72 as a cytoprotective factor in response to stress is highlighted by its extraordinary conservation throughout evolution, existing relatively unchanged from *E. coli* to mammals (136). The Hsp70 family of chaperones contains multiple isoforms, although not all are part of the inducible HSR. In order to clarify this discussion, a brief outline of nomenclature is useful. In humans, up to 13 different isoforms have been proposed – HSPA1A, HSPA1B, HSPA1L, HSPA2, HSPA5, HSPA6, HSPA7, HSPA8, HSPA9, HSPA12A, HSPA12B, HSPA13, and HSPA14 (137). Of these, six function in the cytosol and nucleus, whereas two are localized to the ER and mitochondria (HSPA5 and HSPA9, respectively). HSPA5 is better known as Grp78/BiP, and will be referred to as such. Of the cytosolic HSPA members, HSPA2 is expressed primarily in both the testis and the brain, whereas HSPA1L is almost exclusively expressed in the testis. Conversely, HSPA8 is constitutively expressed in most tissues, and is referred to as heat shock cognate 70, or Hsc70. Little is known about HSPA12-HSPA14. Importantly, only three of the HSPA family members are known to be stress-inducible: HSPA1A, HSPA1B, and HSPA6. HSPA1A and HSPA1B genes are located adjacent to one another on

Table 1 HSP70 superfamily: HSPA (HSP70) and HSPH (HSP110) families

	Gene name	Protein name	Old names	Human gene ID	Mouse ortholog ID
HSP A					
1	HSPA1A	HSPA1A	HSP70-1; HSP72; HSPA1	3303	193740
2	HSPA1B	HSPA1B	HSP70-2	3304	15511
3	HSPA1L	HSPA1L	hum70t; hum70t; Hsp-hom	3305	15482
4	HSPA2	HSPA2	Heat-shock 70kD protein-2	3306	15512
5	HSPA5	HSPA5	BIP; GRP78; MIF2	3309	14828
6	HSPA6	HSPA6	Heat shock 70kD protein 6 (HSP70B′)	3310	X
7	HSPA7[a]	HSPA7	Heat shock 70kD protein 7	3311	X
8	HSPA8	HSPA8	HSC70; HSC71; HSP71; HSP73	3312	15481
9	HSPA9	HSPA9	GRP75; HSPA9B; MOT; MOT2; PBP74; mot-2	3313	15526
10	HSPA12A	HSPA12A	FLJ13874; KIAA0417	259217	73442
11	HSPA12B	HSPA12B	RP23-32L15.1; 2700081N06Rik	116835	72630
12	HSPA13[b]	HSPA13	Stch	6782	110920
13	HSPA14	HSPA14	HSP70-4; HSP70L1; MGC131990	51182	50497
HSP H					
1	HSPH1	HSPH1	HSP105	10808	15505
2	HSPH2[b]	HSPH2	HSPA4; APG-2; HSP110	3308	15525
3	HSPH3[b]	HSPH3	HSPA4L; APG-1	22824	18415
4	HSPH4[b]	HSPH4	HYOU1/Grp170; ORP150; HSP12A	10525	12282

[a] Annotated as pseudogene, but possibly a true gene
[b] Under consultation with HGNC and the scientific community

Table 4.1. Hsp70 chaperone family proposed nomenclature. Systematic re-naming of known Hsp70 family chaperones, shown adjacent to traditional names found in the literature.

chromosome 6 (6p21.3 region), and encode functionally identical proteins that differ in sequence by only two amino acids. Between the two, the HSPA1A isoform is typically expressed at levels 2-3 times higher than HSPA1B. For the purposes of this thesis, Hsp72 will refer to the total protein encoded by the two isoforms, HSPA1A and HSPA1B.

Hsp72's role in cancer is has been well documented (138, 139). Increased expression of Hsp72 is commonly found in human tumors (11), and is thought to help manage the stress of a malignant phenotype and offer resistance to apoptosis (133, 140). Notably, Hsp72 is strongly induced by certain chemotherapeutic agents, especially proteasome inhibitors (32, 33). Induction of heat shock proteins is implicated in resistance to proteasome inhibitors such as bortezomib (BZ) (141, 142).

Our group previously investigated the cytotoxic effects of BZ on bladder cancer cells within the context of combination therapy (143, 144). In this study, we sought to screen a larger panel of bladder cancer cells for sensitivity to BZ, and to determine cytoprotective mechanisms that may be contributing to BZ resistance. We identified the Hsp72 chaperone as one of the most highly induced genes in bladder cancer cells exposed to BZ, therefore, we hypothesized that Hsp72 induction likely was a potent inhibitor of BZ-induced cell death in bladder cancer. Here, we discovered that in a subset of bladder cancer cells, BZ robustly induced Hsp72 protein levels, but discovered that HSPA1A and HSPA1B mRNA expression differed dramatically between cell lines. Some cell lines (253JB-V and SW780) expressed both HSPA1A and A1B mRNA; however others (UM-UC10 and UM-UC13) expressed almost undetectable levels of HSPA1A but highly expressed the A1B isoform. This was found to be a result of decreased HSF1 binding at the HSPA1A promoter in these cells because of heavy DNA methylation in the region. Knockdown of HSPA1B in UM-UC10

cells depleted Hsp72 protein levels and enhanced BZ sensitivity, whereas overexpression of HSPA1A in UM-UC10 and –UC13 raised total Hsp72 protein levels and inhibited BZ-induced cell death. Knockdown of total Hsp72 sensitized resistant 253JB-V cells to bortezomib both *in vitro* and *in vivo*, and chemical inhibition of HSF1 also sensitized these cells *in vitro*. Overall, this study supports the further development of HSF1 and Hsp72 inhibitors for cancer therapy, and also further investigation of the etiology and functional significance of HSPA1A promoter methylation in bladder and other solid tumors.

4.2 Results

4.2.1 Differential induction of HSPA1A in bladder cancer cells. We selected four representative human bladder cancer cell lines (253J B-V, SW780, UM-UC10, and UM-UC13) for characterization of the molecular biological mechanisms that determine cellular responsiveness to the proteasome inhibitor bortezomib. We first confirmed that the cell lines were heterogeneous with respect to their sensitivities to bortezomib-induced cell death as determined using propidium iodide staining and FACS analysis (PI-FACS) to measure loss of plasma membrane integrity (Fig. 4.2). We then used whole genome mRNA expression profiling (Illumina platform) to identify the gene expression patterns associated with drug sensitivity and/or resistance. Bortezomib induced strong dose-dependent upregulation of mRNA encoding the major inducible isoform of Hsp72 (HSPA1A) in the most bortezomib-resistant cell line (253J B-V) but not in the most drug-sensitive line (UM-UC13) (Fig. 4.3). We confirmed these results using quantitative real-time RT-PCR, demonstrating that HSPA1A mRNA was strongly induced by bortezomib in 253JB-V and SW780 cells (~25-60 fold over untreated levels), whereas expression increased only slightly

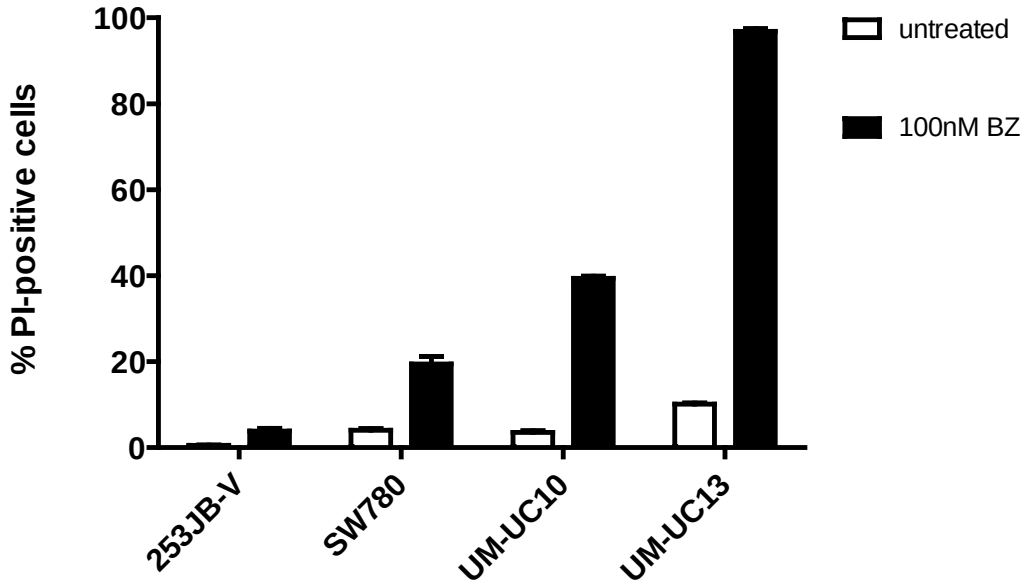

Figure 4.1. Bortezomib-induced cell death in subset of bladder cancer cell lines. Effects of bortezomib on cell death. Bladder cancer cell lines were incubated with or without 100nM bortezomib for 24 hours and PI/FACS was used to quantify cell death. Mean ± SEM, n = 3.

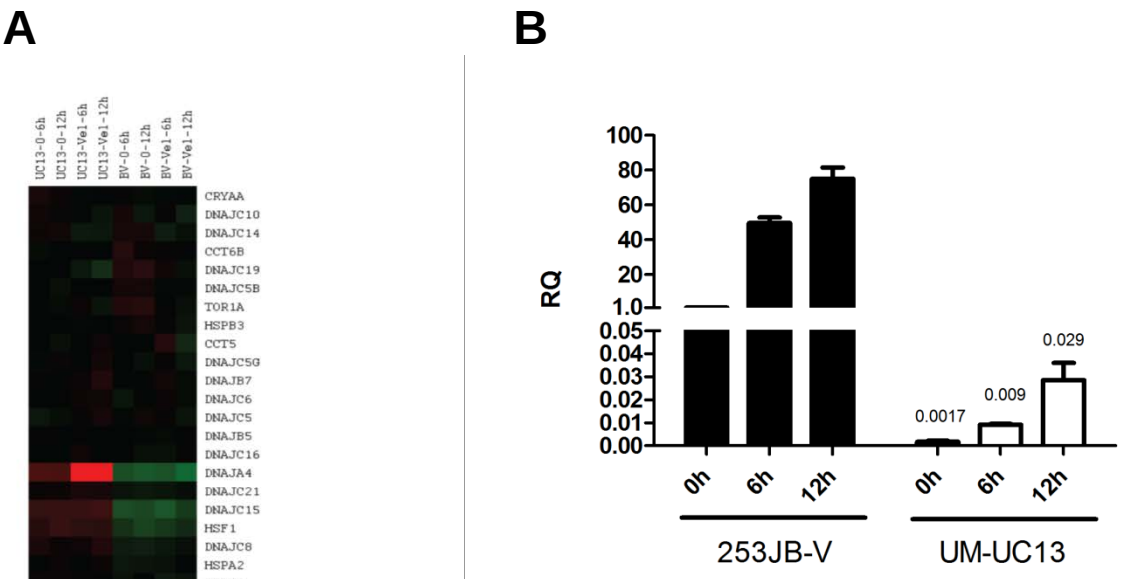

Figure 4.2 Bortezomib fails to induce HSPA1A in BZ-sensitive bladder cancer cells. A) Heat map depicting the effects of bortezomib on gene expression in 253J B-V and UM-UC13 cells. Cells were incubated with or without bortezomib for 6 or 12 h, and global gene expression patterns were compared using the Illumina platform. (Arrow designates HSPA1A). B) Validation of differential bortezomib-mediated HSPA1A induction by quantitative real-time PCR. The same RNA samples from UM-UC13 and 253JB-V used in microarray analyses and an independent set of RNA samples were subjected to real-time PCR analysis to measure the level of HSPA1A expression. Values represent mean ± SEM (N≥3).

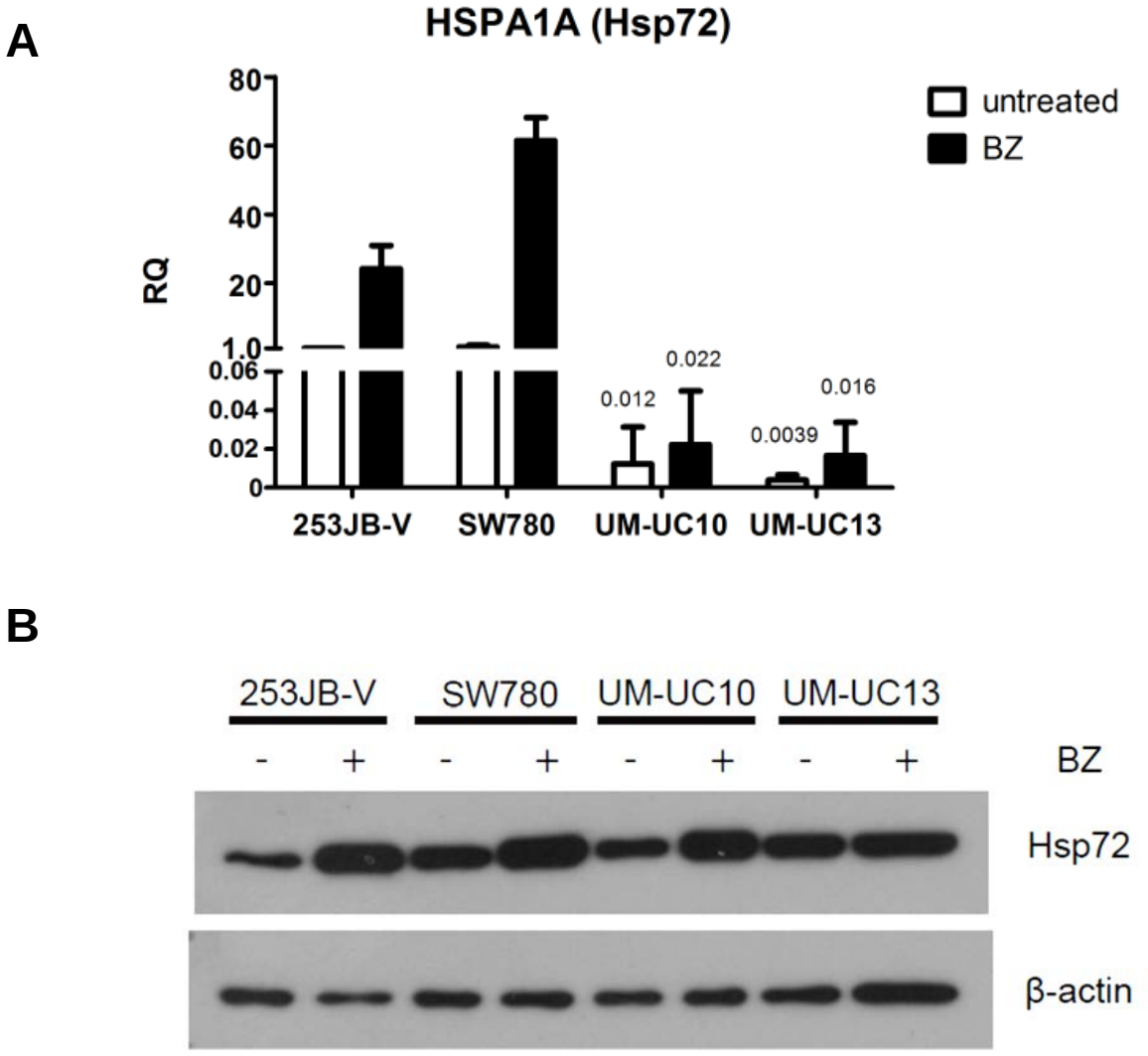

Figure 4.3 Comparison of HSPA1A mRNA and Hsp72 protein levels among bladder cancer cells. A) Effects of bortezomib on the mRNA expression of Hsp72 isoform HSPA1A in 4 bladder cancer cell lines (253JB-V, SW780, UM-UC10, UM-UC13). Cells were exposed to 30nM bortezomib for 6 h and HSPA1A was measured by quantitative RT-PCR. RQ = relative quantity (to GAPDH). Values represent mean ± SEM (N≥3) B) Effects of bortezomib on Hsp72 protein levels. Cells were incubated for 16-18 h with 30nM of bortezomib, and Hsp72 levels were measured in whole cell lysates by immunoblotting. Blots are representative of two independent experiments.

induced (~2-4 fold over untreated levels) in UM-UC10 and UM-UC13 cells (Fig. 4.4A). We also noticed very low basal HSPA1A mRNA expression in UM-UC10 and UM-UC13 cells (~50-250 fold lower than 253JB-V and SW780) and these differences were exacerbated upon bortezomib exposure such that HSPA1A expression levels were ~1000-3000 fold lower in UM-UC10 and UM-UC13 cells than in 253JB-V and SW780 (Fig. 4.4A). However, immunoblotting revealed comparable Hsp72 protein levels in all 4 cell lines (Fig. 4.4B).

4.2.2 HSPA1B isoform compensates for loss of HSPA1A expression in UM-UC10 and UM-UC13 cells. Hsp72 is encoded by two independent genetic loci (HSPA1A and HSPA1B) that produce highly homologous protein products. We therefore characterized HSPA1B expression in the HSPA1A^{low} cells. We used primers specific for the two isoforms of Hsp72, HSPA1A and HSPA1B, as well as a primer that recognized both (pan) isoforms for comparison. Our data revealed that the HSPA1A^{low} cells (UM-UC10, UM-UC13) had higher expression of the HSPA1B isoform at baseline than did the HSPA1A-high cells (253JB-V, SW780) (Fig. 4.5A). In addition, HSPA1B expression was more robustly induced following bortezomib exposure in the HSPA1A^{low} cells lines that lacked the A1A isoform (Fig. 4.5B). Importantly, expression measured by the pan-primer was similar across all four cell lines, corroborating the immunoblotting data (Fig. 4.4B). These data suggest that increased HSPA1B expression compensated for the lack of HSPA1A and accounted for the Hsp72 protein expression in the UM-UC10 and UM-UC13 cells.

4.2.3 Lack of HSPA1A inducibility in UM-UC10 and UM-UC13 cells is due to promoter methylation. Heat shock factor-1 (HSF1) activation controls the global heat shock response

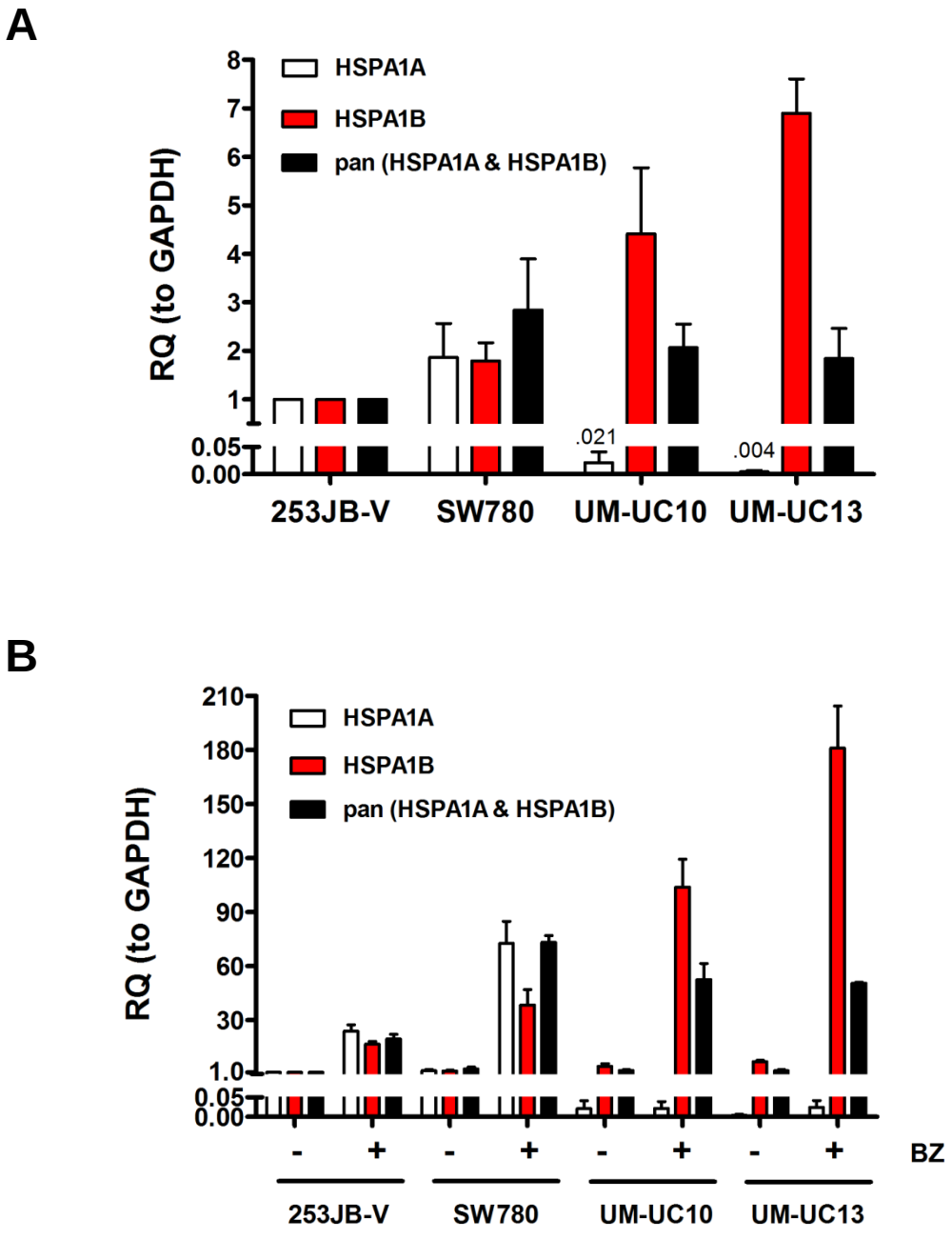

Figure 4.4 Increased HSPA1B expression compensates for loss of HSPA1A expression in UM-UC10 and UM-UC13 cells. A. Basal expression of HSPA1A and HSPA1B isoforms across the four cell lines. **B.** Bortezomib-induced expression of HSPA1A and HSPA1B across the four cell lines. Specific primers for each isoform, as well as a pan-primer that recognized both isoforms, were used to measure expression by quantitative RT-PCR. Values represent mean $\pm$ SE (n = 2).

and stress-induced upregulation of Hsp72 (145). To test whether HSF1 expression was influencing differences in HSPA1A expression among our cell lines, we measured HSF1 mRNA and protein levels in the 253JB-V ($HSPA1A^{high}$) and UM-UC13 ($HSPA1A^{low}$) cells. We observed modest differences in basal and BZ-induced HSF1 mRNA levels between 253JB-V and UM-UC13 cells; specifically, 253JB-V showed a 2-fold increase in HSF1 levels upon drug exposure, whereas UM-UC13 showed only ~1.3 fold increase, but had 2-fold higher HSF1 mRNA expression at baseline than did 253JB-V (Fig. 4.6A). However, protein levels appeared essentially equal between both cell types (Fig. 4.6B). Furthermore, other HSF1 targets were strongly induced, including the aforementioned HSPA1B (Fig. 4.5) and DNAJB1 (Hsp40) (Fig. 4.7) in the UM-UC10 and UM-UC13 cells, suggesting that there was no generalized defect in endogenous HSF1 activation in these cells. We therefore reasoned that the UM-UC10 and UM-UC13 cells might possess specific defect(s) in HSF1-mediated activation of the HSPA1A promoter. Consistent with this idea, chromatin immunoprecipiation (ChIP) revealed that 253J B-V cells possessed higher levels of HSF1 binding to the HSPA1A promoter at baseline and following bortezomib exposure than did UM-UC13 (~2-fold and ~5-fold higher, respectively) (Fig. 4.8). The fold-induction of HSF1 binding by bortezomib was ~9-fold vs. ~4-fold in 253JB-V and UM-UC13, respectively. Analysis of the HSPA1A promoter using the UCSC Genome Browser revealed that it lies within a CpG island that is methylated in other cancer cell lines (Fig 4.9). Using methylation-specific PCR, we confirmed that the HSPA1A promoter was strongly methylated in the UM-UC10 and UM-UC13 but not in the 253J B-V or SW780 cells (Fig.4.10A), which possibly accounted for defective bortezomib-induced HSPA1A

A

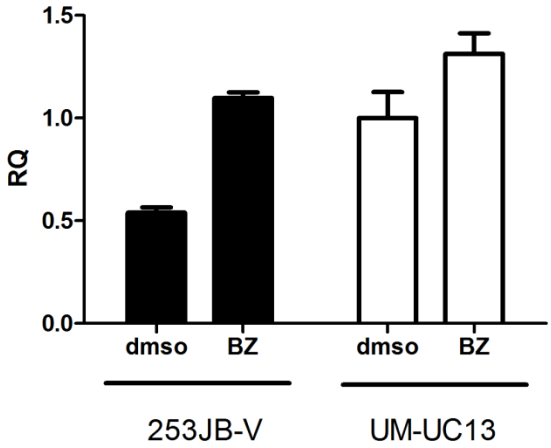

B

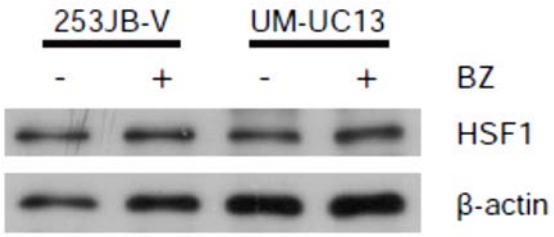

Figure 4.5 Examination of HSF1 mRNA and protein levels between HSPA1A^{high} and HSPA1A^{low} cells. Expression of HSF1. 253J B-V and UM-UC13 bladder cancer cell lines were exposed to bortezomib for 12 h and A) HSF1 mRNA expression (columns represent mean ± SE n=2) and B) protein levels (representative of two independent experiments) were measured by quantitative RT-PCR and immunoblotting, respectively.

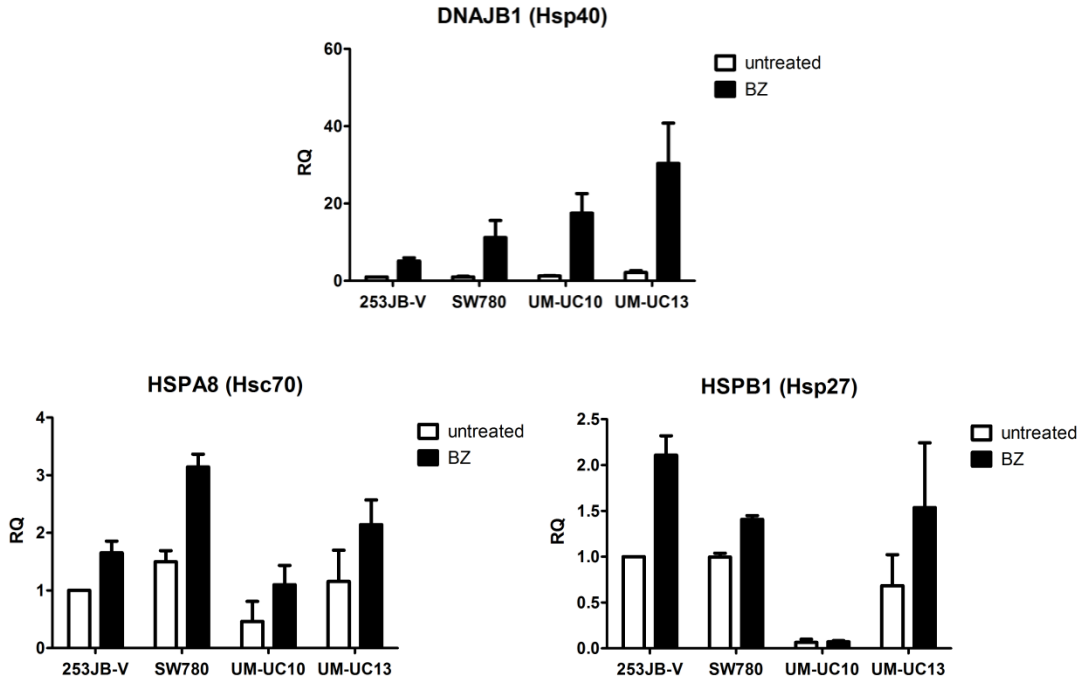

Figure 4.6 Bortezomib-induced expression of other HSF1 targets. Effects of bortezomib on endogenous transcriptional targets of HSF1. Bortezomib-resistant (253J B-V, SW780) and –sensitive (UM-UC10, UM-UC13) cells were incubated with 30nM bortezomib for 6 h and HSF-1 target induction was measured by quantitative RT-PCR. Note that induction of other HSF1 targets (i.e., HSP40, HSP27) still occurred in HSPA1A^{low} UM-UC10 and UM-UC13 cells. Mean ± SEM, n = 3.

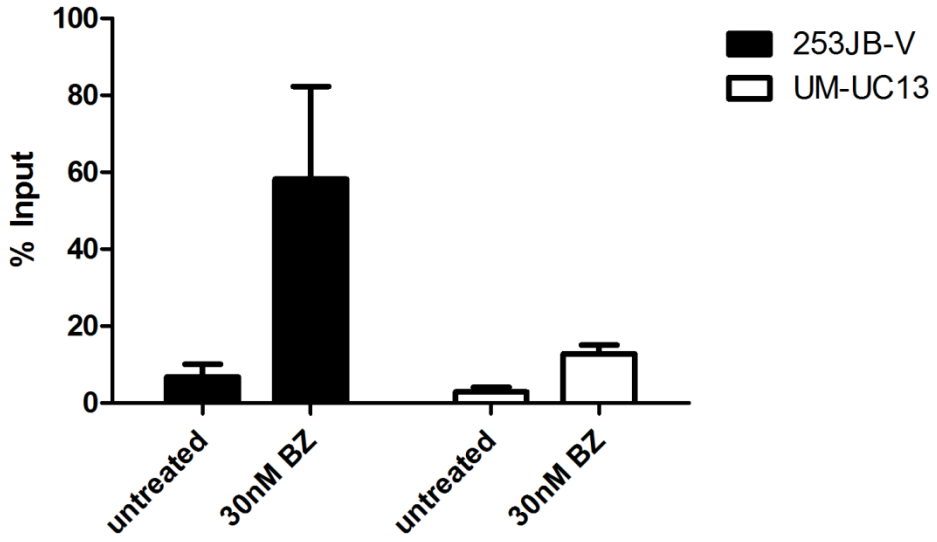

Figure 4.7 Reduced HSF1 binding to HSPA1A promoter region in sensitive cells. Chromatin immunoprecipitation (ChIP) analysis of HSF1 binding to the HSPA1A promoter. Note that basal and bortezomib-induced HSF1 binding is greatly reduced in the bortezomib-sensitive UM-UC13 cells.

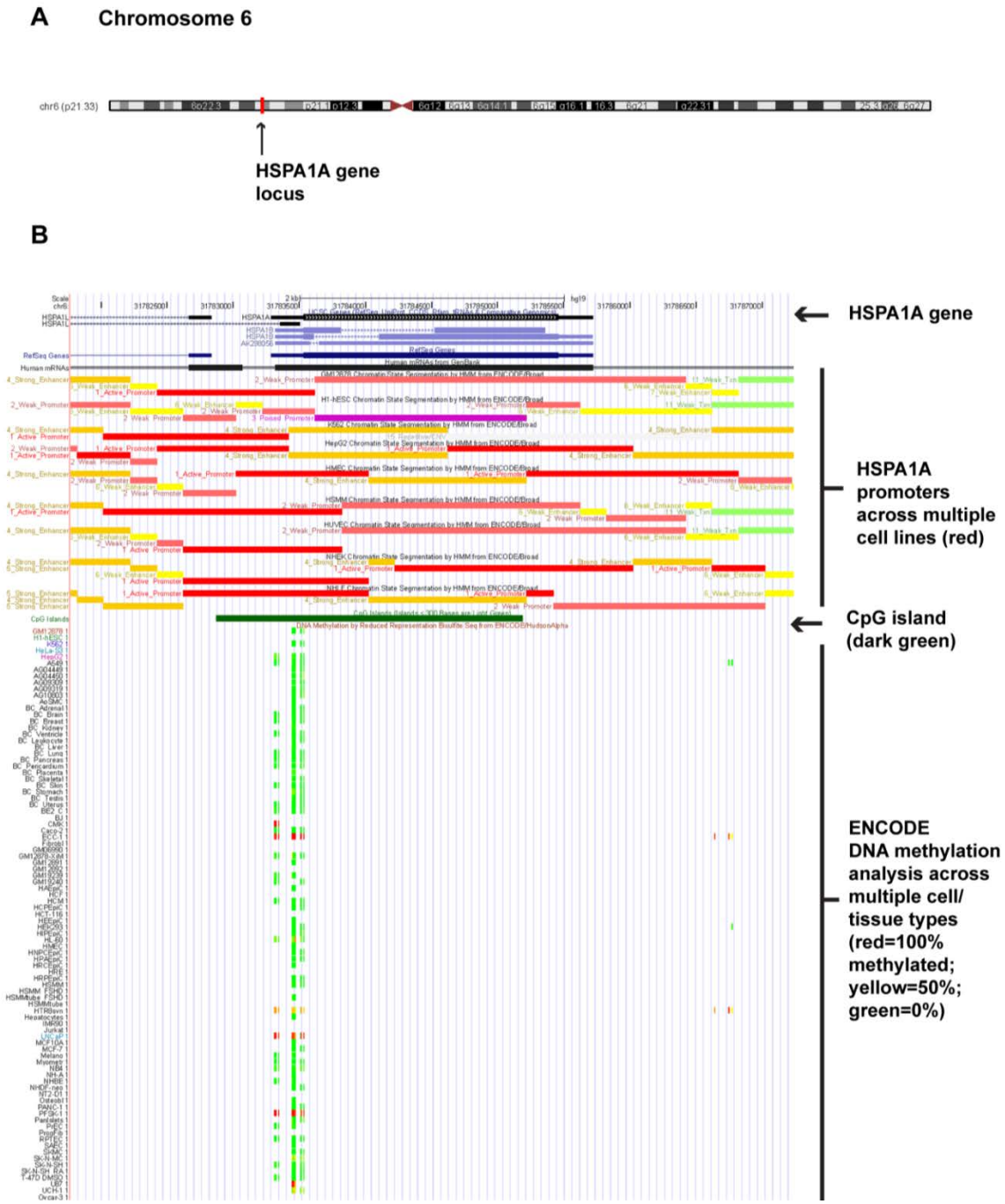

Figure 4.8 The HSPA1A promoter contains a CpG island that is commonly methylated in cancer. A) HSPA1A gene locus on Chromosome 6. Specific location is 6p21.3. B) UCSC Genome Browser screenshot depicting a CpG island (dark green bar) at HSPA1A consensus promoter regions in multiple cell lines (red bars). Below, DNA methylation analysis of the HSPA1A promoter region across multiple cell lines and tissues types. Unmethylated= green; 50% methylated = yellow; 100% methylated= red. Note that 8 out of 9 cell lines with significant methylation (orange-red color) were derived from human tumors.

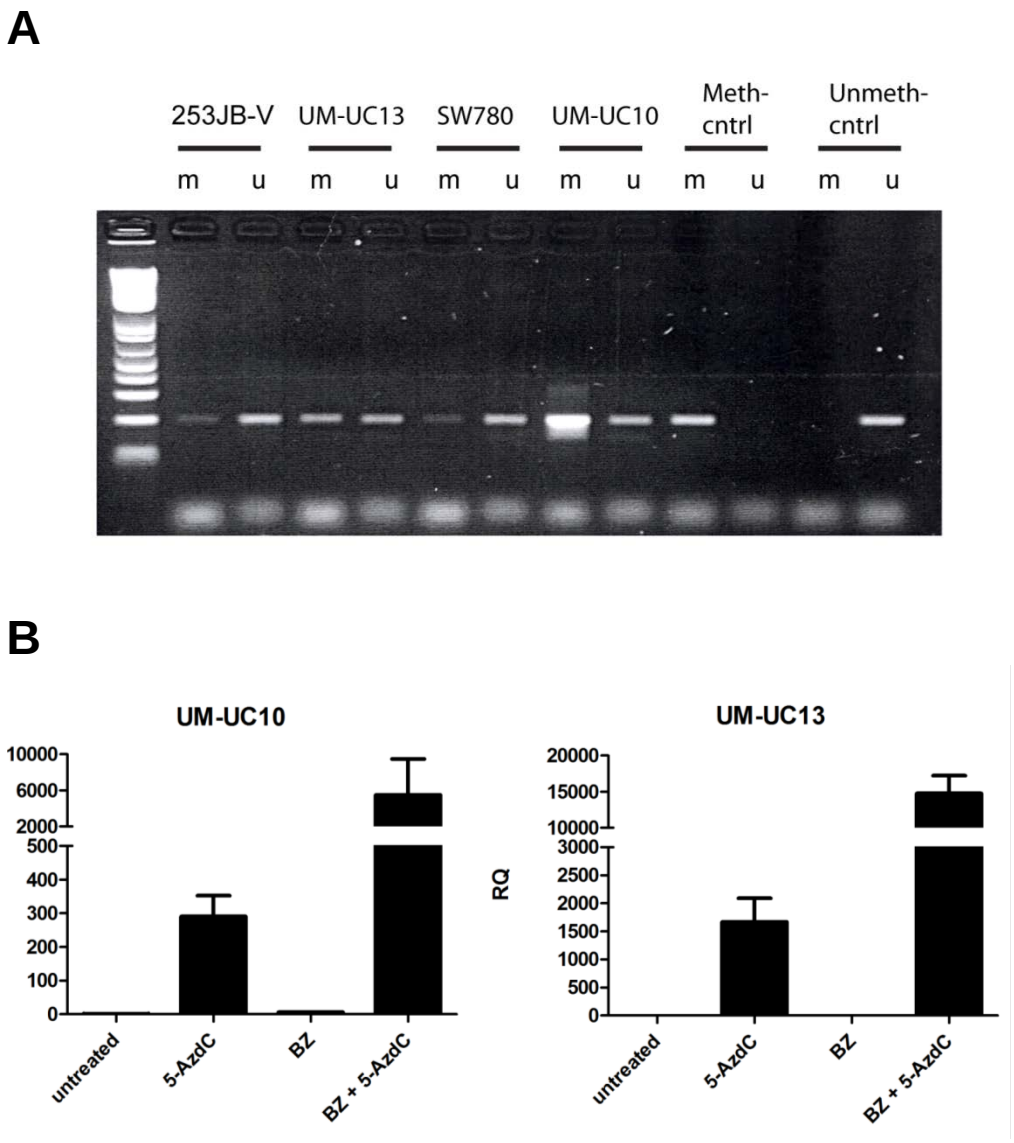

Figure 4.9 Methylation of the HSPA1A promoter in bortezomib-sensitive human bladder cancer cells. A) Methylation-specific PCR was used to assess chromatin methylation in drug-sensitive (UM-UC10, UM-UC13) and drug-resistant (253J B-V, SW780) cell lines as described in Materials and Methods. m, methylated; u, unmethylated. B) The DNA methyltransferase inhibitor 5-aza-2'-deoxycytidine restores HSPA1A expression in bortezomib-sensitive cells. Cells were incubated with 5 μM 5-AC for 5 days and then incubated with or without 30nM bortezomib for 6 h, and HSPA1A expression was measured by quantitative real-time PCR. Mean ± SEM, n = 3.

induction. To directly test this possibility, we examined the effects of the histone methyltransferase inhibitor 5-aza-2'-deoxycytidine on basal and bortezomib-induced HSPA1A mRNA levels in the UM-UC10 and UM-UC13 cells. The inhibitor induced large increases in both basal and proteasome inhibitor-induced HSPA1A levels in both bortezomib-sensitive cell lines (Fig. 4.10B). Together, these results demonstrate that chromatin methylation is responsible for the defective HSPA1A induction observed in UM-UC10 and UM-UC13 cells.

4.2.4 Modulation of HSPA1A and HSPA1B expression in the HSPA1A^{low} cells. Since UM-UC10 and UM-UC13 lacked HSPA1A expression, we examined whether replacing the HSPA1A isoform would promote bortezomib resistance. To address this, we stably overexpressed HSPA1A in both UM-UC10 and -UC13 cells using a lentiviral vector. HSPA1A mRNA expression was confirmed using qRT-PCR and Hsp72 total protein increases by immunoblotting (Fig. 4.11A). HSPA1A overexpressing cells and empty vector transduced cells were then exposed to bortezomib and we discovered that overexpression significantly reduced bortezomib-induced cell death (Fig. 4.11B). Conversely, because UM-UC10 and -UC13 cells appeared to be relying solely on HSPA1B mRNA for Hsp72 protein expression, we hypothesized that these cells may be particularly susceptible to targeting of HSPA1B. To test this, we used siRNA to transiently silence HSPA1B in UM-UC10 cells. Analysis of knockdown efficiencies revealed that the commercially available siRNAs cannot specifically target individual isoforms (i.e., siHSPA1A silenced HSPA1B) (Fig. 4.12A). Nonetheless, a combination of siHSPA1A and siHSPA1B sequences yielded the best (though not complete) overall knockdown of the A1B isoform at both the RNA and protein

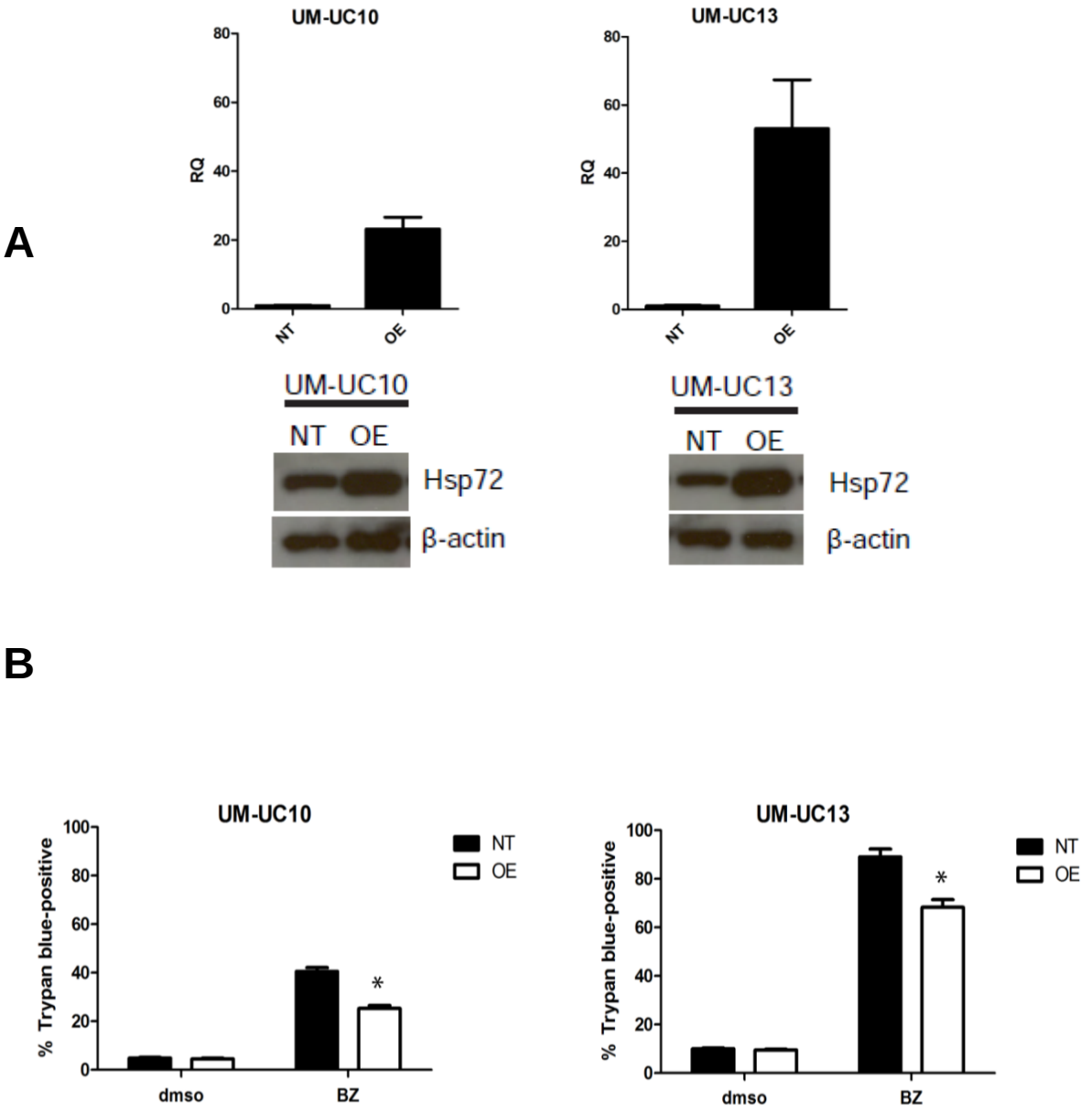

Figure 4.10 Overexpression of HSPA1A reduces bortezomib-induced cell death in HSPA1A^{low} cells. A) Effects of enforced HSPA1A overexpression on HSPA1A levels in UM-UC10 and UM-UC13 cells. Cells were stably transduced with a lentiviral HSPA1A expression construct, and HSPA1A levels were measured by quantitative RT-PCR. Mean ± SEM, n = 3. Protein levels of Hsp72 were measured by immunoblotting (blots representative of two independent experiments). B) Effects of HSPA1A overexpression on bortezomib-induced cell death. Cells transduced with empty vector (NT) or with the HSPA1A expression construct were exposed to 30 nM bortezomib for 24 h and plasma membrane integrity was measured by trypan blue uptake. (The presence of RFP in the expression construct prevented our use of the PI/FACS cell death assay.) Mean ± SEM, n = 3. *, $p<0.02$

level (Fig. 4.12B). Using this strategy, we confirmed that blockade of HSPA1B induction sensitized UM-UC10 cells to bortezomib (Fig. 4.13).

4.2.5 Hsp72 induction inhibits bortezomib-induced cell death. To more directly determine whether bortezomib-induced Hsp72 upregulation promoted resistance, we stably knocked down Hsp72 in 253JB-V bortezomib-resistant cells using a lentiviral shRNA vector. Baseline HSPA1A mRNA levels were reduced by more than 75% in the cells, but shRNA-mediated suppression of HSPA1A mRNA (Fig. 4.14A) and Hsp72 protein (Fig. 4.14B) was less impressive following exposure to bortezomib, presumably because the proteasome inhibitor produced such a strong upregulation of Hsp72. Nonetheless, stable Hsp72 knockdown significantly enhanced bortezomib-induced loss of plasma membrane integrity as measured by propidium iodide uptake (Fig. 4.14C). Previous studies concluded that Hsp72 induction serves a cytoprotective function within the integrated stress response (ISR) by stabilizing lysosomes (134). As such, we compared the effects of bortezomib on lysosomal integrity in the 253JB-V cells transduced with control vector (253JB-V NT) or the KD9 HSPA1A-specific shRNA construct. Bortezomib had little to no effect on lysosomal integrity in the 253JB-V NT cells but induced strong, concentration-dependent loss of lysosomal integrity in the 253JB-V-KD9 cells (Figure 4.15). Together, these results confirm that bortezomib-induced Hsp72 induction functions to promote lysosomal integrity and to inhibit cell death. Finally, we examined whether pharmacologic HSF1 inhibition would also promote bortezomib-induced cell death. The chemical HSF1 inhibitor KNK-437 strongly attenuated bortezomib-induced HSPA1A induction (Fig. 4.16A) and promoted cell

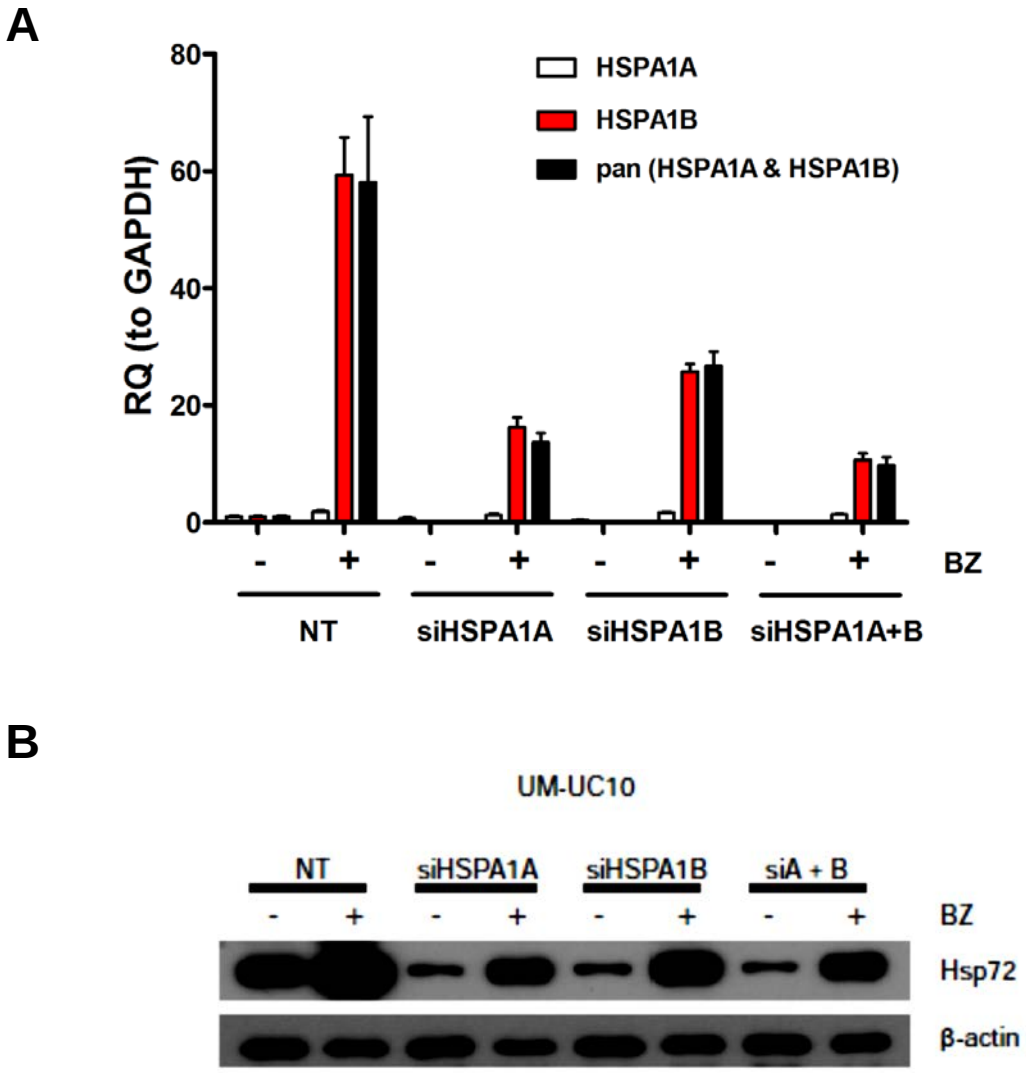

Figure 4.11 Knockdown of HSPA1B in HSPA1A^{low} cells. Knockdown of HSPA1B in UM-UC10 cells. A) knockdown efficiencies of siRNA against HSPA1A, HSPA1B, or both isoforms as measured by quantitative RT-PCR following exposure to 30nM bortezomib for 6 h. B) corresponding knockdown of Hsp72 protein levels by the difference siRNA sequences following exposure to 30nM BZ for 14 h. Data are representative of two independent experiments.

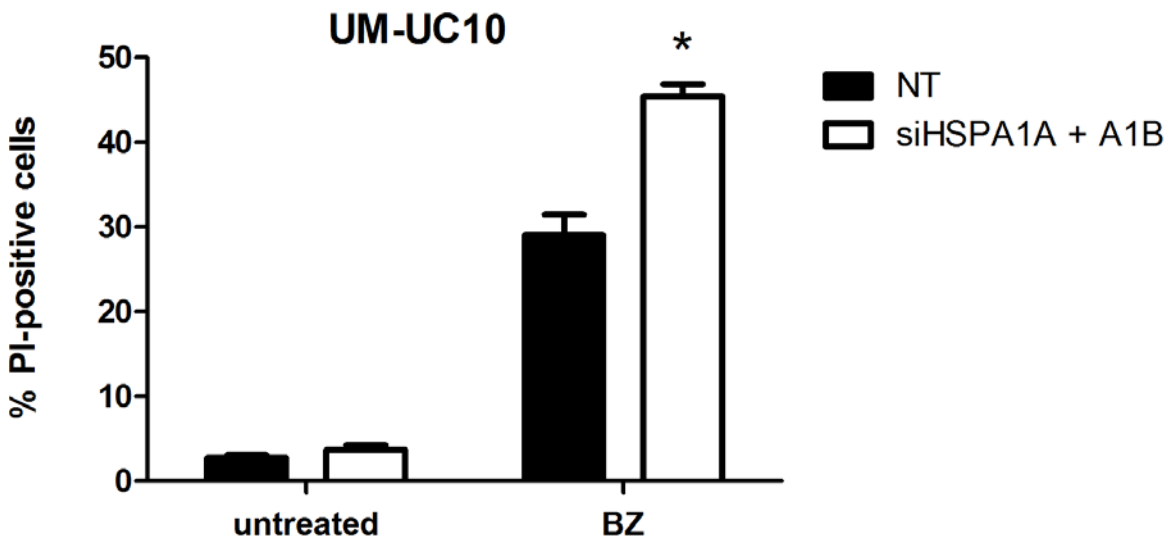

Figure 4.12 Knockdown of HSPA1B enhances BZ-induced cell death in HSPA1A^{low} cells. Effect of HSPA1B knockdown on bortezomib-induced cell death in UM-UC10 cells. Following 72 h knockdown, cells were exposed to 30nM bortezomib for 24 h and cell death measured by PI/FACS analysis. Values represent mean $\pm$ SE (n=3).*P<0.05.

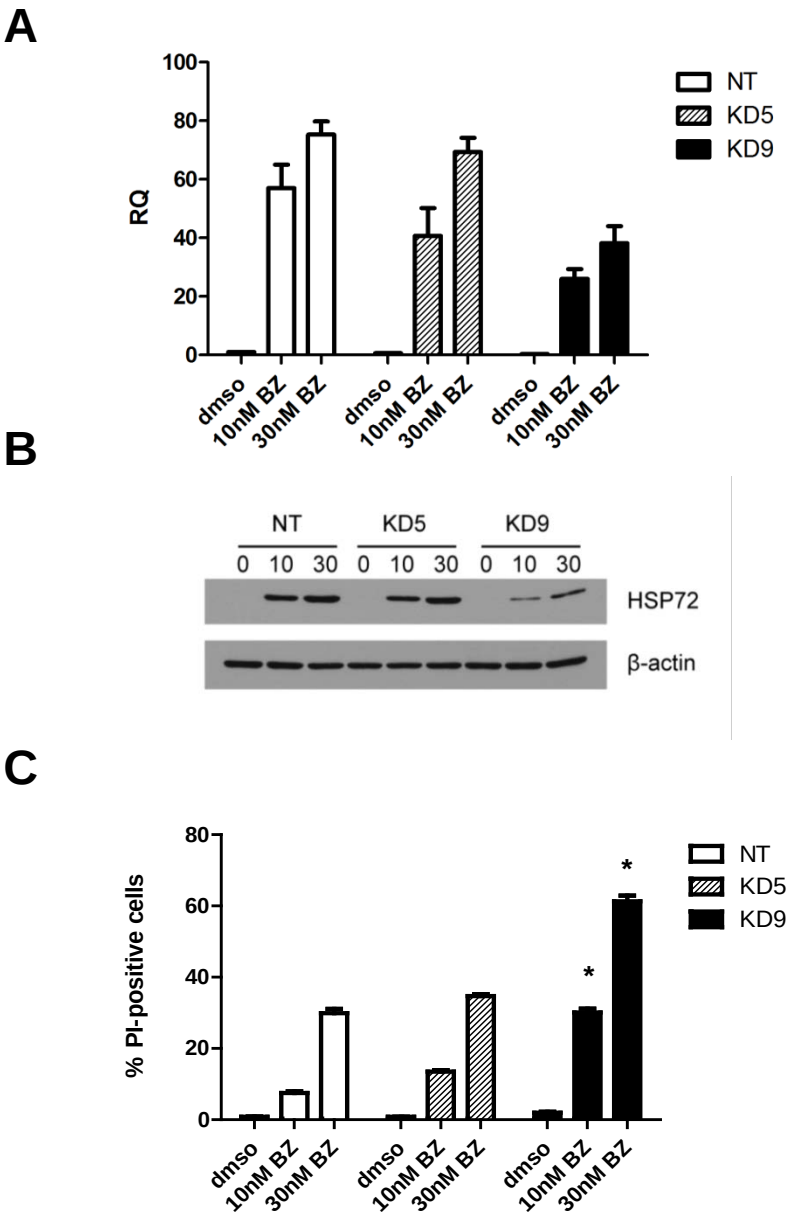

Figure 4.13 Knockdown of HSPA1A enhances bortezomib sensitivity. A) Effects of stable HSPA1A knockdown on basal and bortezomib-induced HSPA1A expression. 253J B-V cells were transduced with a non-targeting (NT) or HSPA1A-specific (KD5, KD9) lentiviral shRNA constructs as described in Materials and Methods. Cells were then incubated with or without indicated concentrations of bortezomib for 6 h and HSPA1A expression was measured by quantitative RT-PCR. Mean ± SEM, n = 3. B) Effects of stable HSPA1A knockdown on HSP72 protein levels. Cells were incubated for 12 h with indicated concentrations of bortezomib (nM), and HSP72 levels were measured in whole cell lysates by immunoblotting. C) Effects of stable HSPA1A knockdown on bortezomib-induced cell death. Cells were incubated with the indicated concentrations of bortezomib for 48 h and PI/FACS analyses were used to quantify cell death. Mean ± SEM, n = 3. *, $p<0.01$

A

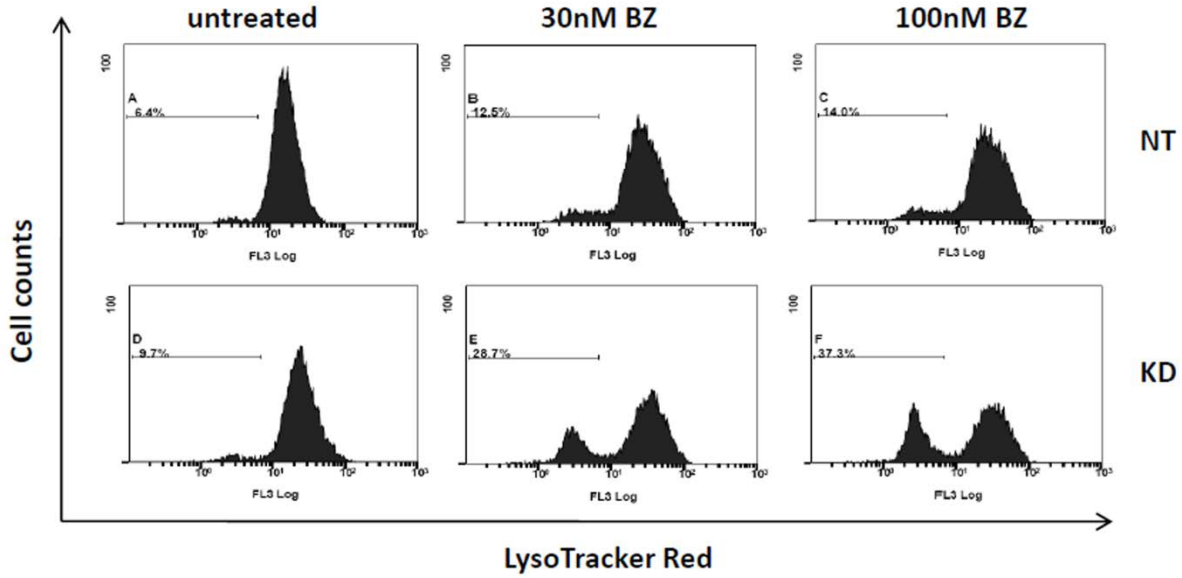

B

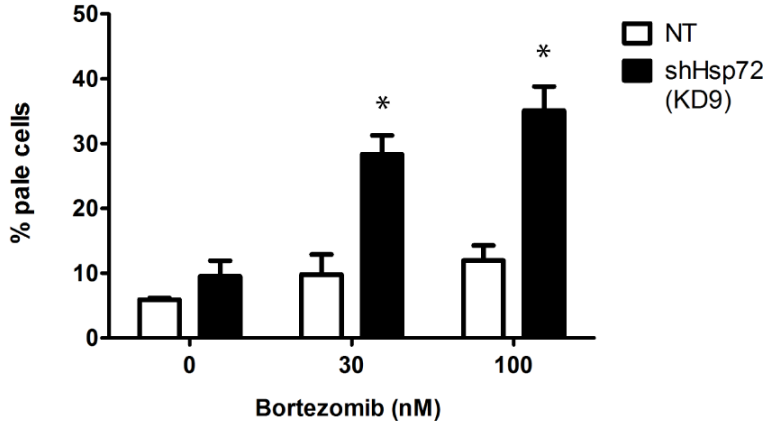

Figure 4.14 Hsp72 knockdown promotes loss of lysosomal integrity. Effects of stable HSPA1A knockdown on lysosomal membrane integrity. A) Cells were exposed to the indicated concentrations of bortezomib for 12 h prior to staining with Lysotracker Red, and loss of red fluorescence was measured by FACS. Cells with loss of lysosomal integrity were designated as "Lysotracker-pale" cells by the gated regions. B) Results were quantified as % Lysotracker-pale cells (mean $\pm$ SEM; n=3). *, $P < 0.03$.

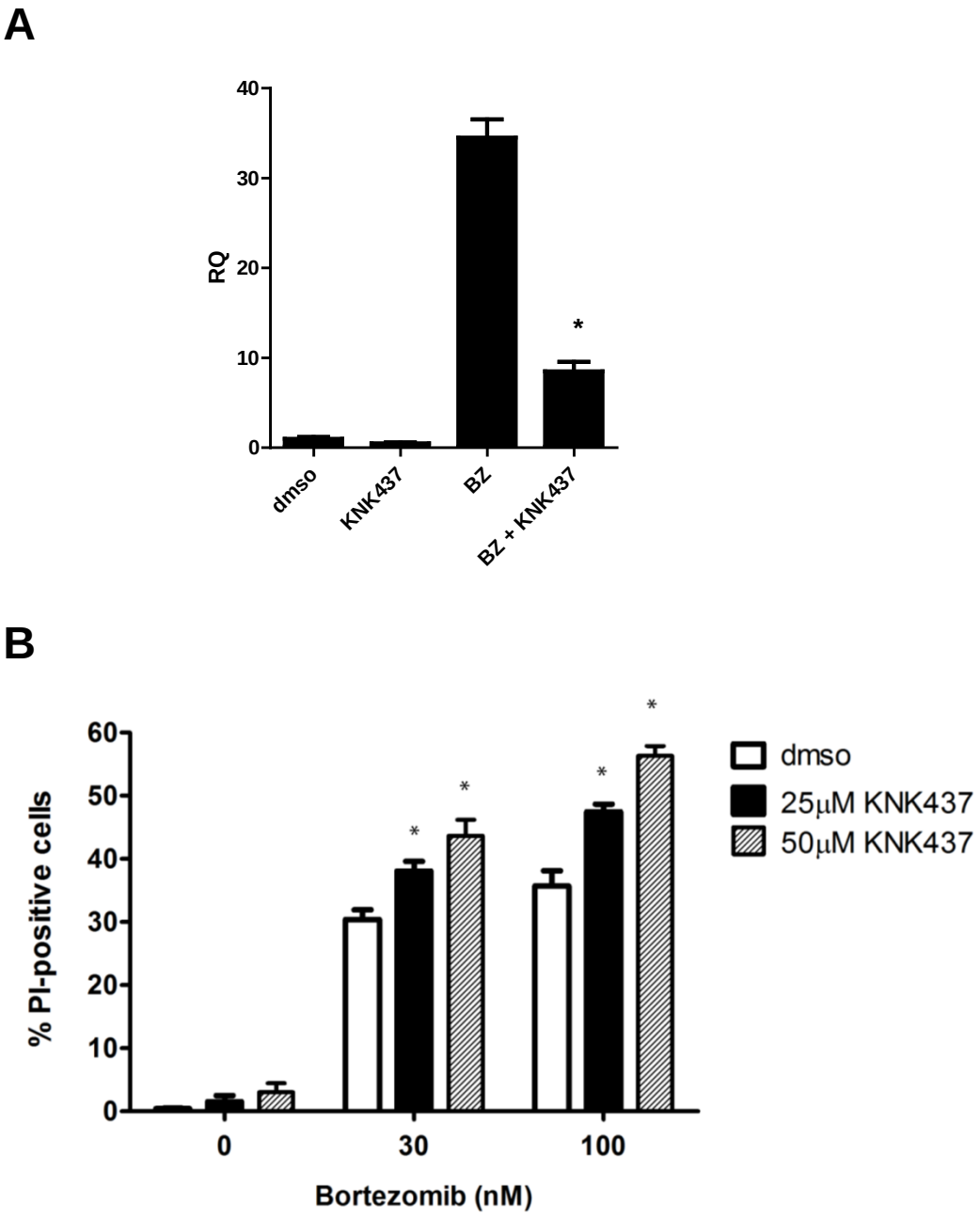

Figure 4.15 Pharmacologic inhibition of HSF1 promotes bortezomib sensitivity in vitro. A) Effects of KNK-437 on bortezomib-induced HSPA1A induction. Bortezomib-resistant 253J B-V cells were exposed to 25 μM KNK-437 with or without 100nM bortezomib for 12 h, and HSPA1A levels were measured by quantitative RT-PCR. Mean ± SEM, n = 3. A) Effects of KNK-437 on cell death. 253J B-V cells were exposed to 25 or 50 μM KNK-437 in combination with 30 or 100nM bortezomib for 48 h, and loss of plasma membrane integrity was quantified by PI/FACS. Mean ± SEM, n = 3. *, $P<0.05$.

death (Fig. 4.16B) in the 253JB-V cells. These data support the idea that chemical inhibitors of HSF1 and/or Hsp72 can be used to promote bortezomib-induced cell death.

4.2.6 Hsp72 knockdown promotes bortezomib-induced tumor growth inhibition in vivo. In a final series of experiments we examined whether stable Hsp72 knockdown would promote the growth-inhibitory effects of bortezomib in 253JB-V tumors in vivo. We established subcutaneous tumors using 253J B-V cells transduced with either the non-targeting (NT) or Hsp72-specific KD9 shRNA constructs and dosed animals with bortezomib (1 mg/kg, the MTD) twice weekly via i.v. injection. Using quantitative real-time RT-PCR, we confirmed that bortezomib increased HSPA1A mRNA levels in vivo and that the shRNA construct inhibited these effects (Fig. 4.17A). The untreated 253JB-V KD9 tumors displayed somewhat slower tumor growth than did the 253JB-V NT tumors, but the differences did not reach statistical significance. Biweekly therapy with bortezomib had no significant effects on the growth of the control 253JB-V.NT tumors (Fig. 4.17B), consistent with our previous findings (143). Conversely, bortezomib almost completely suppressed the growth of the tumors derived from the 253JB-V cells transduced with the HSPA1A-specific shRNA construct (Fig. 4.17B).

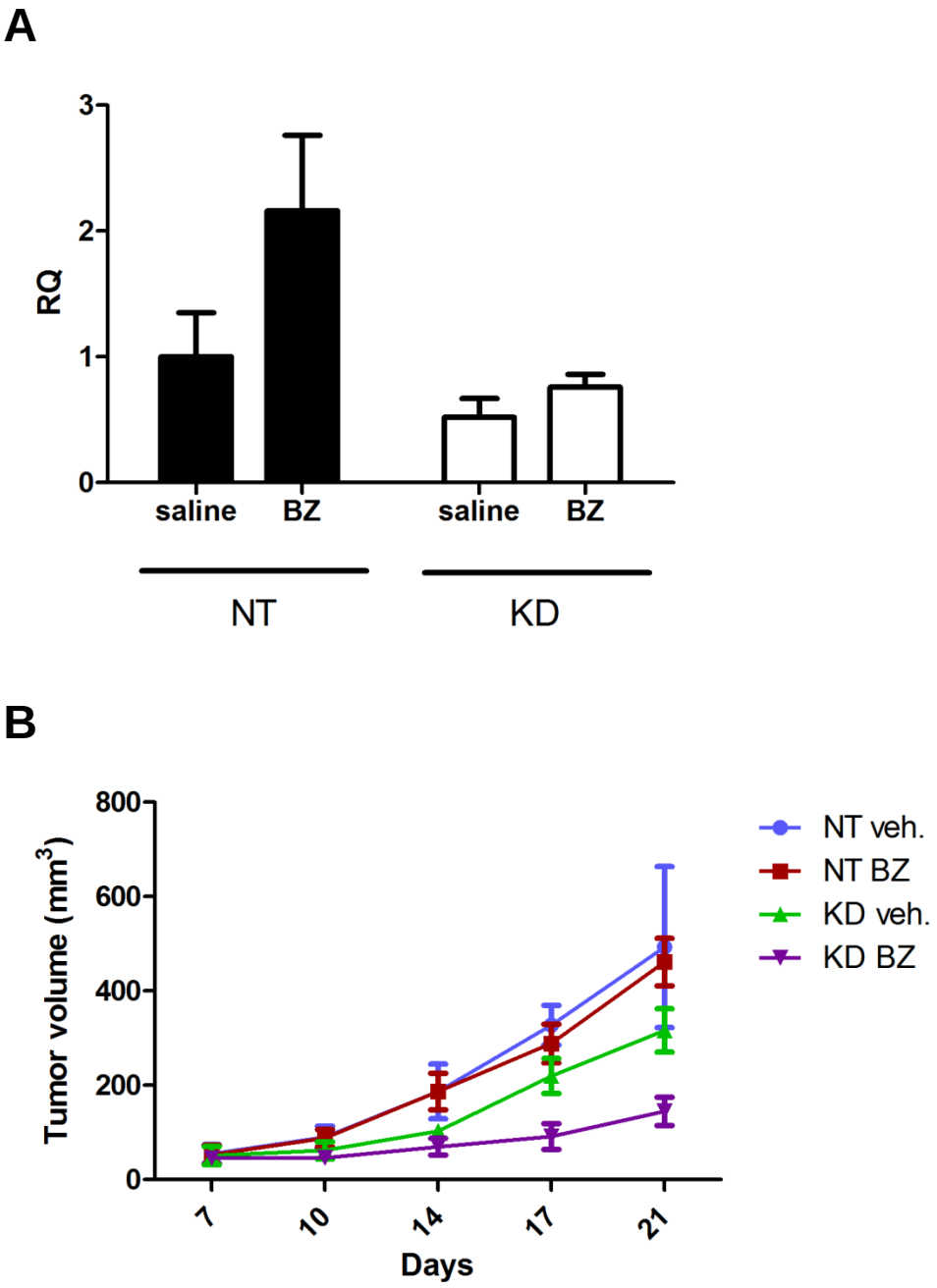

Figure 4.16 Knockdown of HSPA1A promotes bortezomib-induced growth inhibition *in vivo*. A) Effects of bortezomib on HSPA1A induction. Animals were injected twice with 1 mg/kg bortezomib (3 days apart), tumor RNA was harvested, and HSPA1A expression was measured by quantitative RT-PCR. Mean ± SEM, n = 3. B) Effects of bortezomib on tumor growth. Athymic nude mice were inoculated s.c. with 253JB-V.KD9 or 253JB-V.NT cancer cells. When tumors became palpable (5-7 days), the mice were treated i.v. biweekly with bortezomib at 1mg/kg/dose or with saline control. Tumor volumes were measured twice a week after the start of treatment. Values represent mean ± SE (N=5).

4.3. Discussion

Our study is the first to specifically examine Hsp72 modulation in combination with bortezomib in bladder cancer cells *in vitro* and *in vivo.* The data demonstrate that Hsp72 protects cancer cells from proteasome inhibitor-induced stress and cell death. We propose that the cytoprotective effects of Hsp72 are in part due to its known role in promoting lysosomal integrity (134, 146), as 253JB-V cells stably transduced with Hsp72-specific shRNA showed dramatic increases in lysosomal instability over non-targeting control transduced cells. Proteasome inhibition activates autophagy and increases flux through the autophagy-lysosomal system as a compensatory mechanism. It is likely that the increased lysosomal instability caused by Hsp72 depletion has deleterious effects on autophagy function, which is thought to aid in clearing misfolded protein aggregates during proteotoxic stress.

Furthermore, we discovered that among the four cell lines tested,bortezomib-sensitive cells displayed much lower levels of both basal and drug-induced HSPA1A than bortezomib-sensitive cells (Fig. 4.4). This was due to methylation of the HSPA1A promoter region in the sensitive cells, which prevented HSF1 binding and suppressed HSPA1A expression (Figs. 4.8 - 4.10). Intrigued by these data, we expanded our analysis to include a total of 20 bladder cancer cell lines in hopes of revealing a correlation between lack of HSPA1A expression and BZ sensitivity. However, the correlation was not apparent, either using basal or BZ-induced expression (Fig. 4.18 A,B). Overall, approximately 40% of the cell lines had extremely low HSPA1A expression, suggesting that methylation of the HSPA1A promoter region may be prevalent in bladder cancer. It is unclear why HSPA1A promoter methylation would be propagated in cancer, but

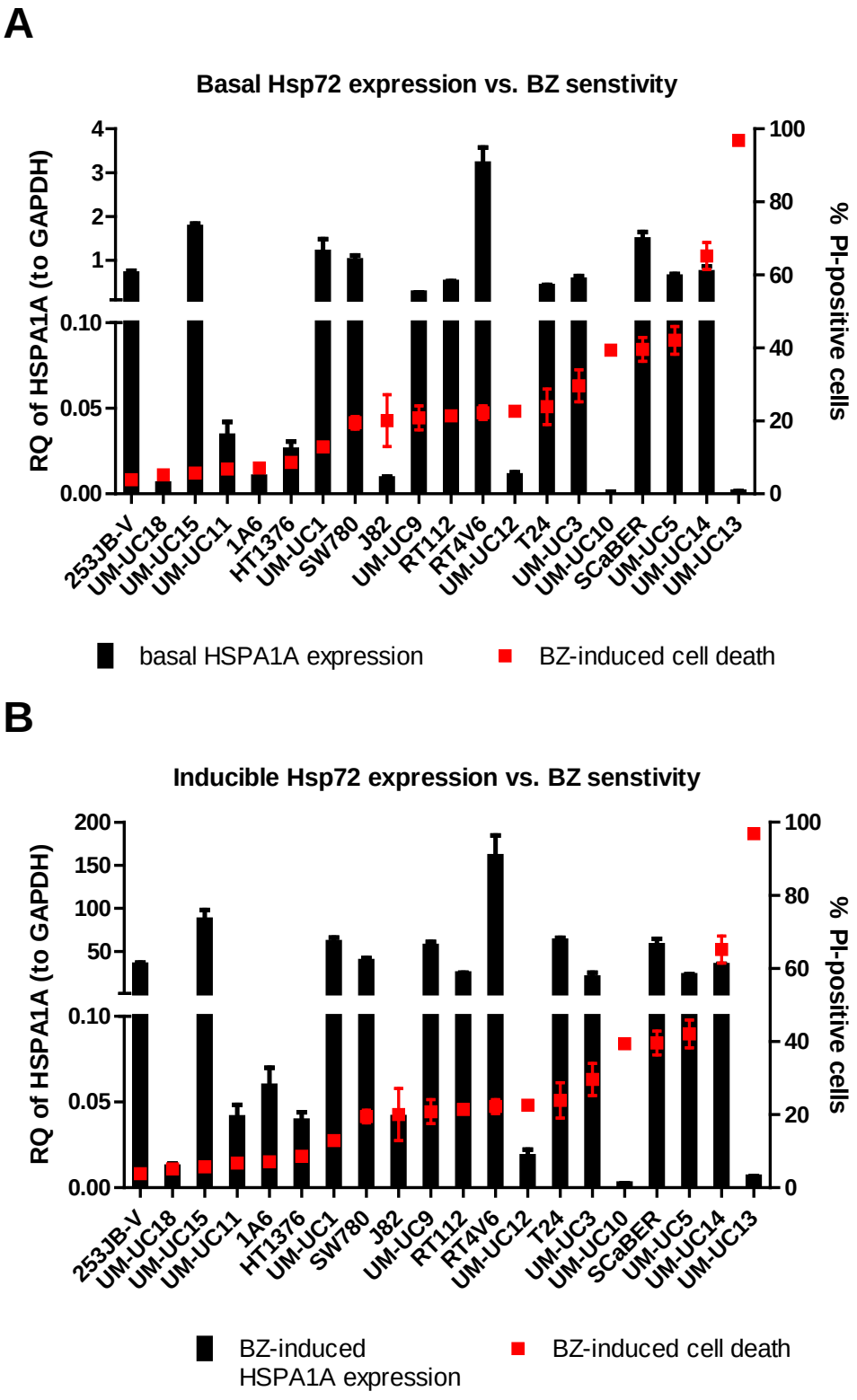

Figure 4.17 Relationship between basal and inducible Hsp72 expression and bortezomib sensitivity. A) Basal expression of Hsp72 (black) vs. BZ-induced cell death (red). B) BZ-induced Hsp72 expression (black) vs. BZ-induced cell death (red).

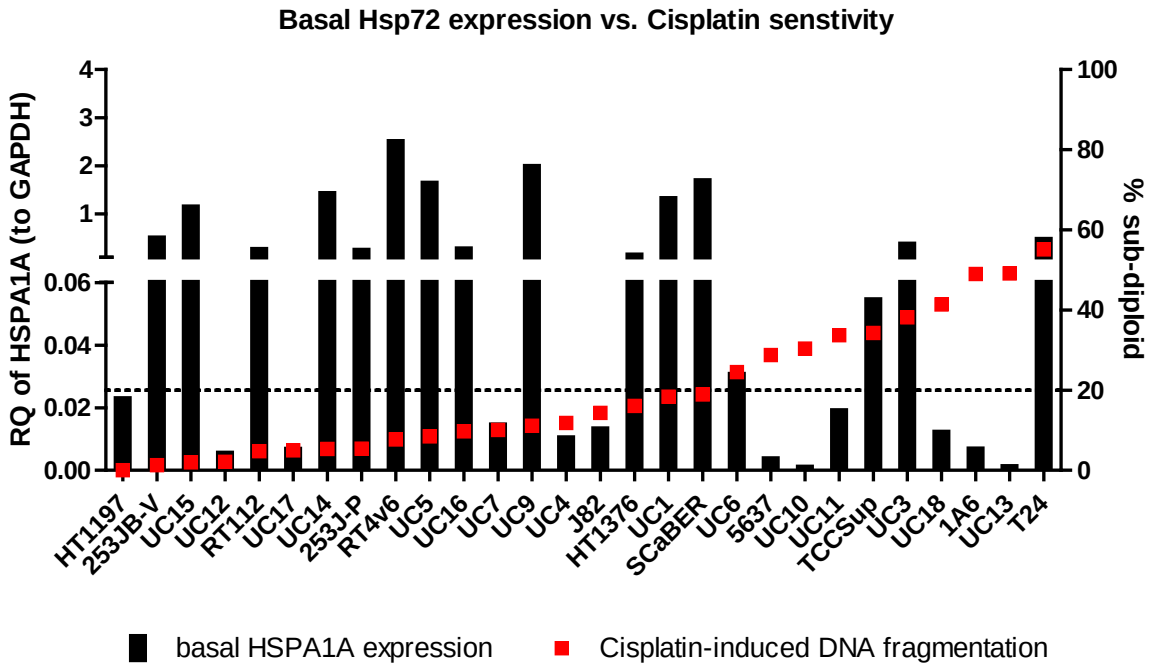

Figure 4.18 Relationship between basal Hsp72 expression and cisplatin sensitivity. Basal expression of Hsp72 (black) vs. cisplatin-induced apoptosis (red). For Hsp72 expression, cells were exposed to 30nM BZ for 6h and then HSPA1A expression measured by RT-PCR. For cisplatin-induced DNA fragmentation (% sub-diploid), cell were exposed to 10uM cisplatin for 48h, then DNA fragmentation was measured by PI-FACS.

perhaps the CpG island surrounding the promoter becomes methylated as part of global epigenetic alterations involved in bladder cancer progression (147, 148). In gastric cancer, the Epstein-Barr virus has been shown to upregulate DNA methyltransferase (DNMT1) and promote methylation of the Hsp72 promoter region (149). HSPA1A promoter methylation in bladder cancer bears further investigation as a potential biomarker of sensitivity to other chemotherapeutic drugs such as cisplatin (Fig. 4.13). Importantly, we demonstrated that bladder cancer cells lacking HSPA1A depend heavily on HSPA1B expression to maintain Hsp72 protein levels. Based on these results, selective targeting of HSPA1B in cells with hypermethylation at the HSPA1A promoter could confer synthetic lethality.

The involvement of molecular chaperones and the heat shock response in cancer is an area of intense interest. Hsp90, through its role as a molecular "holdase", interacts with numerous oncoproteins to ensure proper function and interactions (150). Pioneering work with Hsp90 inhibitiors validated chaperones as attractive targets, and these have displayed some clinical activity in cancer (151). Conversely, the development of Hsp72 inhibitors is noticeably lacking because of difficulty thus far in targeting the ATPase domain (152). Recent work demonstrated that the small molecule 2-phenyethynesulfonamide or pfithrin-μ (PES) is a relatively specific inhibitor of Hsp72, binding the C-terminal substrate-binding-domain and preventing key interactions with co-factors such as Hsp40, CHIP, and Bag-1 while avoiding interactions with other chaperones such as constitutive Hsc70 and Hsp90 (111). PES also interacts with p53, and likely has other pleiotropic effects, making it unsuitable for use in patients, but it nonetheless provides a rationale for targeting the C-terminus substrate-binding-domain as an alternative approach to inhibiting Hsp72's functionality. Overall, our study supports the further development of Hsp72 inhibitors for

single agent and combination therapy in solid tumors; Hsp72 is an attractive, tumor-specific target because of its low expression unstressed normal cells versus high expression in stressed cancer cells.

Chapter 5: EVALUATION OF THE EFFECTS OF A SELECTIVE HDAC6 INHIBITOR ON PROMOTING BORTEZOMIB-INDUCED CANCER CELL DEATH

5.1 Introduction

Histone deacetylase (HDAC) proteins are typically classified into three major groups based on evolutionary relationships and homology to yeast deacetylases (153). Class I HDACs consist of HDAC1, HDAC2, HDAC3, and HDAC8, while Class II includes HDAC4, HDAC5, HDAC6, HDAC7, HDAC9, and HDAC10. Class III HDACs are somewhat distinct from the two classical HDAC groups, and consist of silent information regulator 2 (Sir2) family members, better known as sirtuins (SIRTs) (154). HDAC6 is unique among Class I and II HDACs both structurally and functionally (Figure 5.1). In addition to being the only HDAC with two deacetylase domains (DD1,2), HDAC6 contains two nuclear export signals (NES1-2) as well as a tetradecapeptide repeat-cytoplasmic anchoring domain (SE14), contributing to its almost exclusive cytosolic localization. HDAC6 also uniquely contains a zinc-finger ubiquitin-binding domain (UBD) near its C-terminus. Thus, HDAC6 would more aptly be referred to as a "protein deacetylase", as it almost exclusively targets cytosolic non-histone substrates (Table 5.1), with no known effects on nuclear histones.

Of the cytosolic substrates, α- tubulin is the best characterized; pharmacologic inhibition or genetic silencing of HDAC6 rapidly and robustly increases the levels of acetylated α-tubulin. Acetylation of tubulin confers a more stable, rigid microtubule network (155, 156) and thus has important consequences on intracellular trafficking, mitotic division, and cellular adhesion/motility. Accordingly, in addition to its role in shuttling cargo for degradation, recent literature also implicates a critical role for HDAC6 in cell migration and invasion. Seminal work from Tso-Pang Yao's group demonstrated that

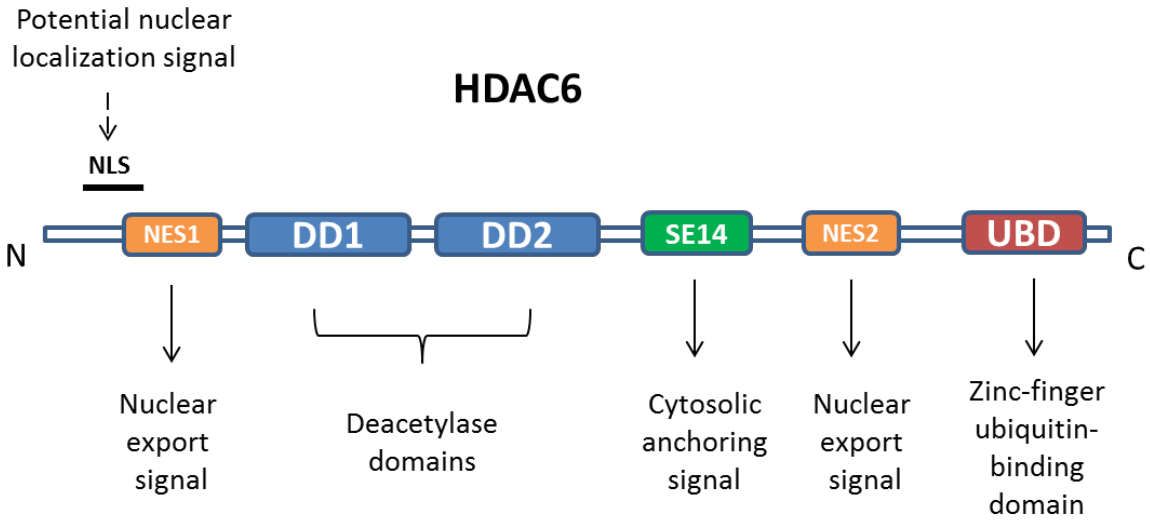

Figure 5.1 Functional domains of HDAC6 protein. A potential nuclear localization signal (NLS) flanks a nuclear export signal (NES1) near the N-terminus (157). However, the presence of another NES (NES2) as well as a cytosolic anchoring signal (SE14) collectively keep HDAC6 localized to the cytosol. Two catalytic deacetylase domains (DD1&2) interact with substrates including α-tubulin, Hsp90, and cortactin. Finally, a zinc-finger ubiquitin-binding domain (UBD) near the C-terminus allows HDAC6 to directly bind ubiquitylated proteins.

Substrates	HDAC6-related function	Potential therapeutic target diseases
α-tubulin	Tubulin deacetylation	Antigen presentation deficiencies
	Regulation of immune synapse formation, HIV-1 viral infection	HIV-1 viral infection (AIDS)
	Cell migration and chemotaxis	Tumor cell metastasis (cancer)
Cortactin	Cortactin deacetylation	Biological disorders associated with actin-based cell migration
	Regulation of cellular migration and F-actin binding	
Hsp90	Hsp90 deacetylation	Neurodegenerative disorders
	Governs misfolded protein degradation and clearance, and regulates GR (Glucocorticoid Receptor) and gene transcription activation	
Interacting proteins		
p97 (VCP,Cdc48p)	AAA-ATPase in endoplasmic reticulum-associated proteosomal degradation	Neurodegenerative disorders
$p150^{glued}$ (dynactin)	Adaptor protein for the molecular motors dyneins and kinesins	
mDia2	Osteoclast maturation	Diseases related to deficiencies in bone formation, resorption and regeneration
Ubiquitin	Signal for cellular processes, such as protein degradation and endocytosis	Neurodegenerative disorders
PLAP	Phospholipase A2 activation protein controlling prostaglandin levels and phospholipase activity	
NF-κB (p50,65)	Transcription factor in inflammation and cell growth control	Gene expression-related deficiencies
Runx2	Transcription factor essential for skeletal development	
Sumoylated p300	Transcriptional co-regulator with lysine acetyltransferase activity	Gene expression-related deficiencies
PP1	Phosphatase, regulation of the interaction between PP1 and Akt	Deficiencies in cell migration and survival

Table 5.1 HDAC6 substrates, interacting proteins, and related biological functions.

*Reprinted from *Trends in Cell Biology*, 116, Agustin Valenzuela-Fernandez, J. Roman Cabrero, Juan M. Serrador, Francisco Sanches-Madrid, HDAC6: a key regulator of cytoskeleton, cell migration and cell-cell interactions, 291-297, Copyright (2008), with permission from Elsevier. Reference # (158).

HDAC6 deacetylase activity was necessary for chemotactic-induced cell invasion across a matrix (159). HDAC6 inhibition leading to hyperacetylated tubulin was also shown to negatively affect the capability of cells to undergo dynamic cell-cell adhesions, which is necessary for migration (160). The actin cytoskeletal network is also targeted by HDAC6 through deacetylation of cortactin. Cortactin is an F-actin interacting protein that stimulates actin polymerization, and hyperacetylation of cortactin by HDAC6 inhibition was found to reduce association with F-actin and inhibit cellular motility (161). Related to its cytoskeletal functions, HDAC6 has also been linked to a fascinating structure called the primary cilium. A single primary cilium exists in most mammalian cells (although it is commonly lost upon malignant transformation), arising from centrioles and playing a role in Hedgehog, Wnt, and other essential signaling pathways (162). HDAC6 was found to be phosphorylated by the Aurora A kinase and to regulate disassembly of primary cilia in human retinal pigment epithelial cells (163).

Another important substrate of HDAC6 is the Hsp90 chaperone protein (164). As previously discussed, Hsp90 interacts with numerous client proteins, many of which are important for cancer, and these interactions are strongly influenced by its acetylation status, which is modulated by HDAC6. HDAC6 also appears to plays a role in controlling activation of the heat shock response (HSR) through dissociation of the Hsp90-HSF1 complex. At steady state, HDAC6 and the ATPase p97/VCP exist bound to the Hsp90-HSF1 repressive complex; upon stress, HDAC6 leaves to bind ubiquitylated proteins, and p97/VCP uses its segregase activity to disrupt the Hsp90-HSF1 interaction, allowing HSF1 to trimerize and translocate to the nucleus to induce the HSR (165). The capability of HDAC6 to directly bind both single and poly-ubiquitin chains via its C-terminal UBD also

has important functional implications for proteostasis. As previously discussed, HDAC6's ubiquitin-binding ability coupled with its ability to associate with dynein motor complexes allows it to coordinate the transport of misfolded/ aggregated proteins along microtubules to perinuclear aggresomes (Section 1.3.2d). HDAC6 has also been found to regulate autophagy through its role in coordinating an F-actin network that promotes fusion of autophagosomes and lysosomes (166).

The myriad functions of HDAC6 in response to proteotoxic stress has led to the concept of HDAC6 as a novel "stress surveillance factor" (167) . Interestingly, an essential role for HDAC6 in tumorigenesis was also proposed (168), which supports the idea that cancer cells pirate stress-coping mechanisms to promote their malignant phenotype. Along these lines, HSF1 has also been found to promote tumorigenesis (2).

A concerted effort has been made over the past decade to discover and develop HDAC6-specific inhibitors for use in cancer and other diseases. Pan-HDAC inhibitors such as tricostatin A (TSA) and suberoylanilide hydroxamic acid (SAHA/ clinically: Vorinostat) inhibit HDAC6, but also inhibit other Class I and II HDACs making it difficult to attribute functions to any specific HDAC. The first major success in targeting HDAC6 directly came from a large chemical library screen that identified a compound called tubacin as a relatively selective inhibitor of HDAC6 and tubulin deacetylation (169). Other compounds soon followed with greater selectivity, such as tubastatin A (170), NK84 (171), and LBH589 (172).

Here we compared the effects of a selective HDAC6 inhibitor (Compound A) to those of type I-selective (MS275) and pan-selective (SAHA) HDAC inhibitors on pancreatic and bladder cancer cell viability, alone and in combination with the proteasome inhibitor

bortezomib (BZ). We hypothesized that the selective HDAC6 inhibitor would have the strong effects on BZ-induced proteotoxicity, and enhance BZ-induced cell death. To validate chemical inhibitor data, we also genetically silenced HDAC6 and Type I HDACs in select cell lines. Overall, our data argue against a unique role for HDAC6 in promoting survival following proteasome inhibition, but rather support the continued evaluation of Type I HDAC inhibitors in combination with PIs. Instead, Compound A was a potent inhibitor of tumor cell invasion, supporting its continued development as an inhibitor of metastasis.

5.2 Results

5.2.1 *Validation of on-target effects of Compound A*- We first sought to determine the specificity of the novel HDAC6-selective inhibitor Compound A by comparing its effects on protein acetylation (acetylated α-tubulin vs. acetylated histone H3) by immunoblotting (Fig. 5.2). We directly compared the effects of Compound A (Cpd. A) to those of a class I-specific inhibitor (SNDX/MS-275). Dose-response analyses revealed that concentrations of Cpd A as low as 0.1μM (100nM) were sufficient to increase levels of acetyl-tubulin, whereas concentrations as high as 10μM had no effects on acetyl-H3 levels, indicating that Cpd. A has robust and selective effects on HDAC6. MS-275, on the other hand, produced strong increases in acetyl-H3 levels at 5-10μM but little to no effects on levels of acetyl-tubulin. Overall these data point to Cpd. A as a potent and selective HDAC6 inhibitor.

5.2.2 *Effects of the HDAC inhibitors on bortezomib-induced cell death*- To evaluate the toxicity of Cpd. A as a single agent in our cancer cell lines, we used the colorimetric MTT

A

Compound A

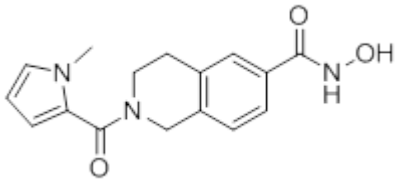

B

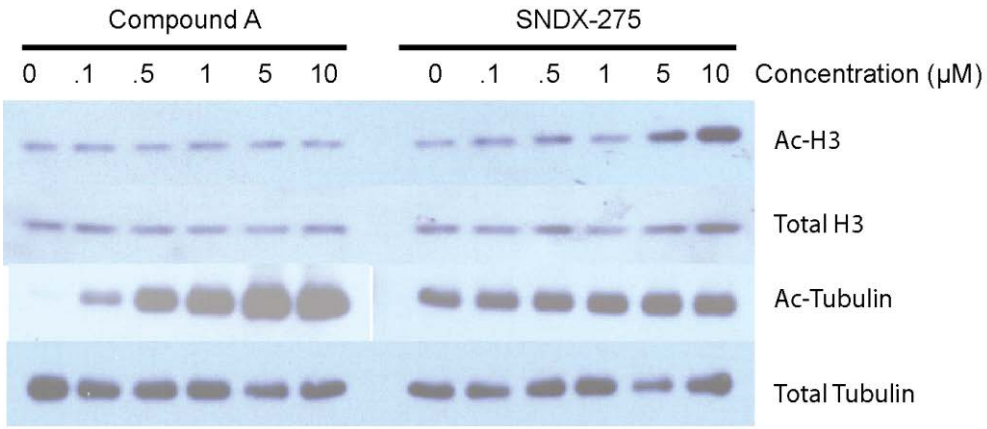

Figure 5.2 Structure and specificity of Compound A. A) Chemical structure of Compound A, B)253JB-V human bladder cancer cells were treated for 24h with a dose response (0.1-10μM) of either Compound A or SNDX-275 (MS-275) and levels of acetylated and total histone H3 and α-tubulin were measured by immunoblotting. Compound A increased levels of acetyl-tubulin at 0.1μM but had no effect on acetyl-H3 at doses up to 10μM.

assay to examine its concentration-dependent effects of Cpd. A on cell growth and metabolic activity. For comparison, we also included the pan-HDAC inhibitor SAHA as well as the Class I-specific SNDX-275. Our data indicate that in the human pancreatic cancer line L3.6pl, SAHA and SNDX-275 decreased formazan salt production (an indicator of metabolically active, viable cells) at concentrations $\geq$ 5μM, whereas formazan salt production was relatively unchanged by Cpd. A at concentrations up to 10μM (Fig. 5.3). To further investigate the toxicity of Cpd. A, we performed additional experiments measuring cumulative cell death (via outer membrane integrity) and apoptosis (via DNA fragmentation) across a panel of 10 human pancreatic cancer cell lines (Fig. 5.4). In both assays, Cpd. A induced minimal amounts of cell death and apoptosis (red columns, Fig. 5.4A and B, respectively). Because of our interest in the ability of a selective HDAC6 inhibitor to synergize with proteasome inhibitors, we combined Cpd. A, SNDX-275, or SAHA with BZ and measured growth inhibition, total cell death, and apoptosis. While Cpd. A showed significant enhancement of BZ-induced growth inhibition with the MTT assay in L3.6pl cells (Fig. 5.3), it did not significantly enhance cell death or apoptosis across the panel of pancreatic cancer cell lines (with the exception of the T3M4 line). Interestingly, SNDX-275, while slightly more toxic as a single agent, significantly augmented BZ-induced cell death in multiple cell lines (Fig. 5.4). In a subset of 3 pancreatic cell lines (Fig. 5.5), SAHA appeared to be more effective than either SNDX-275 or Cpd. A at enhancing BZ-induced cell death. These effects were even more striking in a BZ-resistant bladder cancer cell line, 253JB-V, where both SNDX-275 and SAHA strongly sensitized cells to BZ-induced death, measured by DNA fragmentation and outer membrane integrity at 24 and 48

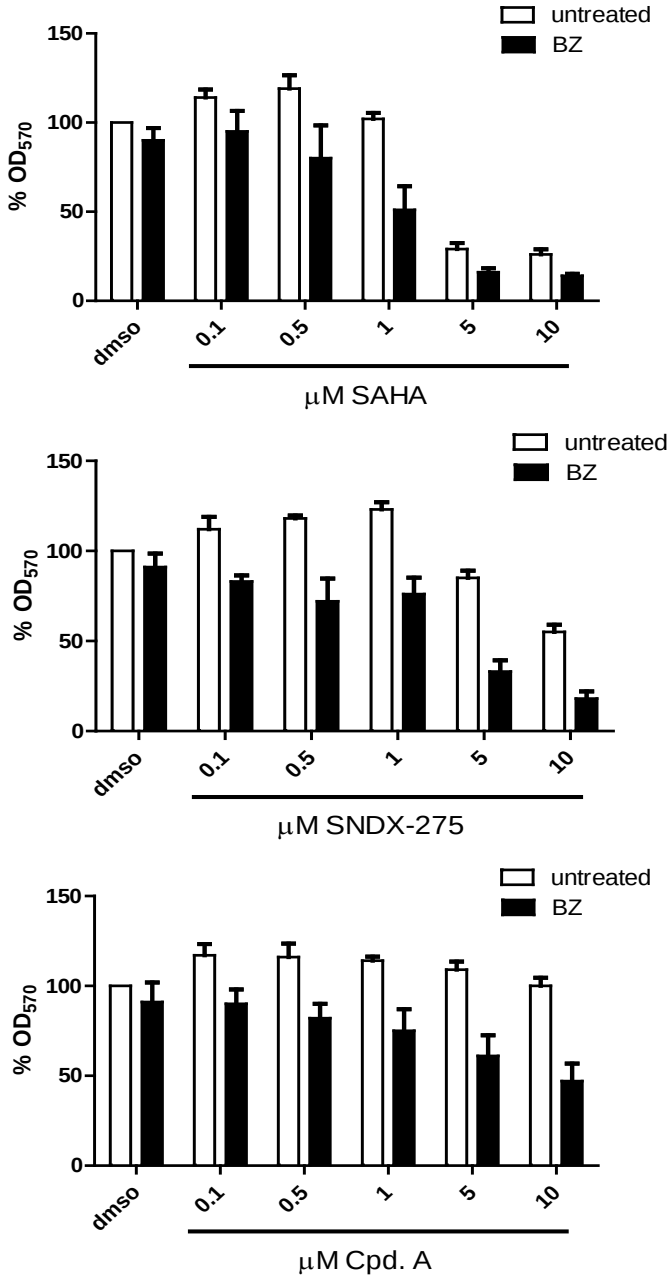

Figure 5.3 Compound A does not cause significant growth inhibition as a single agent, but enhances growth inhibition in combination with BZ. L3.6pl human pancreatic cancer cells were exposed to indicated concentrations of SAHA (top), SNDX-275 (middle), or Cpd. A (bottom) alone or in combination with 10nM BZ for 48h. MTT reagent was added then solubilized, and optical density at 575nm was measured. Columns represent mean $\pm$ SE (n=3; n=2 for SNDX-275).

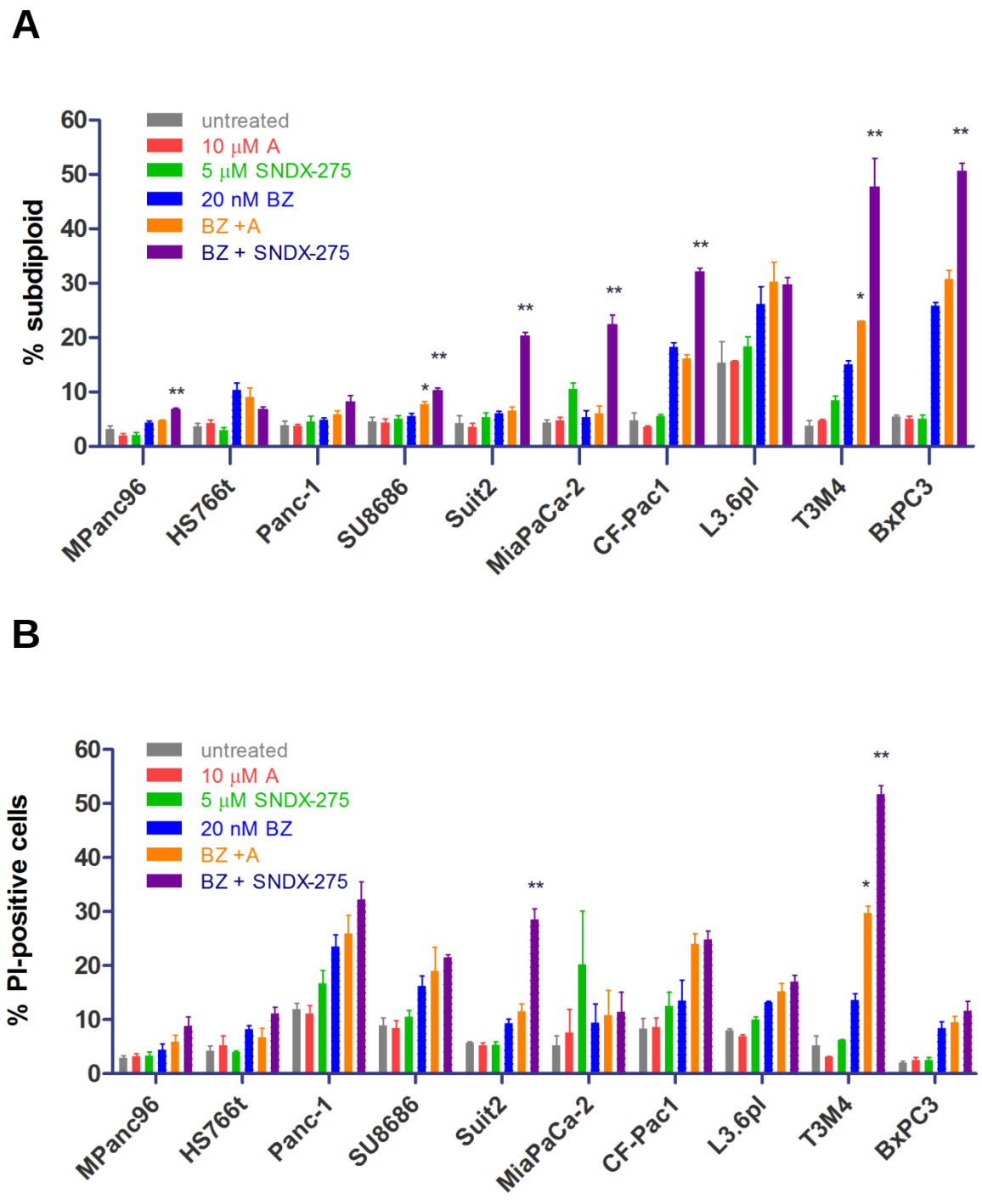

Figure 5.4 Effects of SNDX-275 vs. Cpd. A on BZ-induced DNA fragmentation and cumulative cell death in pancreatic cancer cell lines. Cells were exposed to compounds for 24h. A) DNA fragmentation (% subdiploid); B) outer membrane permeability (% PI-positive) as measured by FACS. Columns represent mean $\pm$ SE (n=3). Asterisks denote $P \leq 0.05$ compared to BZ alone for indicated columns (*BZ+A vs. BZ; **BZ+SNDX-275 vs. BZ).

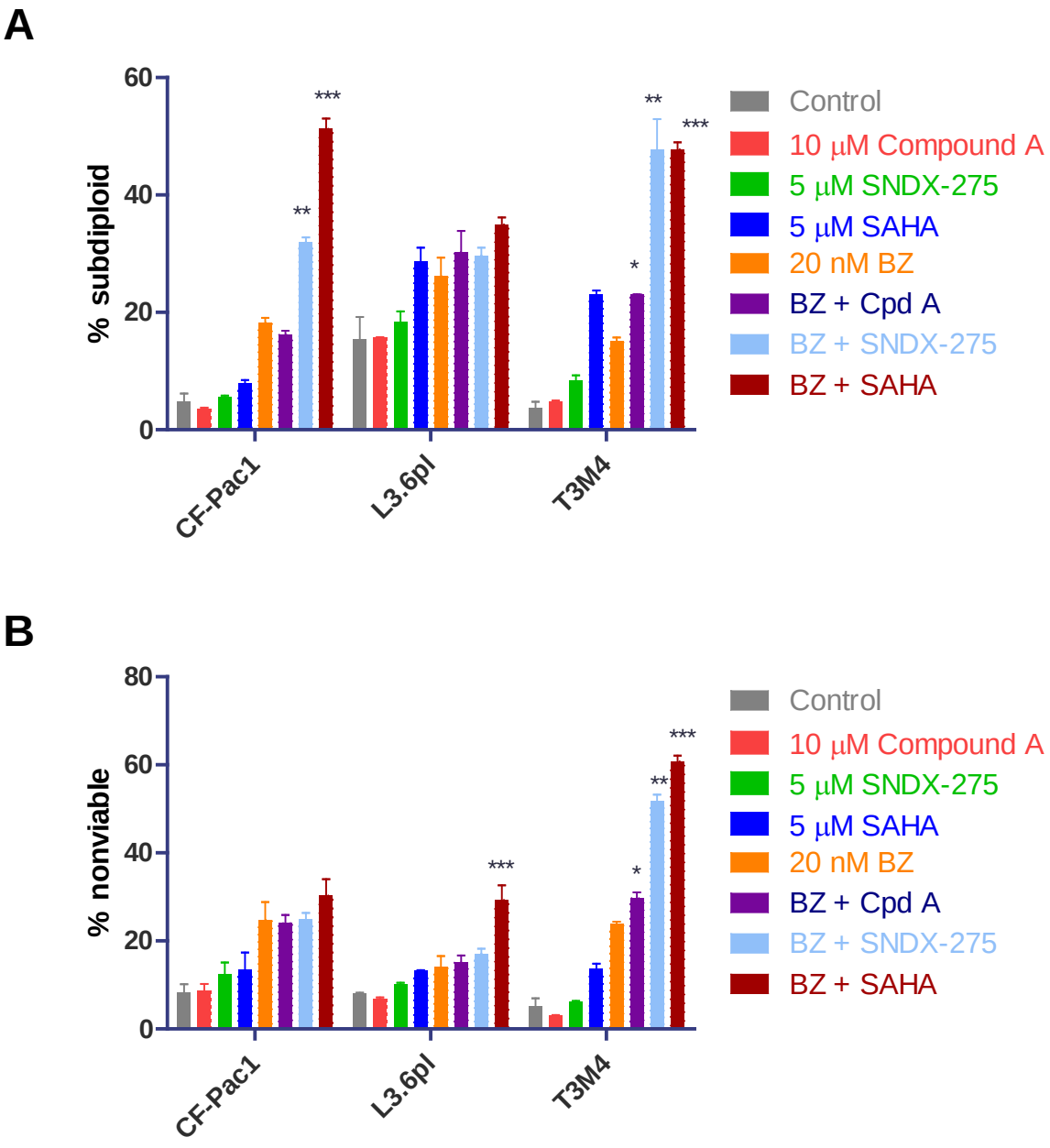

Figure 5.5 Comparison of Cpd. A with both SNDX-275 and SAHA alone and in combination with BZ. CF-Pac1, L3.6pl, and T3M4 pancreatic cancer cells were exposed to indicated concentrations of compounds for 24h. A) DNA fragmentation (% subdiploid) or outer membrane permeability (% PI-positive) were measured by FACS. Columns represent mean $\pm$ SE (n=3). Asterisks denote $P \leq 0.05$ compared to BZ alone (*BZ+A vs. BZ; **BZ+SNDX-275 vs. BZ; ***BZ+SAHA vs. BZ).

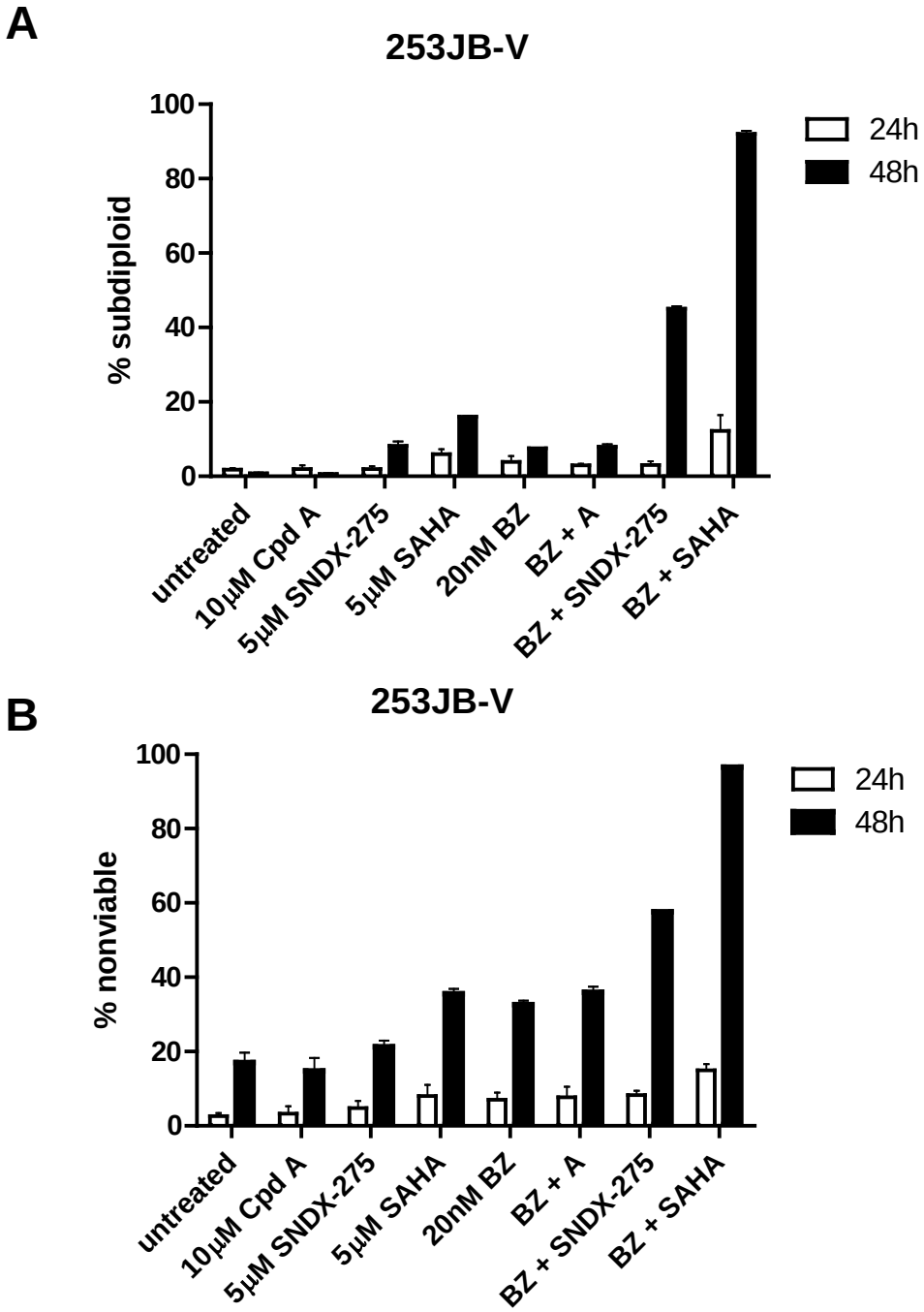

Figure 5.6 Effects of Compound A vs. SNDX-275 and SAHA alone and in combination with BZ in 253JB-V bladder cancer cells. Cells were exposed to the indicated doses of compounds for 24 and 48h and FACS was used to measure apoptosis and cumulative death by A) DNA fragmentation (% subdiploid) and B) outer membrane integrity (% nonviable), respectively. Columns represent mean ± SE. Asterisks represent P< 0.05 (**BZ+SNDX-275 vs. BZ; ***BZ+SAHA vs. BZ).

hours (Fig. 5.6). Compound A was not effective in combination with BZ in these cells either, showing that the results were not pancreatic cancer-specific. Overall, the data suggest that inhibitors of Class I HDACs are more potent than HDAC6 inhibitors in terms of augmenting the cytotoxic effects of PI's in solid tumor cells.

5.2.3 *Knockdown of HDAC6 and Class I HDACs* – To validate the data obtained with the chemical HDAC inhibitors, we next performed transient siRNA-mediated silencing of HDAC6 and HDACs 1,2, and 3 in T3M4 pancreatic cancer cells. Knockdown efficiencies were robust for each target (≥70%), but surprisingly none of the siRNAs significantly sensitized cells to BZ (Fig. 5.7). Though not statistically significant, it appeared that knockdown of HDAC1, either alone or combined with the knockdown of HDACs 2, 3, or both, enhanced BZ-induced cell death to a greater degree than did HDAC6 knockdown, and also to a greater degree than knockdown of HDACs 2 and 3 individually. Likewise, transient knockdown of HDAC6 in another pancreatic cancer cell line, L3.6pl, also provided little sensitization to BZ (Fig. 5.8). To confirm these results in a different model, we generated 253JB-V cells with stably silenced HDAC6 and HDAC1 using lentiviral delivery short hairpin RNA (shRNA) in pGIPZ plasmids. Knockdown was confirmed at the RNA and protein level (Fig. 5.7A) and cells were interrogated for increased apoptosis (DNA fragmentation) in response to 48h BZ exposure (Fig. 5.7B). Here, stable knockdown of HDAC1 significantly sensitized 253JB-V cells to BZ, whereas HDAC6 knockdown did not enhance BZ-induced apoptosis. Overall, these data seem to suggest a critical role for HDAC1 in protecting cells from proteasome inhibitors, and partially explains our results suggesting SNDX-275 as a better combination strategy with PI's than an HDAC6 inhibitor.

The mechanisms behind this sensitization are presently unknown, and are likely pleitropic due to the chromatin-modifications resulting from HDAC1 inhibition.

5.2.4 *Effects of HDAC6 inhibition on BZ-induced cell death in MM cells*- Because the majority of literature on proteasome inhibitors and HDAC6 was generated in multiple myeloma models, we decided to compare the effects of Cpd. A and SNDX-275 alone and in combination with BZ in four different MM cell lines (U266, MM1, OPM2, and RPMI 8226) (Fig. 5.10). In contrast to SNDX-275, Cpd. A was relatively non-toxic as a single agent. When combined with BZ, Cpd. A showed moderately sensitization in each of the four cell lines, but this was not statistically significant. Alternatively, SNDX-275, when combined with BZ, showed clear sensitization in three out of the four cell lines. Overall, these data support the conclusions drawn from our solid tumor cells.

5.3 Discussion

In this study, we demonstrate that the type I-selective HDAC inhibitor SNDX-275 is a more potent chemosensitizer than a novel HDAC6-selective inhibitor (Cpd. A) when the drugs are combined with the proteasome inhibitor bortezomib. Despite strong preclinical biological evidence for an essential role for HDAC6 in protein aggregate clearance, our data show that inhibiting these effects has modest impact on survival in multiple solid tumor and MM cell lines; rather, specific hematologic tumors such as MM may be a niche application. The role for HDAC6 as a regulator of aggresome formation (65) and autophagy (173) is clear. However, these processes are dependent not only on HDAC6's catalytic activity but also its ubiquitin-binding capacity. At present, no small molecules have been developed to target the HDAC6 UBD (Fig. 5.1); rather, all current inhibitors target the catalytic domain(s) (including Compound A). This is a significant caveat, because HDAC6's functions are only

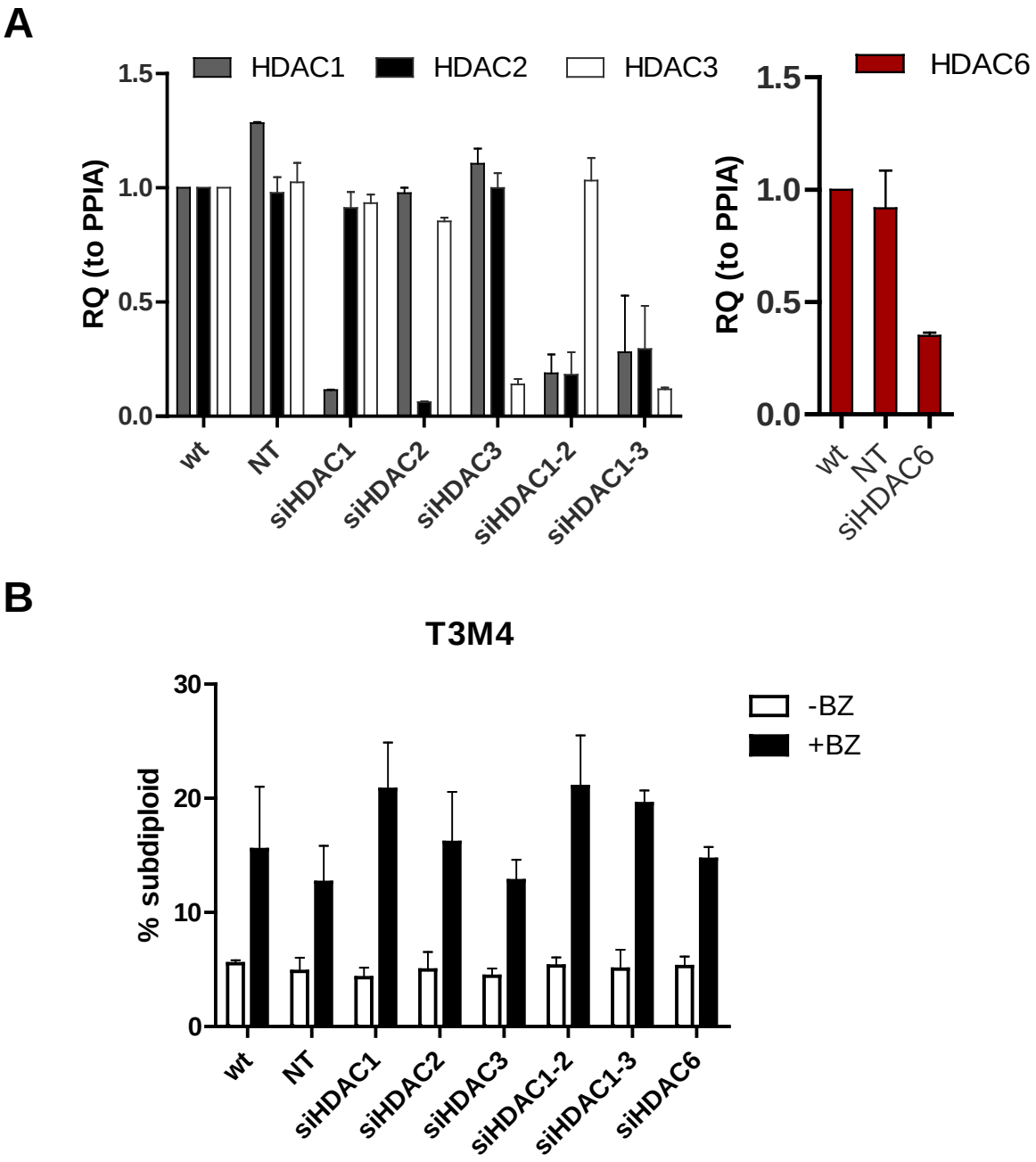

Figure 5.7 Effects of HDACs 1, 2, 3 and 6 knockdown on BZ-induced cell death in T3M4 pancreatic cancer cells. A) HDACs were silenced for 48-72h, and qRT-PCR was used to determine relative quantities of each target to a control gene (PPIA). Columns represent mean ± SE (n=2). B) Following silencing, cells were exposed to 20nM BZ for 24h, and apoptosis (% subdiploid) measured by FACS. Columns represent mean ± SE (n=3).

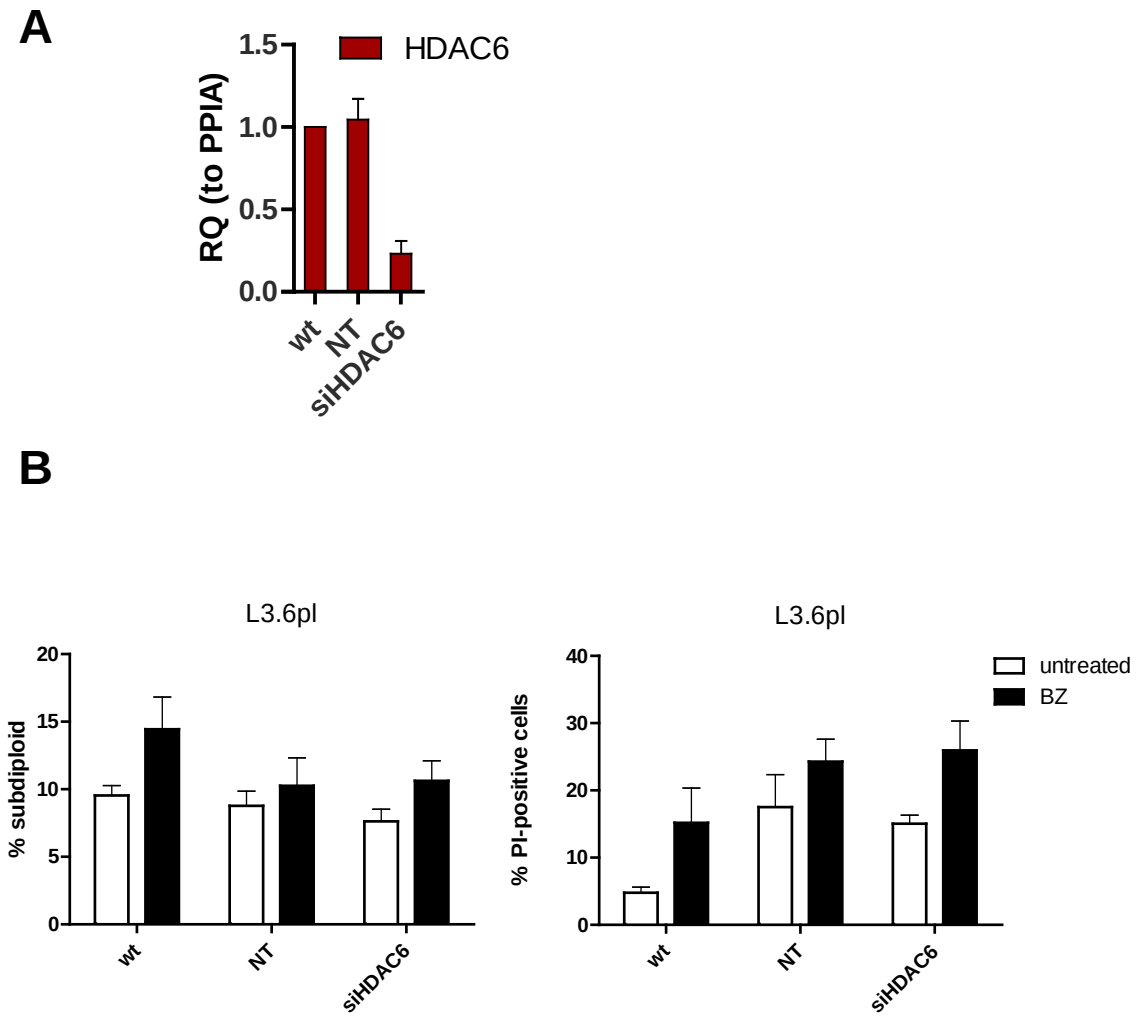

Figure 5.8 Effects of HDAC6 knockdown on BZ-induced cell death in L3.6pl pancreatic cancer cells. A) HDACs were silenced for 48-72h, and qRT-PCR was used to determine relative quantities of each target to a control gene (PPIA). Columns represent mean ± SE (n=2). B) Following silencing, cells were exposed to 20nM BZ for 24h, and apoptosis (% subdiploid; left panel) or outer membrane permeability (% PI-positive; right panel) was measured by FACS. Columns represent mean ± SE (n=3).

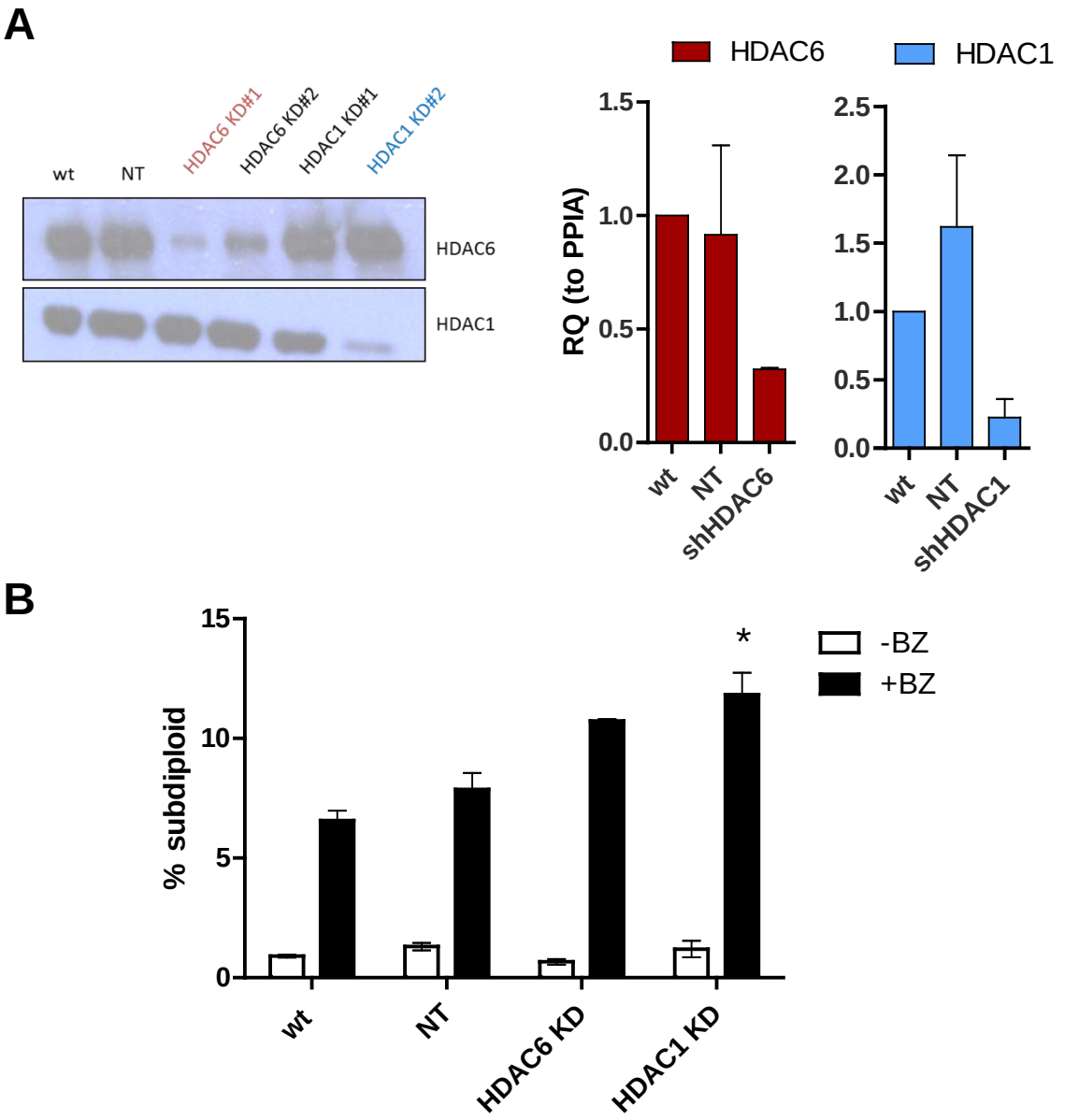

Figure 5.9 Comparison of HDAC1 vs. HDAC6 stable knockdown on BZ sensitivity in 253JB-V bladder cancer cells. Cells were stably transfected with pGIPZ plasmids in lentiviral vectors and selected using antibiotics. A) Two different knockdown constructs were evaluated for protein knockdown of each target (left panel), and the most potent-HDAC6 #1 (red) and HDAC1 #2 (blue) were validated by qRT-PCR (right panel) Data is representative of at least 2 independent experiments. B) Stably transfected cells were exposed to 20nM BZ for 48h and DNA fragmentation (% subdiploid) was measured by FACS. Columns represent mean $\pm$ SE (n=3). Asterisk denotes $P < 0.05$.

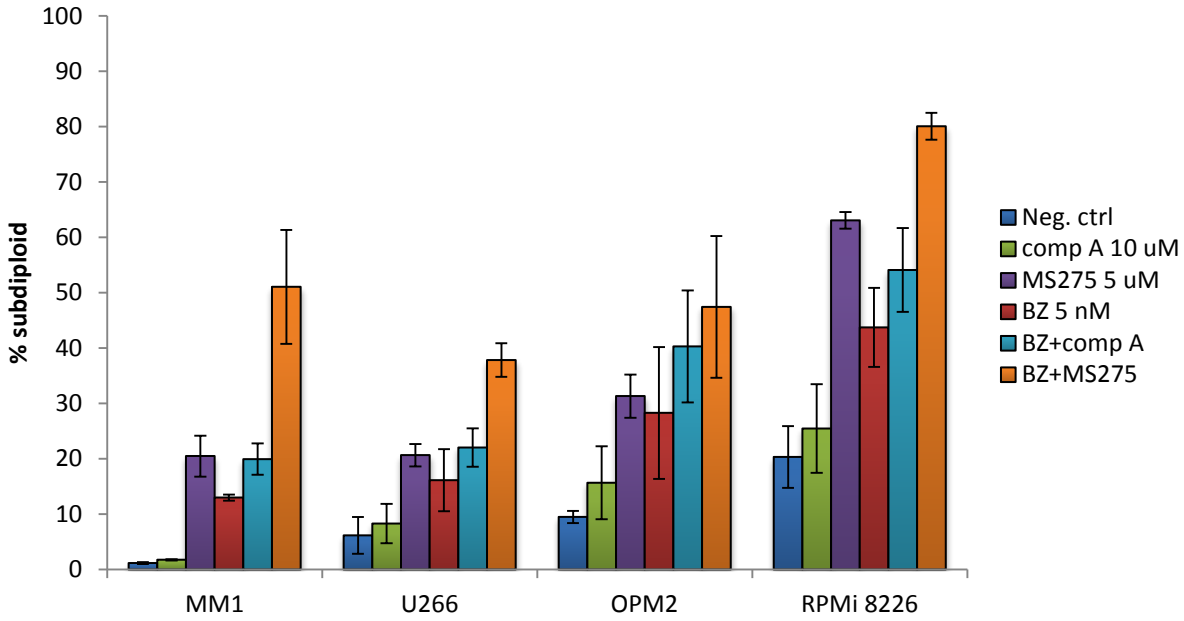

Figure 5.10 Effects of Compound A and SNDX-275 on BZ-induced death in MM cells. Cells were grown in suspension and then exposed to indicated concentrations of drugs for 24h. FACS analysis was used to determine the percent apoptotic cells (% subdiploid) as evidenced by fragmented DNA. Columns represent mean $\pm$ SE (n=3).

partially inhibited by the available chemical inhibitors. To address this, we used siRNA and shRNA knockdown to decrease expression of type I HDACs or HDAC6, and surprisingly, the results largely confirmed what we had observed with the chemical inhibitors, in that knockdown of HDAC1 had stronger effects on BZ-induced cell death than did knockdown of HDAC6.

Our results contrast with published work using other HDAC6-selective inhibitors. Much of this work was done in MM models; for example tubacin, a moderately selective HDAC6 inhibitor, was found to enhance BZ-induced cell death in MM (174). However, it should be mentioned that the dose of tubacin used in this study (5 μM) has off-target effects on Class I HDACs, as evidenced in a previous study by Haggarty, et al. in which as little as 0.2μM of tubacin was enough to noticeably raise acetylated-histone H3 levels (169). Notably, data on the effects of tubacin exposure on acetylated-histone H3 levels were lacking in the Hideshima, et al. study (174). Recently, similar results were found in MM cells and xenografts using a novel more selective HDAC6 inhibitor known as ACY-1215 (175). In solid tumor cells, the HDAC6-selective inhibitor NK84 displayed synergy with bortezomib in ovarian cancer (171), and our own group demonstrated that HDAC siRNA sensitized L3.6pl pancreatic cancer cells to bortezomib (used at higher concentrations than (104). Cumulatively, targeting HDAC6 has yielded consistent but not dramatic sensitization to PIs in multiple studies. Two possible explanations exist for why our results do not match the studies mentioned here. The first could be related to the chemical properties of Compound A; however, it seems to be a very selective and potent inhibitor of HDAC6 (Fig. 5.2). The second could be related to the cell types used in this study (pancreatic and bladder cancer); thus far the only other solid tumor cells in which a selective HDAC6 inhibitor has

been tested in combination with PIs is ovarian cancer, which may express extremely high levels of HDAC6 (171).

Because of the somewhat disappointing results of Compound A in our pancreatic and bladder cancer cells, we sought to examine its activity in MM cells (Fig. 5.9). Here, Compound A was non-toxic as a single agent, but combination with BZ provided modest but consistent increases in cell death over BZ alone in 4 different MM cell lines. However, SNDX-275 was more potent at enhancing the effects of BZ in these cells as well, although significant toxicity with single-agent SNDX-275 was observed. This supports previous findings, and suggests that MM may be the most appropriate disease site for HDAC6 + proteasome inhibitor based therapy.

In our MM, pancreatic, and bladder cancer cells, the Type I and pan- HDAC inhibitors, SNDX-275 and SAHA, respectively, consistently enhanced BZ-induced cell death and displayed greater toxicity as single agents than did Compound A. HDAC inhibitor-mediated sensitization to PIs has also been reported previously in the literature in a variety of tumor types (125, 176-178). Whereas the rationale for combining HDAC6 inhibitors with PIs is fairly clear, it is not presently understood how/why inhibition of Type I HDACs sensitizes cells to PIs (179). Furthermore, it is not clear whether Type I HDAC inhibitors sensitize cells to PIs, or vice versa. Indeed, recent data indicate that HDAC inhibitor-induced decreases in proteasome activity play a significant role in the cytotoxicity of HDAC inhibition (180). Operating under the hypothesis that HDACi's sensitize cells to PIs, a couple of interesting studies have highlighted the role of HDAC1 in PI-induced death. Kikuchi, et al. demonstrated that knockdown of HDAC1 alone sensitized MM cells to BZ, whereas HDAC1 overexpression promoted resistance (181). Buglio, et al. found that

combinations of a novel HDAC1-selective inhibitor (MGCD0103) and BZ in Hodgkin's lymphoma synergize to produce greater levels of cell death than either drug alone (182). Importantly, our results identify novel effects of Type I HDACs on protein aggregation/aggresome formation as a potential explanation for their activity in combination with PIs. The disruption of large aggresome-like structures seen with SNDX-275 could be a result of altered gene expression levels, or perhaps by shuttling of nuclear HDACs into the cytosol to directly interact with the aggresome machinery. Regardless, these results bear further evaluation and may lead to previously undiscovered roles for nuclear HDACs.

Chapter 6. CONCLUSIONS & FUTURE DIRECTIONS

Taken together, the components of this thesis describe key new findings that expand the body of knowledge with respect to the consequences of proteasome inhibition in cancer. In this section, the central conclusions from previous chapters (Chps. 3-5) will be outlined, and future strategies by which to expand these discoveries will be discussed.

6.1 Conclusions

Chapter 3: Lack of inducible eIF2α phosphorylation is associated with sensitivity to bortezomib in pancreatic cancer cells. Here, the data led to several key conclusions. Firstly, I showed that the induction of eIF2α-P at clinically relevant doses of BZ is cytoprotective, and not cytotoxic (as other groups have argued). Based on my observations, the dose appears to be critical for observing this cytoprotective effect. High-doses of PIs (e.g. >100nM of BZ) may overwhelm the cell too rapidly to for global translational repression by eIF2α-P to be useful; rather the pro-apoptotic actions of eIF2α-P-induced transcription factors such as CHOP may become dominant under these conditions. Secondly, I identified a subset of pancreatic cancer cells that possess high levels of constitutive eIF2α-P in resting conditions. This was found to be controlled by the eIF2α kinase GCN2. Thirdly, we demonstrated that this phenotype adversely affected cellular response to BZ, and we found less efficient translation attenuation, increased protein aggregation, increased oxidative stress, and increased cell death upon BZ exposure in these cells. Lastly, I identified HRI, and to a lesser extent PERK, as the eIF2α kinases activated by BZ exposure, and showed that silencing of HRI alone and in combination with PERK sensitizes resistant cells to BZ.

Chapter 4: Hsp72 induction protects bladder cancer cells from bortezomib-induced cell death. In this chapter, we conclude that modulation of Hsp72 in bladder cancer significantly affects the anti-cancer activity of BZ. Chemical inhibition of the HSR or direct silencing of Hsp72 enhanced the cytotoxic effects of BZ *in vitro* and *in vivo*, while overexpression of Hsp72 decreased BZ-induced cell death. We also discovered heterogeneity in expression of the major Hsp72 isoform (HSPA1A) in human bladder cancer cells; some cells expressed both HSPA1A and HSPA1B and robustly induced both genes following exposure to BZ, whereas others expressed nearly undetectable levels HSPA1A that could not be induced. This was due to methylation of the HSPA1A promoter region in these cells, which inhibited HSF1 binding. These HSPA1A^{low} cells compensated for their lack of A1A isoform expression by increasing expression of the HSPA1B isoform such that total protein levels of Hsp72 were similar to cells expressing both isoforms. When we stably overexpressed HSPA1A in HSPA1A^{low} cells, we found that this increased levels of Hsp72 and partially protected these cells from BZ-induced cell death. Likewise, knockdown of HSPA1B in HSPA1A^{low} cells sensitized them to BZ. Overall, extremely low HSPA1A levels were present in approximately 40% of bladder cancer cell lines tested, indicating that methylation of the HSPA1A promoter may be fairly common in bladder cancer. However, low HSPA1A expression did not correlate with BZ sensitivity, presumably because of the compensation by HSPA1B. Collectively, our data provide support for functional redundancy between the A1A and A1B isoforms.

Chapter 5: Evaluation of the effects of a selective HDAC6 inhibitor on promoting bortezomib-induced cancer cell death. Here, we first concluded that Compound A was indeed selective for HDAC6 over Class 1 HDACs because it promoted

robust accumulation of acetylated tubulin while not affecting acetylated histone-H3 levels. However, we did not look at the acetylation levels of other HDAC6 substrates such as Hsp90 and cortactin, or acetylation levels of other histones, so this is an obvious limitation to this study. Secondly, our data demonstrated that inhibition of Class I HDACs via SNDX-275 was more potent than Compound A at enhancing BZ-induced cell death as measured by both DNA fragmentation and plasma membrane permeatility. This observation was corroborated by similar results from both transient (siRNA) and stable (shRNA) silencing of HDAC6 vs. Class I HDACs, in which the knockdown of Class I HDACs (in particular HDAC1) appeared to have stronger effects on promoting BZ-induced cell death than did HDAC6 knockdown. However, genetic silencing of the Class I HDACs did not completely recapitulate the dramatic sensitization provided by the SNDX-275 chemical inhibitor, indicating that this drug may have other off-target effects that are essential for enhancing the activity of BZ. Class I HDAC inhibitors have been previously shown to cause ROS production, and based on my data from Chp. 3, this represents an attractive explanation as to why SNDX-275 increases the toxicity of BZ and other PIs (125). Collectively, these data lead us to the ultimate conclusion that HDAC6 is not an effective target for synergy with PIs in solid tumors.

6.2 Future directions

Chapter 3. Our study detailing the relationship between eIF2α phosphorylation and BZ sensitivity in pancreatic cancer provides two important discoveries that upon further experimental validation, could have measurable impact on the way PI's are used clinically. The first promising idea is that of eIF2α-P as a biomarker for an underlying stress that may

render cancer cells more sensitive to PI's. Having only used 10 cell lines in one tissue type, our data suggest a strong correlation between high basal eIF2α-P and PI-sensitivity, but it is premature to call this a "biomarker". Further studies will need to be done comparing eIF2α-P and BZ sensitivity in additional cancer cell lines (at least n=30), and immunohistochemical analysis of eIF2α-P levels in Velcade®-responsive and -unresponsive tumors would also be necessary (perhaps through tissue microarray). It is likely that constitutive eIF2α-P is merely a "readout" of a more global perturbation in intracellular homeostasis. We speculate that because GCN2 appears to control constitutive eIF2α-P, GCN2-related metabolic stress pathways may be contributing to eIF2α-P in our BZ-sensitive cells. Whole-genome expression profiling comparing expression levels of these pathways between BZ-sensitive and BZ-resistant cell lines could provide useful clues as to the origins of constitutive eIF2α-P and perhaps provide a multi-faceted genetic "signature" to predict sensitivity to PI's. At present, the functional consequences of constitutive eIF2α-P in our sensitive cells are not clear. One would predict that high basal eIF2α-P would significantly decrease global rates of protein synthesis, and we found that CF-Pac1 and T3M4 cells incorporated ~20-25% less ^{3}H-leucine than did Suit2 and mPanc96 cells (Fig. 3.5), indicating less active protein synthesis (although these differences were not statistically significant). However, basal expression levels of CHOP were not significantly different between cells with high or low eIF2α-P (Fig. 3.13), suggesting that the constitutive phosphorylation at steady state is not completely mimicking the effects of stress-inducible phosphorylation on downstream signaling pathways. To more carefully explore the function of basal/constitutive eIF2α-P in our pancreatic cancer cells, future experiments should include stable ovexpression of the GADD34 phosphatase cofactor, which should reduce

constitutive phosphorylation in our BZ-sensitive cells and perhaps restore inducible phosphorylation and decrease BZ-sensitivity. Alternatively, the constitutive eIF2α-P could be an adaptive response to cell stress that is important for survival in some cells, and in this case one would expect that GADD34 overexpression could promote spontaneous cell death.

The second exciting discovery from Chapter 3 that bears further exploration is the identification of HRI as the primary BZ-activated eIF2α kinase in pancreatic cancer (and likely other solid tumor) cells. Further experiments directly measuring HRI phosphorylation are needed to confirm this activation (since no phospho-specific HRI antibodies are currently available, this would have to be done using immunoprecipiation with a phospho-serine antibody). In addition, another key future experiment would be to probe $HRI^{-/-}$ MEFs for enhanced sensitivity to PI's, similar to previous experiments using eIF2α mutant MEFs (Fig. 3.20). If our hypothesis regarding the centrality of the cytoprotective response elicited by HRI- eIF2α-P is correct, targeting HRI could be a potent strategy to overcome resistance to PI's. Kinases are among the most "druggable" targets and such approaches have proven effective in targeting cancer (183). Interestingly, $HRI^{-/-}$ mice develop normally and are fertile, with only minor hematologic side effects. This suggests that HRI inhibition may be well-tolerated systemically, and provides rationale for the development of small molecule HRI inhibitors for use in combination with PI's and perhaps other proteotoxic stressors such as arsenicals.

In **Chapter 4**, our study describing Hsp72 as a resistance factor to BZ in bladder cancer presents two important future directions. First, this study supports the continued development of Hsp72-specific inhibitors for use in cancer therapy, particularly in combination with other proteotoxic stress-inducing drugs such as PIs. Multiple research

groups are working to achieve this, and inhibitors should become available within a few years. Secondly, our data suggest a high incidence of HSPA1A promoter methylation in bladder cancer, which may open a therapeutic window for selective targeting of the HSPA1B isoform. Although we did not observe a significant correlation between extremely low HSPA1A expression and BZ sensitivity, the potential of HSPA1A promoter methylation as a biomarker bears further investigation. Because of the multitude of cytoprotective functions of Hsp72 (protein folding, anti-apoptosis, lysosomal stability), it would be expected that shutting off the HSPA1A promoter and relying exclusively on the HSPA1B locus could have significant consequences for a malignant cell. We hope to analyze HSPA1A promoter methylation in patient bladder tumor samples in the future, with hopes of 1) identifying the prevalence, and 2) probing for correlations with outcomes and survival.

Chapter 5. Because of our unexpected conclusion that Type I HDAC inhibition is more effective than HDAC6 inhibition in promoting BZ-induced cell death in solid tumor cells, we are now actively pursuing intriguing new data in which HDAC6 inhibition by Compound A may effectively reduce solid tumor cell migration and invasion. We are currently evaluating Compound A *in vitro* for its effects on pancreatic and bladder cancer cell migration using the traditional scratch assay, and on invasion by chemotactic movement through a 3D matrigel chamber. Ultimately, we seek to apply Compound A to a mouse model of metastatic bladder cancer developed by other investigators in our group and measure circulating tumor cells and metastases with and without Compound A. Presently, the clinical usefulness for an anti-metastatic agent would be rather limited because it remains difficult to accurately predict which tumors will metastasize. Furthermore, administration of an anti-metastatic agent after distant metastases were already established

would not be optimal. A scenario would have to arise where metastasis was identified very early (perhaps through finding small numbers of circulating tumor cells) and was followed by immediate administration of the anti-metastatic agent for a specified duration. Alternatively, a well-tolerated anti-metastatic agent could be useful following resection of a tumor that displayed aggressive phenotypes but had not yet visibly metastasized. The agent could then be administered following surgery in order to prevent the development of metastases from the residual un-resectable tumor cells that had already invaded peripheral tissue. Despite the challenges just mentioned, the anti-metastatic potential of HDAC6 inhibition is an important phenotype that may become valuable in the future since selective HDAC6 inhibition is thought to be better tolerated systemically than inhibition of Type I HDACs.

6.3 Final Discussion

In an effort to combine my conclusions across all of these projects and tumor types, I would like to comment in a broad sense on what my observations have led me to believe about the mechanisms that most significantly contribute to proteasome inhibitor-induced cytotoxicity. Based on my results, if I were to now rank the three pathways studied in my thesis in terms of their centrality to controlling cellular outcome following PI, they would rank in the following order: 1) eIF2α phosphorylation/ translational control, 2) Hsp72 induction/ heat shock response, and 3) the HDAC6/ aggresome pathway. Here, I discuss why I believe this hierarchy to be true.

Believing that the simplest, most intuitive explanation is often correct, let me build on the assumption that the primary consequence of PIs is the bulk accumulation of

misfolded proteins with nowhere to go. The goal of the cell is then obviously to stop this accumulation, so what is the most efficient way to accomplish this? The simplest explanation is to stop making more misfolded proteins. This is why I believe eIF2α phosphorylation to be central to determining cellular fate following PI. As protein production is shutting down, secondary response mechanisms come into play since the cell must handle the misfolded species that had already accumulated. This is where the heat shock response (HSR) and chaperones come into play. The cell increases the level of chaperones (such as Hsp72) to "sequester" these toxic proteins. Finally, the misfolded substrates must be disposed of somehow, but because the proteasome is blocked, the cell must utilize an alternative strategy called autophagy. This simplistic model can be conceptualized as a clogged tub filling up with water (Fig 6.1). Now imagine if the proteasome is blocked but the cell does not stop protein synthesis when it should. Everything else downstream becomes almost irrelevant, presenting essentially insurmountable odds for the chaperone network and autophagy. By adopting this 30,000 foot view of cellular biology, one can "rank" the relative inputs into the PI-induced stress response and predict which pathways could be disrupted to best augment the activity of PIs. A graphical view of the activation of these essential pathways is provided in Fig. 6.2.

The most intriguing aspect of intrinsic tumor biology identified over the course of my studies has been the discovery that basal phosphorylation levels of eIF2α differ between cancer cell lines. I and others in our group have seen this phenomenon in multiple pancreatic, bladder, and prostate cancer cells, and I have also spoken with other investigators at conferences who had noticed similar phenomena, but had not investigated it

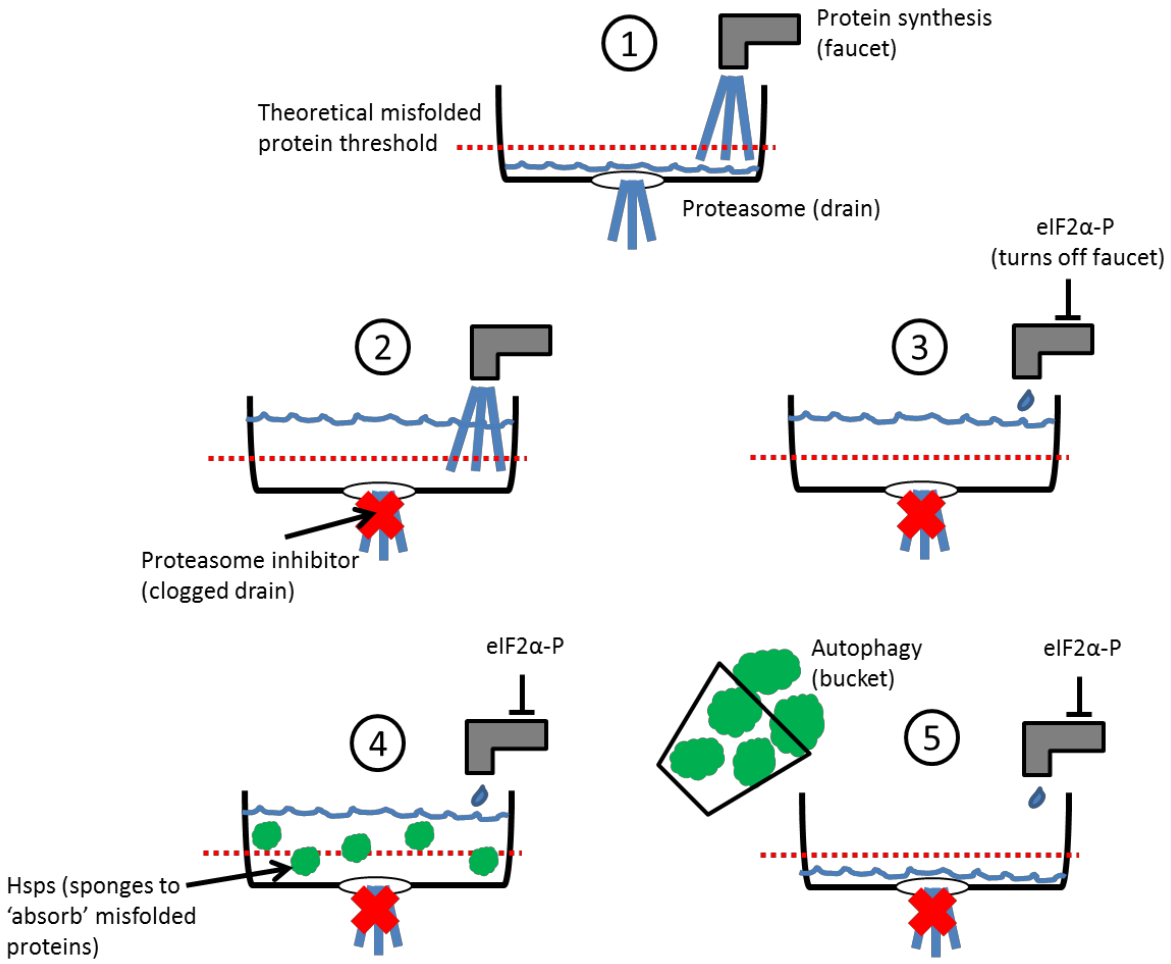

Figure 6.1 The "bathtub" effect. Theoretical diagram outlining how 3 critical stress response pathways work to relieve the stress caused by proteasome inhibition. 1) Proteostasis is maintained by a proteomic balance of synthesis and degradation, or inflow/outflow. 2) If the proteasome (outflow) becomes blocked, then the balance is disrupted and unwanted proteins accumulate above the tolerated "threshold." 3) Inflow must then be stopped (accomplished by eIF2α phosphorylation turning off protein synthesis, or the "faucet"). 4) The cell must now restore proteostasis. Inducible molecular chaperones or heat shock proteins (Hsps) sequester or "soak up" the accumulated misfolded proteins. 5) The chaperone-misfolded substrate complexes (often coalesced into large aggregates to facilitate degradation) are then engulfed, or "scooped up" by autophagosomes (buckets) for recycling. Collectively, this effort reduces the levels or misfolded proteins to below the threshold, assuming that proteasome activity is soon restored.

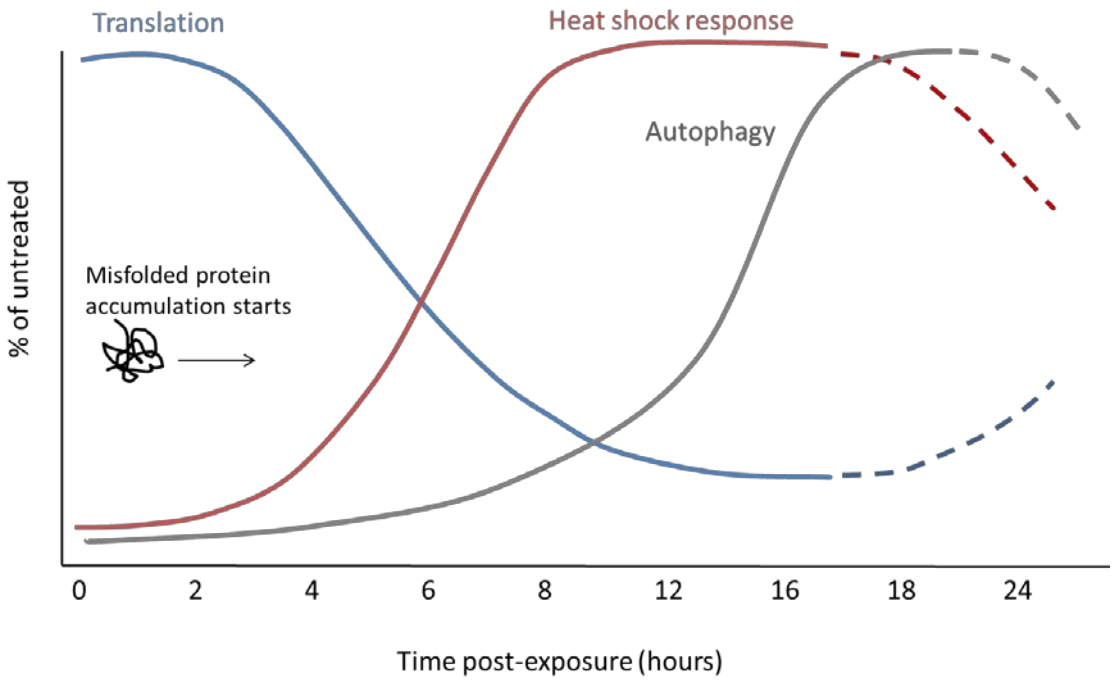

Figure 6.2 Temporal depiction of the three major systems needed for response to proteasome inhibitors. Graphical interpretation of the relative rates of translation, induction of the heat shock response, and activation of autophagy following exposure to a PI (x-axis = hours post-exposure). Translation repression and the heat shock response are the most rapid responses (significant changes within 4-8h), with autophagy activation occurring later (12-18h). Following resolution of stress, these systems should begin to move back towards steady-state levels (dashed lines).

further. My work (Chp. 3) is the first time that this elevated basal phosphorylation has been linked to enhanced sensitivity to a chemotherapeutic agent. Because of the centrality of eIF2α phosphorylation in mitigating proteoxic stress, this basal phosphorylation status may be useful in predicting response to other proteotoxic stress-inducing agents such as arsenicals or Hsp90 inhibitors. Additionally, basal eIF2α-P levels could also predict how a cell responds to targeted therapeutics against signaling pathways that influence protein synthesis such as the Akt/PI3K pathway.

Presumably Hsp72 induction and especially aggregate handling by HDAC6 would be more critical to cells which possessed constitutive, un-inducible eIF2α phosphorylation because levels of misfolded and aggregated proteins would be higher due to continued translation. However, I noticed roughly similar levels of Hsp72 induction irrespective of their phospho-eIF2α status; likewise, HDAC6 inhibition provided little sensitization to BZ in cells with constitutive, un-inducible eIF2α phosphorylation (with the exception of T3M4). Because of the underwhelming effects of HDAC6 inhibition in my hands, and because of recent findings in the literature, I believe that instead of targeting the aggresome pathway, more direct inhibitors of autophagy would be much more effective in combination with PIs. Constitutively high autophagy has been found in pancreatic cancer (124), and this autophagy was shown to be required for tumorigenesis. Activated Ras has also been found to drive increased basal autophagy to promote tumorigenesis, which may explain why this system is highly activated in pancreatic cancers (5). My data also suggest that basal autophagy correlates with basal eIF2α phosphorylation, and in cells where eIF2α is un-inducible, autophagy appears to be un-inducible as well. The mechanistic link between eIF2α and autophagy is presently unclear, and our group has had difficulty in identifying a stress-

responsive transcription factor that drives ATG gene upregulation. A scenario can be imagined where activated Ras drives metabolic changes that activate the GCN2 kinase and raise basal eIF2α phosphorylation, which then signals the up-regulation of autophagy to maintain energy for the Ras-driven cell.

Indeed other plausible mechanisms not examined in this thesis may also influence the cytotoxicity of PIs in cancer cells. Two such possibilities, known as EMT (epithelial-to-mesenchymal transition) and mitochondrial priming, involve characteristics of cancer cells that have the potential to convey pan-resistance to a broad spectrum of chemotherapeutic agents. EMT collectively refers to a reversible process through which cells transition from an epithelial morphology with tight cell-cell interactions into more fibroblast-like cells with decreased polarity and cell-cell interactions. It is hypothesized that this transition confers a more metastatic phenotype to cancer cells, allowing them to break free of the primary tumor and invade surrounding tissue to enter circulation. EMT has also been associated with broad-spectrum drug resistance; indeed recent work from our group has indicated that a more mesenchymal phenotype leads to resistance to standard chemotherapeutic agents in pancreatic cancer preclinical models (98). In this study by Arumugam, et al., many of the same cell lines that I found sensitive to BZ were also more sensitive to the conventional chemotherapeutic agents gemcitabine, cisplatin, and 5-fluorouracil (5-FU). In addition, by reversing EMT through genetic silencing of a pro-mesenchymal transcription factor known as Zeb-1, we were able to sensitize resistant, mesenchymal Suit2 cells to BZ. We did not evaluate the P-eIF2α status of the Zeb-1 silenced cells however, which is needed to conclude if EMT affects basal phosphorylation levels or translational control in any way. In our hands, mesenchymal cells do not have appear to have lower rates of translation, so it is

likely that Zeb-1 knockdown promotes BZ-induced cell death by other mechanisms. Through unpublished work from our group and the work of others, inhibition of Class I HDACs may be another strategy to reverse EMT (184). This could be an important explanation for why SNDX-275 was more potent than Compound A in sensitizing cells to BZ. Overall, the relationship between EMT and protein quality control networks bears further exploration.

The idea of mitochondrial priming is relatively new and has been developed by seminal work from the laboratory of Anthony Letai at the Dana-Farber Cancer Institute. Through direct introduction of BH3-only pro-apoptotic peptides, his group has found that certain cancer cells are intrinsically resistant to apoptosis, whereas other cancer cells are more "primed" and readily undergo apoptosis. This "priming" refers to the relative "proximity to the apoptotic threshold" of mitochondria isolated from cancer cells as measured by their ability to undergo mitochondrial outer membrane permeabilization (MOMP) upon direct exposure to PUMA, BMF, and BIM BH3-only peptides (185). This is an attractive explanation for broad-spectrum drug resistance in cancer, and although not tested here, could be another contributing factor to the BZ sensitivity/resistance of the pancreatic and bladder cancer cells that were studied.

In conclusion, I hope that this thesis provides key contributions to understanding how proteasome inhibitors function as anti-cancer agents, and how cancer cell heterogeneity influences their efficacy. A final model summarizing my view of the cellular response to proteasome inhibition and suggested locations for therapeutic targeting is presented in Fig. 6.3. It is an exciting time for cancer research, and I am grateful that I was able to spend five

and half years of my life addressing perhaps the biggest biomedical challenge of my generation at such a world-class institution. Much is left to be uncovered, and as I have stood on the shoulders of those before me, I hope that this work provides a solid foundation for others to come.

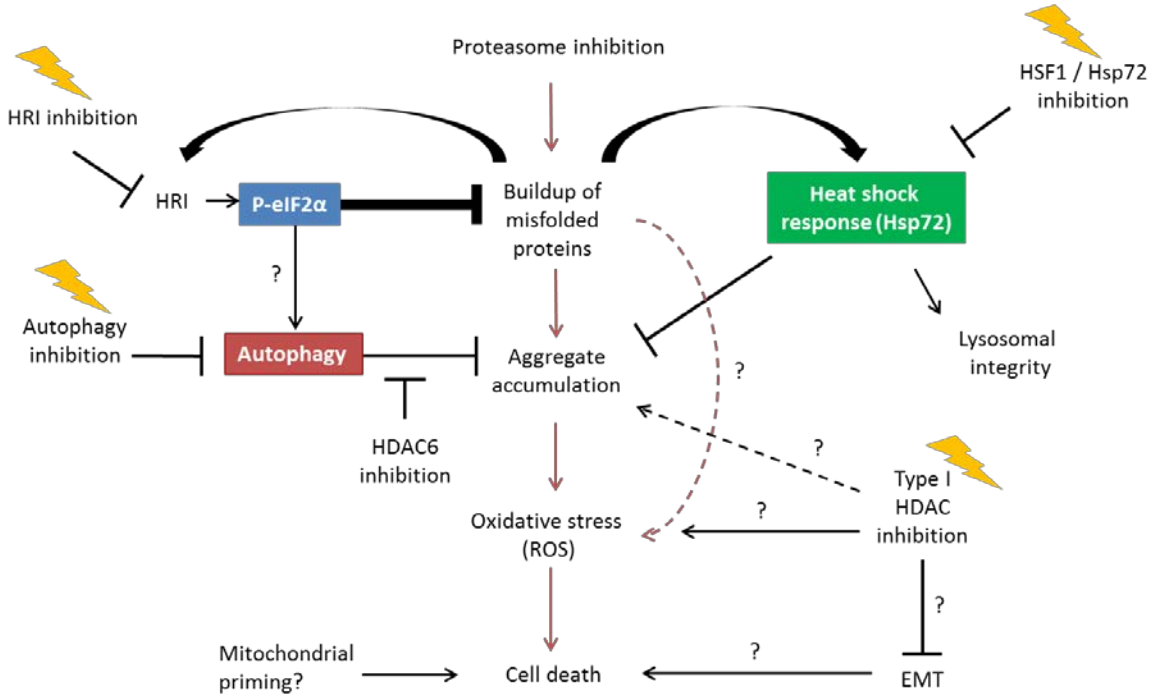

Figure 6.3 Overall model depicting the various inputs into cellular outcome following proteasome inhibition. Left, eIF2α-mediated translational repression plays the most essential role in preventing downstream proteotoxicity, and may potentially play a role in activating autophagy as a secondary degradation system. Right, activation of the heat shock response attempts to inhibits aggregate accumulation and toxicity by refolding or and shielding hydrophobic residues from the cytosol and other proteins. Hsps may also play a role in presenting substrates to autophagy, and may also ensure functionality of autophagy through stabilization of the lysosomal membrane. Finally, HDAC6 inhibition affects only a single input (handling of aggregates for degradation by autophagy), whereas Class I HDAC inhibition may affect multiple, which may explain why Class I inhibition sensitize cells to BZ better than HDAC6 inhibition. Orange lightning bolts indicate the best areas for developing therapeutic strategies to enhance the activity of PIs.

Chapter 7. REFERENCES

1. Luo, J., N. L. Solimini, and S. J. Elledge. 2009. Principles of cancer therapy: oncogene and non-oncogene addiction. Cell 136:823-837.
2. Dai, C., L. Whitesell, A. B. Rogers, and S. Lindquist. 2007. Heat shock factor 1 is a powerful multifaceted modifier of carcinogenesis. Cell 130:1005-1018.
3. Solimini, N. L., J. Luo, and S. J. Elledge. 2007. Non-oncogene addiction and the stress phenotype of cancer cells. Cell 130:986-988.
4. DeNicola, G. M., F. A. Karreth, T. J. Humpton, A. Gopinathan, C. Wei, K. Frese, D. Mangal, K. H. Yu, C. J. Yeo, E. S. Calhoun, F. Scrimieri, J. M. Winter, R. H. Hruban, C. Iacobuzio-Donahue, S. E. Kern, I. A. Blair, and D. A. Tuveson. 2011. Oncogene-induced Nrf2 transcription promotes ROS detoxification and tumorigenesis. Nature 475:106-109.
5. Guo, J. Y., H. Y. Chen, R. Mathew, J. Fan, A. M. Strohecker, G. Karsli-Uzunbas, J. J. Kamphorst, G. Chen, J. M. Lemons, V. Karantza, H. A. Coller, R. S. Dipaola, C. Gelinas, J. D. Rabinowitz, and E. White. 2011. Activated Ras requires autophagy to maintain oxidative metabolism and tumorigenesis. Genes Dev 25:460-470.
6. Torres, E. M., B. R. Williams, and A. Amon. 2008. Aneuploidy: cells losing their balance. Genetics 179:737-746.
7. Zimmerman, S. B., and S. O. Trach. 1991. Estimation of macromolecule concentrations and excluded volume effects for the cytoplasm of Escherichia coli. J Mol Biol 222:599-620.
8. Ritossa, F. 1996. Discovery of the heat shock response. Cell Stress Chaperones 1:97-98.

9. Whitesell, L., and S. L. Lindquist. 2005. HSP90 and the chaperoning of cancer. Nat Rev Cancer 5:761-772.

10. Frydman, J., E. Nimmesgern, K. Ohtsuka, and F. U. Hartl. 1994. Folding of nascent polypeptide chains in a high molecular mass assembly with molecular chaperones. Nature 370:111-117.

11. Morano, K. A. 2007. New tricks for an old dog: the evolving world of Hsp70. Annals of the New York Academy of Sciences 1113:1-14.

12. Petrucelli, L., D. Dickson, K. Kehoe, J. Taylor, H. Snyder, A. Grover, M. De Lucia, E. McGowan, J. Lewis, G. Prihar, J. Kim, W. H. Dillmann, S. E. Browne, A. Hall, R. Voellmy, Y. Tsuboi, T. M. Dawson, B. Wolozin, J. Hardy, and M. Hutton. 2004. CHIP and Hsp70 regulate tau ubiquitination, degradation and aggregation. Hum Mol Genet 13:703-714.

13. Goldberg, A. L. 2000. Probing the proteasome pathway. Nature biotechnology 18:494-496.

14. Chin, L. S., J. A. Olzmann, and L. Li. 2010. Parkin-mediated ubiquitin signalling in aggresome formation and autophagy. Biochemical Society transactions 38:144-149.

15. Goldberg, A. L. 2007. Functions of the proteasome: from protein degradation and immune surveillance to cancer therapy. Biochemical Society transactions 35:12-17.

16. Yang, Z., and D. J. Klionsky. 2010. Mammalian autophagy: core molecular machinery and signaling regulation. Curr Opin Cell Biol 22:124-131.

17. Yang, Z., and D. J. Klionsky. 2010. Eaten alive: a history of macroautophagy. Nat Cell Biol 12:814-822.

18. Dice, J. F. 2007. Chaperone-mediated autophagy. Autophagy 3:295-299.

19. Wu, W. K., K. M. Sakamoto, M. Milani, G. Aldana-Masankgay, D. Fan, K. Wu, C. W. Lee, C. H. Cho, J. Yu, and J. J. Sung. 2010. Macroautophagy modulates cellular response to proteasome inhibitors in cancer therapy. Drug Resist Updat 13:87-92.

20. Lamark, T., V. Kirkin, I. Dikic, and T. Johansen. 2009. NBR1 and p62 as cargo receptors for selective autophagy of ubiquitinated targets. Cell cycle (Georgetown, Tex 8:1986-1990.

21. Kirkin, V., T. Lamark, T. Johansen, and I. Dikic. 2009. NBR1 cooperates with p62 in selective autophagy of ubiquitinated targets. Autophagy 5:732-733.

22. Pankiv, S., T. H. Clausen, T. Lamark, A. Brech, J. A. Bruun, H. Outzen, A. Overvatn, G. Bjorkoy, and T. Johansen. 2007. p62/SQSTM1 binds directly to Atg8/LC3 to facilitate degradation of ubiquitinated protein aggregates by autophagy. The Journal of biological chemistry 282:24131-24145.

23. Xie, Z., and D. J. Klionsky. 2007. Autophagosome formation: core machinery and adaptations. Nat Cell Biol 9:1102-1109.

24. Adams, J., V. J. Palombella, E. A. Sausville, J. Johnson, A. Destree, D. D. Lazarus, J. Maas, C. S. Pien, S. Prakash, and P. J. Elliott. 1999. Proteasome inhibitors: a novel class of potent and effective antitumor agents. Cancer research 59:2615-2622.

25. Adams, J., and M. Kauffman. 2004. Development of the proteasome inhibitor Velcade (Bortezomib). Cancer Invest 22:304-311.

26. Feling, R. H., G. O. Buchanan, T. J. Mincer, C. A. Kauffman, P. R. Jensen, and W. Fenical. 2003. Salinosporamide A: a highly cytotoxic proteasome inhibitor from a novel microbial source, a marine bacterium of the new genus salinospora. Angew Chem Int Ed Engl 42:355-357.

27. Chauhan, D., L. Catley, G. Li, K. Podar, T. Hideshima, M. Velankar, C. Mitsiades, N. Mitsiades, H. Yasui, A. Letai, H. Ovaa, C. Berkers, B. Nicholson, T. H. Chao, S. T. Neuteboom, P. Richardson, M. A. Palladino, and K. C. Anderson. 2005. A novel orally active proteasome inhibitor induces apoptosis in multiple myeloma cells with mechanisms distinct from Bortezomib. Cancer cell 8:407-419.

28. Demo, S. D., C. J. Kirk, M. A. Aujay, T. J. Buchholz, M. Dajee, M. N. Ho, J. Jiang, G. J. Laidig, E. R. Lewis, F. Parlati, K. D. Shenk, M. S. Smyth, C. M. Sun, M. K. Vallone, T. M. Woo, C. J. Molineaux, and M. K. Bennett. 2007. Antitumor activity of PR-171, a novel irreversible inhibitor of the proteasome. Cancer research 67:6383-6391.

29. Kisselev, A. F., W. A. van der Linden, and H. S. Overkleeft. 2012. Proteasome inhibitors: an expanding army attacking a unique target. Chem Biol 19:99-115.

30. Jolly, C., and R. I. Morimoto. 2000. Role of the heat shock response and molecular chaperones in oncogenesis and cell death. J Natl Cancer Inst 92:1564-1572.

31. Bauman, J. W., J. Liu, and C. D. Klaassen. 1993. Production of metallothionein and heat-shock proteins in response to metals. Fundam Appl Toxicol 21:15-22.

32. Kawazoe, Y., A. Nakai, M. Tanabe, and K. Nagata. 1998. Proteasome inhibition leads to the activation of all members of the heat-shock-factor family. Eur J Biochem 255:356-362.

33. Bush, K. T., A. L. Goldberg, and S. K. Nigam. 1997. Proteasome inhibition leads to a heat-shock response, induction of endoplasmic reticulum chaperones, and thermotolerance. The Journal of biological chemistry 272:9086-9092.

34. Liao, W., X. Li, M. Mancini, and L. Chan. 2006. Proteasome inhibition induces differential heat shock protein response but not unfolded protein response in HepG2 cells. J Cell Biochem 99:1085-1095.

35. Morimoto, R. I. 1998. Regulation of the heat shock transcriptional response: cross talk between a family of heat shock factors, molecular chaperones, and negative regulators. Genes Dev 12:3788-3796.

36. Guettouche, T., F. Boellmann, W. S. Lane, and R. Voellmy. 2005. Analysis of phosphorylation of human heat shock factor 1 in cells experiencing a stress. BMC Biochem 6:4.

37. Westerheide, S. D., J. Anckar, S. M. Stevens, Jr., L. Sistonen, and R. I. Morimoto. 2009. Stress-inducible regulation of heat shock factor 1 by the deacetylase SIRT1. Science 323:1063-1066.

38. Hilgarth, R. S., Y. Hong, O. K. Park-Sarge, and K. D. Sarge. 2003. Insights into the regulation of heat shock transcription factor 1 SUMO-1 modification. Biochem Biophys Res Commun 303:196-200.

39. Xu, D., L. P. Zalmas, and N. B. La Thangue. 2008. A transcription cofactor required for the heat-shock response. EMBO Rep 9:662-669.

40. Hahn, J. S., Z. Hu, D. J. Thiele, and V. R. Iyer. 2004. Genome-wide analysis of the biology of stress responses through heat shock transcription factor. Molecular and cellular biology 24:5249-5256.

41. Fritah, S., E. Col, C. Boyault, J. Govin, K. Sadoul, S. Chiocca, E. Christians, S. Khochbin, C. Jolly, and C. Vourc'h. 2009. Heat-shock factor 1 controls genome-wide acetylation in heat-shocked cells. Mol Biol Cell 20:4976-4984.

42. Baird, T. D., and R. C. Wek. 2012. Eukaryotic initiation factor 2 phosphorylation and translational control in metabolism. Adv Nutr 3:307-321.

43. McConkey, D. J., M. White, and W. Yan. 2012. HDAC inhibitor modulation of proteotoxicity as a therapeutic approach in cancer. Adv Cancer Res 116:131-163.

44. Han, A. P., C. Yu, L. Lu, Y. Fujiwara, C. Browne, G. Chin, M. Fleming, P. Leboulch, S. H. Orkin, and J. J. Chen. 2001. Heme-regulated eIF2alpha kinase (HRI) is required for translational regulation and survival of erythroid precursors in iron deficiency. EMBO J 20:6909-6918.

45. Lu, L., A. P. Han, and J. J. Chen. 2001. Translation initiation control by heme-regulated eukaryotic initiation factor 2alpha kinase in erythroid cells under cytoplasmic stresses. Molecular and cellular biology 21:7971-7980.

46. Yerlikaya, A., S. R. Kimball, and B. A. Stanley. 2008. Phosphorylation of eIF2alpha in response to 26S proteasome inhibition is mediated by the haem-regulated inhibitor (HRI) kinase. The Biochemical journal 412:579-588.

47. Matts, R. L., Z. Xu, J. K. Pal, and J. J. Chen. 1992. Interactions of the heme-regulated eIF-2 alpha kinase with heat shock proteins in rabbit reticulocyte lysates. The Journal of biological chemistry 267:18160-18167.

48. Uma, S., V. Thulasiraman, and R. L. Matts. 1999. Dual role for Hsc70 in the biogenesis and regulation of the heme-regulated kinase of the alpha subunit of eukaryotic translation initiation factor 2. Molecular and cellular biology 19:5861-5871.

49. Zhang, F., P. R. Romano, T. Nagamura-Inoue, B. Tian, T. E. Dever, M. B. Mathews, K. Ozato, and A. G. Hinnebusch. 2001. Binding of double-stranded RNA to protein

kinase PKR is required for dimerization and promotes critical autophosphorylation events in the activation loop. The Journal of biological chemistry 276:24946-24958.

50. Pindel, A., and A. Sadler. 2011. The role of protein kinase R in the interferon response. J Interferon Cytokine Res 31:59-70.

51. Harding, H. P., M. Calfon, F. Urano, I. Novoa, and D. Ron. 2002. Transcriptional and translational control in the Mammalian unfolded protein response. Annu Rev Cell Dev Biol 18:575-599.

52. Zhang, P., B. McGrath, S. Li, A. Frank, F. Zambito, J. Reinert, M. Gannon, K. Ma, K. McNaughton, and D. R. Cavener. 2002. The PERK eukaryotic initiation factor 2 alpha kinase is required for the development of the skeletal system, postnatal growth, and the function and viability of the pancreas. Molecular and cellular biology 22:3864-3874.

53. Harding, H. P., Y. Zhang, H. Zeng, I. Novoa, P. D. Lu, M. Calfon, N. Sadri, C. Yun, B. Popko, R. Paules, D. F. Stojdl, J. C. Bell, T. Hettmann, J. M. Leiden, and D. Ron. 2003. An integrated stress response regulates amino acid metabolism and resistance to oxidative stress. Molecular cell 11:619-633.

54. Rzymski, T., M. Milani, L. Pike, F. Buffa, H. R. Mellor, L. Winchester, I. Pires, E. Hammond, I. Ragoussis, and A. L. Harris. 2010. Regulation of autophagy by ATF4 in response to severe hypoxia. Oncogene 29:4424-4435.

55. Obeng, E. A., L. M. Carlson, D. M. Gutman, W. J. Harrington, Jr., K. P. Lee, and L. H. Boise. 2006. Proteasome inhibitors induce a terminal unfolded protein response in multiple myeloma cells. Blood 107:4907-4916.

56. Ron, D., and P. Walter. 2007. Signal integration in the endoplasmic reticulum unfolded protein response. Nature reviews 8:519-529.

57. Kim, I., W. Xu, and J. C. Reed. 2008. Cell death and endoplasmic reticulum stress: disease relevance and therapeutic opportunities. Nat Rev Drug Discov 7:1013-1030.

58. Jiang, H. Y., and R. C. Wek. 2005. Phosphorylation of the alpha-subunit of the eukaryotic initiation factor-2 (eIF2alpha) reduces protein synthesis and enhances apoptosis in response to proteasome inhibition. The Journal of biological chemistry 280:14189-14202.

59. Scheuner, D., B. Song, E. McEwen, C. Liu, R. Laybutt, P. Gillespie, T. Saunders, S. Bonner-Weir, and R. J. Kaufman. 2001. Translational control is required for the unfolded protein response and in vivo glucose homeostasis. Molecular cell 7:1165-1176.

60. Wictome, M., I. Henderson, A. G. Lee, and J. M. East. 1992. Mechanism of inhibition of the calcium pump of sarcoplasmic reticulum by thapsigargin. The Biochemical journal 283 (Pt 2):525-529.

61. Heifetz, A., R. W. Keenan, and A. D. Elbein. 1979. Mechanism of action of tunicamycin on the UDP-GlcNAc:dolichyl-phosphate Glc-NAc-1-phosphate transferase. Biochemistry 18:2186-2192.

62. Szegezdi, E., S. E. Logue, A. M. Gorman, and A. Samali. 2006. Mediators of endoplasmic reticulum stress-induced apoptosis. EMBO Rep 7:880-885.

63. Ellgaard, L., and A. Helenius. 2003. Quality control in the endoplasmic reticulum. Nature reviews 4:181-191.

64. Garcia-Mata, R., Y. S. Gao, and E. Sztul. 2002. Hassles with taking out the garbage: aggravating aggresomes. Traffic 3:388-396.

65. Kawaguchi, Y., J. J. Kovacs, A. McLaurin, J. M. Vance, A. Ito, and T. P. Yao. 2003. The deacetylase HDAC6 regulates aggresome formation and cell viability in response to misfolded protein stress. Cell 115:727-738.

66. Jacobson, A. D., N. Y. Zhang, P. Xu, K. J. Han, S. Noone, J. Peng, and C. W. Liu. 2009. The lysine 48 and lysine 63 ubiquitin conjugates are processed differently by the 26 s proteasome. The Journal of biological chemistry 284:35485-35494.

67. Olzmann, J. A., and L. S. Chin. 2008. Parkin-mediated K63-linked polyubiquitination: a signal for targeting misfolded proteins to the aggresome-autophagy pathway. Autophagy 4:85-87.

68. Seibenhener, M. L., J. R. Babu, T. Geetha, H. C. Wong, N. R. Krishna, and M. W. Wooten. 2004. Sequestosome 1/p62 is a polyubiquitin chain binding protein involved in ubiquitin proteasome degradation. Molecular and cellular biology 24:8055-8068.

69. Garcia-Mata, R., Z. Bebok, E. J. Sorscher, and E. S. Sztul. 1999. Characterization and dynamics of aggresome formation by a cytosolic GFP-chimera. The Journal of cell biology 146:1239-1254.

70. Wigley, W. C., R. P. Fabunmi, M. G. Lee, C. R. Marino, S. Muallem, G. N. DeMartino, and P. J. Thomas. 1999. Dynamic association of proteasomal machinery with the centrosome. The Journal of cell biology 145:481-490.

71. Zhu, K., K. Dunner, Jr., and D. J. McConkey. 2010. Proteasome inhibitors activate autophagy as a cytoprotective response in human prostate cancer cells. Oncogene 29:451-462.

72. Nagaoka, U., K. Kim, N. R. Jana, H. Doi, M. Maruyama, K. Mitsui, F. Oyama, and N. Nukina. 2004. Increased expression of p62 in expanded polyglutamine-expressing cells and its association with polyglutamine inclusions. Journal of neurochemistry 91:57-68.

73. Zatloukal, K., C. Stumptner, A. Fuchsbichler, H. Heid, M. Schnoelzer, L. Kenner, R. Kleinert, M. Prinz, A. Aguzzi, and H. Denk. 2002. p62 Is a common component of cytoplasmic inclusions in protein aggregation diseases. Am J Pathol 160:255-263.

74. Yamamoto, Y., and R. B. Gaynor. 2001. Therapeutic potential of inhibition of the NF-kappaB pathway in the treatment of inflammation and cancer. J Clin Invest 107:135-142.

75. Adams, J. 2004. The development of proteasome inhibitors as anticancer drugs. Cancer cell 5:417-421.

76. Hideshima, T., D. Chauhan, P. Richardson, C. Mitsiades, N. Mitsiades, T. Hayashi, N. Munshi, L. Dang, A. Castro, V. Palombella, J. Adams, and K. C. Anderson. 2002. NF-kappa B as a therapeutic target in multiple myeloma. The Journal of biological chemistry 277:16639-16647.

77. Naugler, W. E., and M. Karin. 2008. NF-kappaB and cancer-identifying targets and mechanisms. Curr Opin Genet Dev 18:19-26.

78. Khanbolooki, S., S. T. Nawrocki, T. Arumugam, R. Andtbacka, M. S. Pino, R. Kurzrock, C. D. Logsdon, J. L. Abbruzzese, and D. J. McConkey. 2006. Nuclear

factor-kappaB maintains TRAIL resistance in human pancreatic cancer cells. Molecular cancer therapeutics 5:2251-2260.

79. Tan, T. T., K. Degenhardt, D. A. Nelson, B. Beaudoin, W. Nieves-Neira, P. Bouillet, A. Villunger, J. M. Adams, and E. White. 2005. Key roles of BIM-driven apoptosis in epithelial tumors and rational chemotherapy. Cancer cell 7:227-238.

80. Zhu, H., L. Zhang, F. Dong, W. Guo, S. Wu, F. Teraishi, J. J. Davis, P. J. Chiao, and B. Fang. 2005. Bik/NBK accumulation correlates with apoptosis-induction by bortezomib (PS-341, Velcade) and other proteasome inhibitors. Oncogene 24:4993-4999.

81. Fribley, A. M., B. Evenchik, Q. Zeng, B. K. Park, J. Y. Guan, H. Zhang, T. J. Hale, M. S. Soengas, R. J. Kaufman, and C. Y. Wang. 2006. Proteasome inhibitor PS-341 induces apoptosis in cisplatin-resistant squamous cell carcinoma cells by induction of Noxa. The Journal of biological chemistry 281:31440-31447.

82. Qin, J. Z., J. Ziffra, L. Stennett, B. Bodner, B. K. Bonish, V. Chaturvedi, F. Bennett, P. M. Pollock, J. M. Trent, M. J. Hendrix, P. Rizzo, L. Miele, and B. J. Nickoloff. 2005. Proteasome inhibitors trigger NOXA-mediated apoptosis in melanoma and myeloma cells. Cancer research 65:6282-6293.

83. Schubert, U., L. C. Anton, J. Gibbs, C. C. Norbury, J. W. Yewdell, and J. R. Bennink. 2000. Rapid degradation of a large fraction of newly synthesized proteins by proteasomes. Nature 404:770-774.

84. Yewdell, J. W., L. C. Anton, and J. R. Bennink. 1996. Defective ribosomal products (DRiPs): a major source of antigenic peptides for MHC class I molecules? J Immunol 157:1823-1826.

85. Meister, S., U. Schubert, K. Neubert, K. Herrmann, R. Burger, M. Gramatzki, S. Hahn, S. Schreiber, S. Wilhelm, M. Herrmann, H. M. Jack, and R. E. Voll. 2007. Extensive Immunoglobulin Production Sensitizes Myeloma Cells for Proteasome Inhibition. Cancer research 67:1783-1792.

86. Suraweera, A., C. Munch, A. Hanssum, and A. Bertolotti. 2012. Failure of amino acid homeostasis causes cell death following proteasome inhibition. Molecular cell 48:242-253.

87. Vabulas, R. M., and F. U. Hartl. 2005. Protein synthesis upon acute nutrient restriction relies on proteasome function. Science 310:1960-1963.

88. Nawrocki, S. T., J. S. Carew, K. Dunner, Jr., L. H. Boise, P. J. Chiao, P. Huang, J. L. Abbruzzese, and D. J. McConkey. 2005. Bortezomib inhibits PKR-like endoplasmic reticulum (ER) kinase and induces apoptosis via ER stress in human pancreatic cancer cells. Cancer research 65:11510-11519.

89. Richardson, P. G., P. Sonneveld, M. W. Schuster, D. Irwin, E. A. Stadtmauer, T. Facon, J. L. Harousseau, D. Ben-Yehuda, S. Lonial, H. Goldschmidt, D. Reece, J. F. San-Miguel, J. Blade, M. Boccadoro, J. Cavenagh, W. S. Dalton, A. L. Boral, D. L. Esseltine, J. B. Porter, D. Schenkein, and K. C. Anderson. 2005. Bortezomib or high-dose dexamethasone for relapsed multiple myeloma. The New England journal of medicine 352:2487-2498.

90. O'Connor, O. A., J. Wright, C. Moskowitz, J. Muzzy, B. MacGregor-Cortelli, M. Stubblefield, D. Straus, C. Portlock, P. Hamlin, E. Choi, O. Dumetrescu, D. Esseltine, E. Trehu, J. Adams, D. Schenkein, and A. D. Zelenetz. 2005. Phase II clinical experience with the novel proteasome inhibitor bortezomib in patients with

indolent non-Hodgkin's lymphoma and mantle cell lymphoma. J Clin Oncol 23:676-684.

91. Belch, A., C. T. Kouroukis, M. Crump, L. Sehn, R. D. Gascoyne, R. Klasa, J. Powers, J. Wright, and E. A. Eisenhauer. 2007. A phase II study of bortezomib in mantle cell lymphoma: the National Cancer Institute of Canada Clinical Trials Group trial IND.150. Ann Oncol 18:116-121.

92. Aghajanian, C., S. Soignet, D. S. Dizon, C. S. Pien, J. Adams, P. J. Elliott, P. Sabbatini, V. Miller, M. L. Hensley, S. Pezzulli, C. Canales, A. Daud, and D. R. Spriggs. 2002. A phase I trial of the novel proteasome inhibitor PS341 in advanced solid tumor malignancies. Clin Cancer Res 8:2505-2511.

93. Fanucchi, M. P., F. V. Fossella, R. Belt, R. Natale, P. Fidias, D. P. Carbone, R. Govindan, L. E. Raez, F. Robert, M. Ribeiro, W. Akerley, K. Kelly, S. A. Limentani, J. Crawford, H. J. Reimers, R. Axelrod, O. Kashala, S. Sheng, and J. H. Schiller. 2006. Randomized phase II study of bortezomib alone and bortezomib in combination with docetaxel in previously treated advanced non-small-cell lung cancer. J Clin Oncol 24:5025-5033.

94. Su, Y., K. I. Amiri, L. W. Horton, Y. Yu, G. D. Ayers, E. Koehler, M. C. Kelley, I. Puzanov, A. Richmond, and J. A. Sosman. 2010. A phase I trial of bortezomib with temozolomide in patients with advanced melanoma: toxicities, antitumor effects, and modulation of therapeutic targets. Clin Cancer Res 16:348-357.

95. Phuphanich, S., J. G. Supko, K. A. Carson, S. A. Grossman, L. Burt Nabors, T. Mikkelsen, G. Lesser, S. Rosenfeld, S. Desideri, and J. J. Olson. 2010. Phase 1

clinical trial of bortezomib in adults with recurrent malignant glioma. J Neurooncol 100:95-103.

96. Yang, C. H., A. M. Gonzalez-Angulo, J. M. Reuben, D. J. Booser, L. Pusztai, S. Krishnamurthy, D. Esseltine, J. Stec, K. R. Broglio, R. Islam, G. N. Hortobagyi, and M. Cristofanilli. 2006. Bortezomib (VELCADE) in metastatic breast cancer: pharmacodynamics, biological effects, and prediction of clinical benefits. Ann Oncol 17:813-817.

97. Chiong, E., A. Dadbin, L. D. Harris, A. L. Sabichi, and H. B. Grossman. 2009. The use of short tandem repeat profiling to characterize human bladder cancer cell lines. J Urol 181:2737-2748.

98. Arumugam, T., V. Ramachandran, K. F. Fournier, H. Wang, L. Marquis, J. L. Abbruzzese, G. E. Gallick, C. D. Logsdon, D. J. McConkey, and W. Choi. 2009. Epithelial to mesenchymal transition contributes to drug resistance in pancreatic cancer. Cancer research 69:5820-5828.

99. Liu, C. H., A. L. Goldberg, and X. B. Qiu. 2007. New insights into the role of the ubiquitin-proteasome pathway in the regulation of apoptosis. Chang Gung Med J 30:469-479.

100. Morgan, W. D., G. T. Williams, R. I. Morimoto, J. Greene, R. E. Kingston, and R. Tjian. 1987. Two transcriptional activators, CCAAT-box-binding transcription factor and heat shock transcription factor, interact with a human hsp70 gene promoter. Mol Cell Biol 7:1129-1138.

101. Wu, B. J., R. E. Kingston, and R. I. Morimoto. 1986. Human HSP70 promoter contains at least two distinct regulatory domains. Proceedings of the National Academy of Sciences of the United States of America 83:629-633.

102. Kent, W. J., C. W. Sugnet, T. S. Furey, K. M. Roskin, T. H. Pringle, A. M. Zahler, and D. Haussler. 2002. The human genome browser at UCSC. Genome Res 12:996-1006.

103. Dreszer, T. R., D. Karolchik, A. S. Zweig, A. S. Hinrichs, B. J. Raney, R. M. Kuhn, L. R. Meyer, M. Wong, C. A. Sloan, K. R. Rosenbloom, G. Roe, B. Rhead, A. Pohl, V. S. Malladi, C. H. Li, K. Learned, V. Kirkup, F. Hsu, R. A. Harte, L. Guruvadoo, M. Goldman, B. M. Giardine, P. A. Fujita, M. Diekhans, M. S. Cline, H. Clawson, G. P. Barber, D. Haussler, and W. James Kent. 2012. The UCSC Genome Browser database: extensions and updates 2011. Nucleic Acids Res 40:D918-923.

104. Nawrocki, S. T., J. S. Carew, M. S. Pino, R. A. Highshaw, R. H. Andtbacka, K. Dunner, Jr., A. Pal, W. G. Bornmann, P. J. Chiao, P. Huang, H. Xiong, J. L. Abbruzzese, and D. J. McConkey. 2006. Aggresome disruption: a novel strategy to enhance bortezomib-induced apoptosis in pancreatic cancer cells. Cancer research 66:3773-3781.

105. Nawrocki, S. T., J. S. Carew, M. S. Pino, R. A. Highshaw, K. Dunner, Jr., P. Huang, J. L. Abbruzzese, and D. J. McConkey. 2005. Bortezomib sensitizes pancreatic cancer cells to endoplasmic reticulum stress-mediated apoptosis. Cancer research 65:11658-11666.

106. Harding, H. P., Y. Zhang, and D. Ron. 1999. Protein translation and folding are coupled by an endoplasmic-reticulum-resident kinase. Nature 397:271-274.

107. Pour, P. M., K. K. Pandey, and S. K. Batra. 2003. What is the origin of pancreatic adenocarcinoma? Mol Cancer 2:13.

108. Morris, J. P. t., and M. Hebrok. 2009. It's a free for all--insulin-positive cells join the group of potential progenitors for pancreatic ductal adenocarcinoma. Cancer cell 16:359-361.

109. Pettengill, O. S., R. A. Faris, R. H. Bell, Jr., E. T. Kuhlmann, and D. S. Longnecker. 1993. Derivation of ductlike cell lines from a transplantable acinar cell carcinoma of the rat pancreas. Am J Pathol 143:292-303.

110. Fribley, A., Q. Zeng, and C. Y. Wang. 2004. Proteasome inhibitor PS-341 induces apoptosis through induction of endoplasmic reticulum stress-reactive oxygen species in head and neck squamous cell carcinoma cells. Molecular and cellular biology 24:9695-9704.

111. Leu, J. I., J. Pimkina, A. Frank, M. E. Murphy, and D. L. George. 2009. A small molecule inhibitor of inducible heat shock protein 70. Molecular cell 36:15-27.

112. Wyttenbach, A., O. Sauvageot, J. Carmichael, C. Diaz-Latoud, A. P. Arrigo, and D. C. Rubinsztein. 2002. Heat shock protein 27 prevents cellular polyglutamine toxicity and suppresses the increase of reactive oxygen species caused by huntingtin. Hum Mol Genet 11:1137-1151.

113. Tabner, B. J., S. Turnbull, O. M. El-Agnaf, and D. Allsop. 2002. Formation of hydrogen peroxide and hydroxyl radicals from A(beta) and alpha-synuclein as a possible mechanism of cell death in Alzheimer's disease and Parkinson's disease. Free radical biology & medicine 32:1076-1083.

114. Bucciantini, M., G. Calloni, F. Chiti, L. Formigli, D. Nosi, C. M. Dobson, and M. Stefani. 2004. Prefibrillar amyloid protein aggregates share common features of cytotoxicity. The Journal of biological chemistry 279:31374-31382.

115. Jenner, P. 2003. Oxidative stress in Parkinson's disease. Annals of neurology 53 Suppl 3:S26-36; discussion S36-28.

116. Rubinsztein, D. C. 2007. Autophagy induction rescues toxicity mediated by proteasome inhibition. Neuron 54:854-856.

117. Talloczy, Z., W. Jiang, H. W. t. Virgin, D. A. Leib, D. Scheuner, R. J. Kaufman, E. L. Eskelinen, and B. Levine. 2002. Regulation of starvation- and virus-induced autophagy by the eIF2alpha kinase signaling pathway. Proceedings of the National Academy of Sciences of the United States of America 99:190-195.

118. Kouroku, Y., E. Fujita, I. Tanida, T. Ueno, A. Isoai, H. Kumagai, S. Ogawa, R. J. Kaufman, E. Kominami, and T. Momoi. 2007. ER stress (PERK/eIF2alpha phosphorylation) mediates the polyglutamine-induced LC3 conversion, an essential step for autophagy formation. Cell death and differentiation 14:230-239.

119. Kuma, A., M. Matsui, and N. Mizushima. 2007. LC3, an autophagosome marker, can be incorporated into protein aggregates independent of autophagy: caution in the interpretation of LC3 localization. Autophagy 3:323-328.

120. Klionsky, D. J., H. Abeliovich, P. Agostinis, D. K. Agrawal, G. Aliev, D. S. Askew, M. Baba, E. H. Baehrecke, B. A. Bahr, A. Ballabio, B. A. Bamber, D. C. Bassham, E. Bergamini, X. Bi, M. Biard-Piechaczyk, J. S. Blum, D. E. Bredesen, J. L. Brodsky, J. H. Brumell, U. T. Brunk, W. Bursch, N. Camougrand, E. Cebollero, F. Cecconi, Y. Chen, L. S. Chin, A. Choi, C. T. Chu, J. Chung, P. G. Clarke, R. S.

Clark, S. G. Clarke, C. Clave, J. L. Cleveland, P. Codogno, M. I. Colombo, A. Coto-Montes, J. M. Cregg, A. M. Cuervo, J. Debnath, F. Demarchi, P. B. Dennis, P. A. Dennis, V. Deretic, R. J. Devenish, F. Di Sano, J. F. Dice, M. Difiglia, S. Dinesh-Kumar, C. W. Distelhorst, M. Djavaheri-Mergny, F. C. Dorsey, W. Droge, M. Dron, W. A. Dunn, Jr., M. Duszenko, N. T. Eissa, Z. Elazar, A. Esclatine, E. L. Eskelinen, L. Fesus, K. D. Finley, J. M. Fuentes, J. Fueyo, K. Fujisaki, B. Galliot, F. B. Gao, D. A. Gewirtz, S. B. Gibson, A. Gohla, A. L. Goldberg, R. Gonzalez, C. Gonzalez-Estevez, S. Gorski, R. A. Gottlieb, D. Haussinger, Y. W. He, K. Heidenreich, J. A. Hill, M. Hoyer-Hansen, X. Hu, W. P. Huang, A. Iwasaki, M. Jaattela, W. T. Jackson, X. Jiang, S. Jin, T. Johansen, J. U. Jung, M. Kadowaki, C. Kang, A. Kelekar, D. H. Kessel, J. A. Kiel, H. P. Kim, A. Kimchi, T. J. Kinsella, K. Kiselyov, K. Kitamoto, E. Knecht, M. Komatsu, E. Kominami, S. Kondo, A. L. Kovacs, G. Kroemer, C. Y. Kuan, R. Kumar, M. Kundu, J. Landry, M. Laporte, W. Le, H. Y. Lei, M. J. Lenardo, B. Levine, A. Lieberman, K. L. Lim, F. C. Lin, W. Liou, L. F. Liu, G. Lopez-Berestein, C. Lopez-Otin, B. Lu, K. F. Macleod, W. Malorni, W. Martinet, K. Matsuoka, J. Mautner, A. J. Meijer, A. Melendez, P. Michels, G. Miotto, W. P. Mistiaen, N. Mizushima, B. Mograbi, I. Monastyrska, M. N. Moore, P. I. Moreira, Y. Moriyasu, T. Motyl, C. Munz, L. O. Murphy, N. I. Naqvi, T. P. Neufeld, I. Nishino, R. A. Nixon, T. Noda, B. Nurnberg, M. Ogawa, N. L. Oleinick, L. J. Olsen, B. Ozpolat, S. Paglin, G. E. Palmer, I. Papassideri, M. Parkes, D. H. Perlmutter, G. Perry, M. Piacentini, R. Pinkas-Kramarski, M. Prescott, T. Proikas-Cezanne, N. Raben, A. Rami, F. Reggiori, B. Rohrer, D. C. Rubinsztein, K. M. Ryan, J. Sadoshima, H. Sakagami, Y. Sakai, M. Sandri, C. Sasakawa, M. Sass, C. Schneider,

P. O. Seglen, O. Seleverstov, J. Settleman, J. J. Shacka, I. M. Shapiro, A. Sibirny, E. C. Silva-Zacarin, H. U. Simon, C. Simone, A. Simonsen, M. A. Smith, K. Spanel-Borowski, V. Srinivas, M. Steeves, H. Stenmark, P. E. Stromhaug, C. S. Subauste, S. Sugimoto, D. Sulzer, T. Suzuki, M. S. Swanson, I. Tabas, F. Takeshita, N. J. Talbot, Z. Talloczy, K. Tanaka, I. Tanida, G. S. Taylor, J. P. Taylor, A. Terman, G. Tettamanti, C. B. Thompson, M. Thumm, A. M. Tolkovsky, S. A. Tooze, R. Truant, L. V. Tumanovska, Y. Uchiyama, T. Ueno, N. L. Uzcategui, I. van der Klei, E. C. Vaquero, T. Vellai, M. W. Vogel, H. G. Wang, P. Webster, J. W. Wiley, Z. Xi, G. Xiao, J. Yahalom, J. M. Yang, G. Yap, X. M. Yin, T. Yoshimori, L. Yu, Z. Yue, M. Yuzaki, O. Zabirnyk, X. Zheng, X. Zhu, and R. L. Deter. 2008. Guidelines for the use and interpretation of assays for monitoring autophagy in higher eukaryotes. Autophagy 4:151-175.

121. Chen, S., J. L. Blank, T. Peters, X. J. Liu, D. M. Rappoli, M. D. Pickard, S. Menon, J. Yu, D. L. Driscoll, T. Lingaraj, A. L. Burkhardt, W. Chen, K. Garcia, D. S. Sappal, J. Gray, P. Hales, P. J. Leroy, J. Ringeling, C. Rabino, J. J. Spelman, J. P. Morgenstern, and E. S. Lightcap. 2010. Genome-wide siRNA screen for modulators of cell death induced by proteasome inhibitor bortezomib. Cancer research 70:4318-4326.

122. Schewe, D. M., and J. A. Aguirre-Ghiso. 2009. Inhibition of eIF2alpha dephosphorylation maximizes bortezomib efficiency and eliminates quiescent multiple myeloma cells surviving proteasome inhibitor therapy. Cancer research 69:1545-1552.

123. He, Y., A. M. Correa, M. G. Raso, W. L. Hofstetter, B. Fang, C. Behrens, J. A. Roth, Y. Zhou, L. Yu, Wistuba, II, S. G. Swisher, and A. Pataer. 2011. The role of PKR/eIF2alpha signaling pathway in prognosis of non-small cell lung cancer. PLoS One 6:e24855.

124. Yang, S., X. Wang, G. Contino, M. Liesa, E. Sahin, H. Ying, A. Bause, Y. Li, J. M. Stommel, G. Dell'antonio, J. Mautner, G. Tonon, M. Haigis, O. S. Shirihai, C. Doglioni, N. Bardeesy, and A. C. Kimmelman. 2011. Pancreatic cancers require autophagy for tumor growth. Genes Dev 25:717-729.

125. Miller, C. P., K. Ban, M. E. Dujka, D. J. McConkey, M. Munsell, M. Palladino, and J. Chandra. 2007. NPI-0052, a novel proteasome inhibitor, induces caspase-8 and ROS-dependent apoptosis alone and in combination with HDAC inhibitors in leukemia cells. Blood 110:267-277.

126. Ling, Y. H., L. Liebes, Y. Zou, and R. Perez-Soler. 2003. Reactive oxygen species generation and mitochondrial dysfunction in the apoptotic response to Bortezomib, a novel proteasome inhibitor, in human H460 non-small cell lung cancer cells. The Journal of biological chemistry 278:33714-33723.

127. Perez-Galan, P., G. Roue, N. Villamor, E. Montserrat, E. Campo, and D. Colomer. 2006. The proteasome inhibitor bortezomib induces apoptosis in mantle-cell lymphoma through generation of ROS and Noxa activation independent of p53 status. Blood 107:257-264.

128. Weniger, M. A., E. G. Rizzatti, P. Perez-Galan, D. Liu, Q. Wang, P. J. Munson, N. Raghavachari, T. White, M. M. Tweito, K. Dunleavy, Y. Ye, W. H. Wilson, and A. Wiestner. 2011. Treatment-induced oxidative stress and cellular antioxidant capacity

determine response to bortezomib in mantle cell lymphoma. Clin Cancer Res 17:5101-5112.

129. Kowaltowski, A. J., N. C. de Souza-Pinto, R. F. Castilho, and A. E. Vercesi. 2009. Mitochondria and reactive oxygen species. Free radical biology & medicine 47:333-343.

130. Stefani, M., and C. M. Dobson. 2003. Protein aggregation and aggregate toxicity: new insights into protein folding, misfolding diseases and biological evolution. J Mol Med (Berl) 81:678-699.

131. Fournier, M. J., C. Gareau, and R. Mazroui. 2010. The chemotherapeutic agent bortezomib induces the formation of stress granules. Cancer Cell Int 10:12.

132. Rafie-Kolpin, M., A. P. Han, and J. J. Chen. 2003. Autophosphorylation of threonine 485 in the activation loop is essential for attaining eIF2alpha kinase activity of HRI. Biochemistry 42:6536-6544.

133. Gyrd-Hansen, M., J. Nylandsted, and M. Jaattela. 2004. Heat shock protein 70 promotes cancer cell viability by safeguarding lysosomal integrity. Cell cycle (Georgetown, Tex 3:1484-1485.

134. Nylandsted, J., M. Gyrd-Hansen, A. Danielewicz, N. Fehrenbacher, U. Lademann, M. Hoyer-Hansen, E. Weber, G. Multhoff, M. Rohde, and M. Jaattela. 2004. Heat shock protein 70 promotes cell survival by inhibiting lysosomal membrane permeabilization. J Exp Med 200:425-435.

135. Garrido, C., M. Brunet, C. Didelot, Y. Zermati, E. Schmitt, and G. Kroemer. 2006. Heat shock proteins 27 and 70: anti-apoptotic proteins with tumorigenic properties. Cell cycle (Georgetown, Tex 5:2592-2601.

136. Cheetham, M. E., and A. J. Caplan. 1998. Structure, function and evolution of DnaJ: conservation and adaptation of chaperone function. Cell Stress Chaperones 3:28-36.

137. Kampinga, H. H., J. Hageman, M. J. Vos, H. Kubota, R. M. Tanguay, E. A. Bruford, M. E. Cheetham, B. Chen, and L. E. Hightower. 2009. Guidelines for the nomenclature of the human heat shock proteins. Cell Stress Chaperones 14:105-111.

138. Calderwood, S. K., M. A. Khaleque, D. B. Sawyer, and D. R. Ciocca. 2006. Heat shock proteins in cancer: chaperones of tumorigenesis. Trends Biochem Sci 31:164-172.

139. Mosser, D. D., and R. I. Morimoto. 2004. Molecular chaperones and the stress of oncogenesis. Oncogene 23:2907-2918.

140. Ravagnan, L., S. Gurbuxani, S. A. Susin, C. Maisse, E. Daugas, N. Zamzami, T. Mak, M. Jaattela, J. M. Penninger, C. Garrido, and G. Kroemer. 2001. Heat-shock protein 70 antagonizes apoptosis-inducing factor. Nat Cell Biol 3:839-843.

141. Heimberger, T., M. Andrulis, S. Riedel, T. Stuhmer, H. Schraud, A. Beilhack, T. Bumm, B. Bogen, H. Einsele, R. C. Bargou, and M. Chatterjee. 2012. The heat shock transcription factor 1 as a potential new therapeutic target in multiple myeloma. British journal of haematology.

142. Shringarpure, R., L. Catley, D. Bhole, R. Burger, K. Podar, Y. T. Tai, B. Kessler, P. Galardy, H. Ploegh, P. Tassone, T. Hideshima, C. Mitsiades, N. C. Munshi, D. Chauhan, and K. C. Anderson. 2006. Gene expression analysis of B-lymphoma cells resistant and sensitive to bortezomib. British journal of haematology 134:145-156.

143. Kamat, A. M., T. Karashima, D. W. Davis, L. Lashinger, M. Bar-Eli, R. Millikan, Y. Shen, C. P. Dinney, and D. J. McConkey. 2004. The proteasome inhibitor

bortezomib synergizes with gemcitabine to block the growth of human 253JB-V bladder tumors in vivo. Molecular cancer therapeutics 3:279-290.

144. Papageorgiou, A., A. Kamat, W. F. Benedict, C. Dinney, and D. J. McConkey. 2006. Combination therapy with IFN-alpha plus bortezomib induces apoptosis and inhibits angiogenesis in human bladder cancer cells. Molecular cancer therapeutics 5:3032-3041.

145. Anckar, J., and L. Sistonen. 2007. Heat shock factor 1 as a coordinator of stress and developmental pathways. Adv Exp Med Biol 594:78-88.

146. Kirkegaard, T., A. G. Roth, N. H. Petersen, A. K. Mahalka, O. D. Olsen, I. Moilanen, A. Zylicz, J. Knudsen, K. Sandhoff, C. Arenz, P. K. Kinnunen, J. Nylandsted, and M. Jaattela. 2010. Hsp70 stabilizes lysosomes and reverts Niemann-Pick disease-associated lysosomal pathology. Nature 463:549-553.

147. Lauss, M., M. Aine, G. Sjodahl, S. Veerla, O. Patschan, S. Gudjonsson, G. Chebil, K. Lovgren, M. Ferno, W. Mansson, F. Liedberg, M. Ringner, D. Lindgren, and M. Hoglund. 2012. DNA methylation analyses of urothelial carcinoma reveal distinct epigenetic subtypes and an association between gene copy number and methylation status. Epigenetics 7:858-867.

148. Dawson, M. A., and T. Kouzarides. 2012. Cancer epigenetics: from mechanism to therapy. Cell 150:12-27.

149. Ryan, J. L., R. J. Jones, S. C. Kenney, A. G. Rivenbark, W. Tang, E. R. Knight, W. B. Coleman, and M. L. Gulley. 2010. Epstein-Barr virus-specific methylation of human genes in gastric cancer cells. Infect Agent Cancer 5:27.

150. Workman, P., F. Burrows, L. Neckers, and N. Rosen. 2007. Drugging the cancer chaperone HSP90: combinatorial therapeutic exploitation of oncogene addiction and tumor stress. Annals of the New York Academy of Sciences 1113:202-216.

151. Trepel, J., M. Mollapour, G. Giaccone, and L. Neckers. 2010. Targeting the dynamic HSP90 complex in cancer. Nat Rev Cancer 10:537-549.

152. Powers, M. V., K. Jones, C. Barillari, I. Westwood, R. L. van Montfort, and P. Workman. 2010. Targeting HSP70: the second potentially druggable heat shock protein and molecular chaperone? Cell cycle (Georgetown, Tex 9:1542-1550.

153. de Ruijter, A. J., A. H. van Gennip, H. N. Caron, S. Kemp, and A. B. van Kuilenburg. 2003. Histone deacetylases (HDACs): characterization of the classical HDAC family. The Biochemical journal 370:737-749.

154. Michan, S., and D. Sinclair. 2007. Sirtuins in mammals: insights into their biological function. The Biochemical journal 404:1-13.

155. Matsuyama, A., T. Shimazu, Y. Sumida, A. Saito, Y. Yoshimatsu, D. Seigneurin-Berny, H. Osada, Y. Komatsu, N. Nishino, S. Khochbin, S. Horinouchi, and M. Yoshida. 2002. In vivo destabilization of dynamic microtubules by HDAC6-mediated deacetylation. EMBO J 21:6820-6831.

156. Piperno, G., M. LeDizet, and X. J. Chang. 1987. Microtubules containing acetylated alpha-tubulin in mammalian cells in culture. The Journal of cell biology 104:289-302.

157. Bertos, N. R., B. Gilquin, G. K. Chan, T. J. Yen, S. Khochbin, and X. J. Yang. 2004. Role of the tetradecapeptide repeat domain of human histone deacetylase 6 in cytoplasmic retention. The Journal of biological chemistry 279:48246-48254.

158. Valenzuela-Fernandez, A., J. R. Cabrero, J. M. Serrador, and F. Sanchez-Madrid. 2008. HDAC6: a key regulator of cytoskeleton, cell migration and cell-cell interactions. Trends in cell biology 18:291-297.

159. Hubbert, C., A. Guardiola, R. Shao, Y. Kawaguchi, A. Ito, A. Nixon, M. Yoshida, X. F. Wang, and T. P. Yao. 2002. HDAC6 is a microtubule-associated deacetylase. Nature 417:455-458.

160. Tran, A. D., T. P. Marmo, A. A. Salam, S. Che, E. Finkelstein, R. Kabarriti, H. S. Xenias, R. Mazitschek, C. Hubbert, Y. Kawaguchi, M. P. Sheetz, T. P. Yao, and J. C. Bulinski. 2007. HDAC6 deacetylation of tubulin modulates dynamics of cellular adhesions. J Cell Sci 120:1469-1479.

161. Zhang, X., Z. Yuan, Y. Zhang, S. Yong, A. Salas-Burgos, J. Koomen, N. Olashaw, J. T. Parsons, X. J. Yang, S. R. Dent, T. P. Yao, W. S. Lane, and E. Seto. 2007. HDAC6 modulates cell motility by altering the acetylation level of cortactin. Molecular cell 27:197-213.

162. Singla, V., and J. F. Reiter. 2006. The primary cilium as the cell's antenna: signaling at a sensory organelle. Science 313:629-633.

163. Pugacheva, E. N., S. A. Jablonski, T. R. Hartman, E. P. Henske, and E. A. Golemis. 2007. HEF1-dependent Aurora A activation induces disassembly of the primary cilium. Cell 129:1351-1363.

164. Kovacs, J. J., P. J. Murphy, S. Gaillard, X. Zhao, J. T. Wu, C. V. Nicchitta, M. Yoshida, D. O. Toft, W. B. Pratt, and T. P. Yao. 2005. HDAC6 regulates Hsp90 acetylation and chaperone-dependent activation of glucocorticoid receptor. Molecular cell 18:601-607.

165. Boyault, C., Y. Zhang, S. Fritah, C. Caron, B. Gilquin, S. H. Kwon, C. Garrido, T. P. Yao, C. Vourc'h, P. Matthias, and S. Khochbin. 2007. HDAC6 controls major cell response pathways to cytotoxic accumulation of protein aggregates. Genes Dev 21:2172-2181.

166. Lee, J. Y., H. Koga, Y. Kawaguchi, W. Tang, E. Wong, Y. S. Gao, U. B. Pandey, S. Kaushik, E. Tresse, J. Lu, J. P. Taylor, A. M. Cuervo, and T. P. Yao. 2010. HDAC6 controls autophagosome maturation essential for ubiquitin-selective quality-control autophagy. EMBO J 29:969-980.

167. Matthias, P., M. Yoshida, and S. Khochbin. 2008. HDAC6 a new cellular stress surveillance factor. Cell cycle (Georgetown, Tex 7:7-10.

168. Lee, Y. S., K. H. Lim, X. Guo, Y. Kawaguchi, Y. Gao, T. Barrientos, P. Ordentlich, X. F. Wang, C. M. Counter, and T. P. Yao. 2008. The cytoplasmic deacetylase HDAC6 is required for efficient oncogenic tumorigenesis. Cancer research 68:7561-7569.

169. Haggarty, S. J., K. M. Koeller, J. C. Wong, C. M. Grozinger, and S. L. Schreiber. 2003. Domain-selective small-molecule inhibitor of histone deacetylase 6 (HDAC6)-mediated tubulin deacetylation. Proceedings of the National Academy of Sciences of the United States of America 100:4389-4394.

170. Butler, K. V., J. Kalin, C. Brochier, G. Vistoli, B. Langley, and A. P. Kozikowski. 2010. Rational design and simple chemistry yield a superior, neuroprotective HDAC6 inhibitor, tubastatin A. J Am Chem Soc 132:10842-10846.

171. Bazzaro, M., Z. Lin, A. Santillan, M. K. Lee, M. C. Wang, K. C. Chan, R. E. Bristow, R. Mazitschek, J. Bradner, and R. B. Roden. 2008. Ubiquitin Proteasome

System Stress Underlies Synergistic Killing of Ovarian Cancer Cells by Bortezomib and a Novel HDAC6 Inhibitor. Clin Cancer Res 14:7340-7347.

172. Catley, L., E. Weisberg, T. Kiziltepe, Y. T. Tai, T. Hideshima, P. Neri, P. Tassone, P. Atadja, D. Chauhan, N. C. Munshi, and K. C. Anderson. 2006. Aggresome induction by proteasome inhibitor bortezomib and alpha-tubulin hyperacetylation by tubulin deacetylase (TDAC) inhibitor LBH589 are synergistic in myeloma cells. Blood 108:3441-3449.

173. Pandey, U. B., Z. Nie, Y. Batlevi, B. A. McCray, G. P. Ritson, N. B. Nedelsky, S. L. Schwartz, N. A. DiProspero, M. A. Knight, O. Schuldiner, R. Padmanabhan, M. Hild, D. L. Berry, D. Garza, C. C. Hubbert, T. P. Yao, E. H. Baehrecke, and J. P. Taylor. 2007. HDAC6 rescues neurodegeneration and provides an essential link between autophagy and the UPS. Nature 447:859-863.

174. Hideshima, T., J. E. Bradner, J. Wong, D. Chauhan, P. Richardson, S. L. Schreiber, and K. C. Anderson. 2005. Small-molecule inhibition of proteasome and aggresome function induces synergistic antitumor activity in multiple myeloma. Proceedings of the National Academy of Sciences of the United States of America 102:8567-8572.

175. Santo, L., T. Hideshima, A. L. Kung, J. C. Tseng, D. Tamang, M. Yang, M. Jarpe, J. H. van Duzer, R. Mazitschek, W. C. Ogier, D. Cirstea, S. Rodig, H. Eda, T. Scullen, M. Canavese, J. Bradner, K. C. Anderson, S. S. Jones, and N. Raje. 2012. Preclinical activity, pharmacodynamic, and pharmacokinetic properties of a selective HDAC6 inhibitor, ACY-1215, in combination with bortezomib in multiple myeloma. Blood 119:2579-2589.

176. Pei, X. Y., Y. Dai, and S. Grant. 2004. Synergistic induction of oxidative injury and apoptosis in human multiple myeloma cells by the proteasome inhibitor bortezomib and histone deacetylase inhibitors. Clin Cancer Res 10:3839-3852.

177. Dasmahapatra, G., T. K. Nguyen, P. Dent, and S. Grant. 2006. Adaphostin and bortezomib induce oxidative injury and apoptosis in imatinib mesylate-resistant hematopoietic cells expressing mutant forms of Bcr/Abl. Leukemia research 30:1263-1272.

178. Adachi, M., Y. Zhang, X. Zhao, T. Minami, R. Kawamura, Y. Hinoda, and K. Imai. 2004. Synergistic effect of histone deacetylase inhibitors FK228 and m-carboxycinnamic acid bis-hydroxamide with proteasome inhibitors PSI and PS-341 against gastrointestinal adenocarcinoma cells. Clin Cancer Res 10:3853-3862.

179. McConkey, D. 2010. Proteasome and HDAC: who's zooming who? Blood 116:308-309.

180. Fotheringham, S., M. T. Epping, L. Stimson, O. Khan, V. Wood, F. Pezzella, R. Bernards, and N. B. La Thangue. 2009. Genome-wide loss-of-function screen reveals an important role for the proteasome in HDAC inhibitor-induced apoptosis. Cancer cell 15:57-66.

181. Kikuchi, J., T. Wada, R. Shimizu, T. Izumi, M. Akutsu, K. Mitsunaga, K. Noborio-Hatano, M. Nobuyoshi, K. Ozawa, Y. Kano, and Y. Furukawa. 2010. Histone deacetylases are critical targets of bortezomib-induced cytotoxicity in multiple myeloma. Blood 116:406-417.

182. Buglio, D., V. Mamidipudi, N. M. Khaskhely, H. Brady, C. Heise, J. Besterman, R. E. Martell, K. MacBeth, and A. Younes. 2010. The class-I HDAC inhibitor

MGCD0103 induces apoptosis in Hodgkin lymphoma cell lines and synergizes with proteasome inhibitors by an HDAC6-independent mechanism. British journal of haematology 151:387-396.

183. Melnikova, I., and J. Golden. 2004. Targeting protein kinases. Nat Rev Drug Discov 3:993-994.

184. Srivastava, R. K., R. Kurzrock, and S. Shankar. 2010. MS-275 sensitizes TRAIL-resistant breast cancer cells, inhibits angiogenesis and metastasis, and reverses epithelial-mesenchymal transition in vivo. Molecular cancer therapeutics 9:3254-3266.

185. Ni Chonghaile, T., K. A. Sarosiek, T. T. Vo, J. A. Ryan, A. Tammareddi, G. Moore Vdel, J. Deng, K. C. Anderson, P. Richardson, Y. T. Tai, C. S. Mitsiades, U. A. Matulonis, R. Drapkin, R. Stone, D. J. Deangelo, D. J. McConkey, S. E. Sallan, L. Silverman, M. S. Hirsch, D. R. Carrasco, and A. Letai. 2011. Pretreatment mitochondrial priming correlates with clinical response to cytotoxic chemotherapy. Science 334:1129-1133.

VITA

Matthew Cooper White was born in Tyler, Texas on October 13th, 1984, the second son of Wesley and Shelia White, and brother of Jeffery White. After graduating from Jacksonville High School (salutatorian) in 2003, he enrolled at Texas A&M University (College Station, TX). There, he met and married his wife, Brittany White, in 2006 and earned a Bachelor of Science degree (cum laude) in Molecular & Cell Biology in 2007. He then began his doctorate work at the Graduate School for Biomedical Sciences (GSBS) at The University of Texas Health Science Center at Houston/ MD Anderson Cancer Center. Following completion of his Ph.D., Matt will start a career in environmental/toxicological consulting as a Health Scientist for ToxStrategies, Austin, TX.